Role of NOD2 and S100A8/S100A9 in the pathogenesis of Coxsackievirus B3-induced myocarditis

vorgelegt von
Dipl.-Biochem.
Irene Müller
geb. in Kasachstan

von der Fakultät III - Prozesswissenschaften
der Technischen Universität Berlin
zur Erlangung des akademischen Grades

Doktor der Naturwissenschaften
- Dr. rer. nat -

genehmigte Dissertation

Promotionsausschuss:

Vorsitzender: Prof. Dr. Peter Neubauer
Gutachter: Prof. Dr. Jens Kurreck
Gutachter: Prof. Dr. Roland Lauster
Gutachter: Prof. Dr. Carsten Tschöpe
Gutachterin: PD Dr. Sophie Van Linthout

Tag der wissenschaftlichen Aussprache: 14. Dezember 2016

Berlin 2017

Diese Arbeit wurde von April 2012 bis April 2016 in der Arbeitsgruppe von Prof. Dr. Carsten Tschöpe, unter der Anleitung von PD Dr. Sophie Van Linthout, an der Charité - Universitätsmedizin Berlin, in der Abteilung Kardiologie und Pulmologie, Campus Rudolf Virchow, angefertigt. Die externe Begutachtung aus der Technischen Universität Berlin, Institut für Biotechnologie FG angewandte Biochemie, erfolgte durch Prof. Dr. Jens Kurreck.

Für meine Familie

CONTENTS

ABSTRACT

Cardiac inflammation plays a crucial role in Coxsackievirus B3 (CVB3)-induced myocarditis and is a consequence of viral-related cardiomyocyte injury, which activates the innate immune system. The nucleotide binding oligomerization domain 2 (NOD2), a cytoplasmatic pattern-recognition receptor (PRR), is responsible for the recognition of single stranded (ss) RNA. The alarmins S100A8 and S100A9 are damage-associated molecular patterns (DAMPs) and have been shown to be of importance in several cardiovascular disorders. NOD2 and the alarmins belong to the innate immune system. Furthermore, the NLR family, pyrin domain containing 3 (NLRP3) inflammasome plays an important role in CVB3 myocarditis, whereby a relationship between NOD2 and NLRP3 has been described. S100A8/S100A9 acts as an inducer of reactive oxygen species (ROS) production, which is an NLRP3 activator. Overall, the role of NOD2, S100A8 and S100A9 in CVB3-induced myocarditis has not been explored so far. Briefly, our group demonstrated recently that NOD2 knockdown ($^{-/-}$) mice are protected from deleterious CVB3-induced effects versus WT CVB3 mice. The aim of our first study was to further investigate the role of NOD2 and its connection to NLRP3 in CVB3-induced myocarditis models. In a second study, we wanted to examine the importance of S100A8 and S100A9 and their connection to NLRP3 in the same experimental models as for NOD2.

In the first study, we demonstrated that NOD2 is up-regulated in CVB3-positive patients compared to acute myocarditis (AMC), dilated cardiomyopathy and control patients. *In vitro*, we further confirmed the relevance of NOD2 in experimental CVB3-mediated myocarditis and determined its link to the NLRP3 inflammasome, as shown by the patients, *in vivo,* and *in vitro* data. In the scope of a second study, we demonstrated that S100A8 and S100A9 are elevated in endomyocardial biopsies of CVB3-positive patients compared to control patients. The S100A9$^{-/-}$ animal study demonstrated the detrimental role of S100A8 and S100A9 in CVB3-induced myocarditis, as shown by reduced cardiac chemokine production, less cardiac immune cell infiltrates, suppression of cardiac oxidative stress and RAGE signaling, lower Coxsackievirus and adenovirus receptor levels and CVB3 copy number, and an improved LV function in S100A9$^{-/-}$ CVB3-infected mice versus WT CVB3 animals. Exogenous application of S100A8 to S100A9$^{-/-}$ CVB3 mice induced a severe myocarditis similar to WT CVB3 mice. In *in vitro* experiments, we confirmed the deteriorating effect of both alarmins. Furthermore, our *in vivo* and *in vitro* results demonstrated a link between alarmins and the NLRP3

inflammasome system. The decreased RAGE and Dia-1 expression in CVB3-infected S100A9$^{-/-}$ mice compared to respective CVB3 controls, which in case of RAGE was also confirmed *in vitro*, may be an indicator for S100A8- and S100A9-signaling via RAGE and Dia-1 in CVB3-induced myocarditis. These data predict a model where in CVB3-induced myocarditis, NOD2 is responsible for CVB3 sensing and NLRP3 activation, and is probably therefore the main source of the inflammatory disorder. In parallel, the CVB3 infection results in an elevation of S100A8 and S100A9, which induces a signaling cascade via RAGE and Dia-1, resulting in an increased inflammatory cell migration and oxidative stress, particularly ROS. The latter is considered to lead to myocardial injury in AMC patients and to exacerbate inflammation. High ROS production in myocarditis in turn boosts the inflammatory disorder. In this vicious circle, ROS activates the NLRP3 inflammasome and in turn boosts the inflammatory disorder. Prevailing pharmacological treatment of myocarditis-associated cardiomyopathy targets mainly the neuroendocrine system but does not directly influence the virus-induced inflammation and oxidative stress. Since NOD2 and NLRP3 are involved in the inflammatory disorder and S100A8 and S100A9 seem to play a role in oxidative stress, these molecules may represent new potential pharmaceutical targets for the treatment of (CVB3-induced) myocarditis.

ABBREVIATIONS

AMC	acute myocarditis
AP-1	activation protein-1
APS	ammonium persulfate
ASC	apoptosis-associated speck-like protein containing a CARD
α-SMA	alpha-smooth muscle actin
BCA	bicinchoninic acid-protein assay
c	concentration
Ca^{2+}	calcium
CAR	Coxsackievirus and adenovirus receptor
CARD	caspase-recruiting domain
CD	cluster of differentiation
CVB3	Coxsackievirus B3
DAMPs	damage-associated molecular patterns
DCM	dilated cardiomyopathy
DCMi	inflammatory DCM
Dia-1	Diaphanous-1
DMEM	Dulbecco's modified eagle medium
DMSO	dimethylsulfoxide
DNA	deoxyribonucleic acid
ECM	extracellular matrix
EDTA	ethylenediaminetetraacetate
EF	ejection fraction
ELISA	enzyme-linked immunosorbant assay

ER	endoplasmatic reticulum
ERK	extracellular-signal regulated kinase
FACS	fluorescence activated cell sorting
FITC	fluorescein isothiocyanate
HF	heart failure
HIV	human immunodeficiency virus
HMGB1	high mobility group box 1 protein
HRP	horseradish peroxidase
HSP	heat shock protein
IFN-β	interferon-beta
IL	interleukin
IKK	inhibitor kappa B kinase
IκB	inhibitor kappa B
IRAK1	interleukin 1 receptor associated kinase 1
JNK	c-jun N-terminal kinase
LPS	lipopolysaccharide
LV	left ventricle
Ly6c	lymphocyte antigen 6 complex locus c1
Ly6g	lymphocyte antigen 6 complex locus g6d
MAPK	mitogen-activated protein kinase
MAVS	mitochondrial antiviral signaling protein
MDP	muramyl dipeptide
MIP-2	macrophage inflammatory protein-2
MOI	multiplicity of infection

MPO	myeloperoxidase
mRNA	messenger RNA
MyD88	myeloid differentiation factor 88
NACHT	nucleotide-binding oligomerization domain
NADPH	nicotinamide adenine dinucleotide phosphate
NF	nuclear factor
NLRs	(NOD)-like receptors
NLRP3	NLR family, pyrin domain containing 3
NOD2	nucleotide-binding oligomerization domain 2
NO	nitric oxide
NOS	nitric oxide synthase
Nox1	NADPH oxidase 1
NFκB	nuclear factor "kappa-light-chain-enhancer" of activated B cells
OD	optical density
PAMPs	pattern-associated molecular patterns
PBS	phosphate-buffered saline
PBS-T	PBS-Tween
PCR	polymerase chain reaction
PKC	protein kinase C
PRR	pattern-recognition receptor
RAGE	receptor for advanced glycation end products
RIPK2	receptor interacting protein kinase 2
RPMI	Roswell Park Memorial Institute
RSV	respiratory-syncytial virus

scr	scrambled
SDS	sodium dodecyl sulfate
siRNA	small interference RNA
ss	single stranded
RNA	ribonucleic acid
ROS	reactive oxygen species
PFU	plaque forming units
RT	room temperature
RLU	relative light units
TEMED	tetramethylethylenediamine
TGF-β	transforming growth factor-beta
TIR	toll-interleukin-1 receptor
TLRs	toll-like receptrors
TMB	tetramethylbenzidin
TNF-α	tumor necrosis factor-alpha
TRIF	TIR-domain containing adaptor inducing IFN-β

1. INTRODUCTION

1.1. Viral myocarditis

1.1.1. Epidemiology of viral myocarditis

Viral myocarditis is defined as an inflammatory cardiac disorder caused by viral infections. Common viral pathogens of myocarditis include the group B of Coxsackievirus[1], adenovirus[2], parvovirus B19[3], hepatitis C virus[4], human immunodeficiency virus (HIV)[5] and influenza virus[6]. It is a main cause of heart failure (HF) in young adults and often leads to chronic myocarditis, dilated cardiomyopathy (DCM), congestive HF and sudden cardiac death[1, 7]. The long-term mortality rate of viral myocarditis is up to 19.2% in 4.5 years[8].

Endomyocardial biopsy (EMB)-based virological examinations are not widely used. Thus, there is a lack of high-value epidemiological reports and the exact incidence and prevalence of viral myocarditis is not known[1]. Kühl *et al.*[3] showed a 67% high prevalence of viral genome in biopsies of patients with DCM.

1.1.2. Etiology of myocarditis

Most information about the pathophysiology of viral myocarditis is available in Coxsackievirus B3 (CVB3)-induced experimental or human myocarditis. In order to internalize the viral genome into the cardiomyocyte, the CVB3 virus and some adenoviruses utilize the Coxsackievirus and adenovirus receptor (CAR)[9]. As a co-receptor, CVB3 utilizes the deflecting decay accelerating factor and the adenovirus particular integrins, such as αvβ3 and αvβ5. Deletion of CAR results in an abolished viral infection and myocarditis[10]. CVB3 enters the organism via the respiratory or gastrointestinal tract and persists in lymph nodes and in the spleen. After affecting the heart, the first phase of infection is induced, where viremia is followed by direct cardiomyocyte injury and innate immunity activation[11]. This

phase includes invasion of macrophages, natural killer cells and cytokine and nitric oxide production, followed by T lymphocyte infiltration. The acute phase takes place for only a few days. Most patients recover during this phase. A subgroup of patients progresses to a second phase, which takes a few weeks to several months, with the onset of adaptive immune responses, mediated by T-cells and B-cells[11-13]. In this sub-acute phase, cytokines and antibodies towards viral and cardiac proteins may lead to cardiac damage. In most patients, the immune response decreases with viral elimination accompanied by an improvement of the left ventricular (LV) function. Nonetheless, some patients progress to a chronic phase, where remodeling and fibrosis takes place[13, 14]. Some patients show a persistent inflammation with no viral evidence, nominal inflammatory DCM (DCMi), whereby the other patients show a persistent virus and no inflammation, nominal chronic heart disease[11]. Although in the last few years, huge progress in the diagnosis methods, and in the understanding of the pathophysiology and treatment of viral myocarditis has been achieved, no standard treatment has been defined[13].

1.2. Innate immunity

1.2.1. TLRs

Innate immunity is initiated by pattern-recognition receptors (PRRs)[15] recognizing pathogen- or/and damage-associated molecular patterns (PAMPs or DAMPs, respectively)[16]. So far, five families of PRRs have been described: C-type lectin receptors, the "Toll-like" receptors (TLRs), retinoic acid inducible gene-I-like receptors, the Pyrin-HIN domain containing family, and the nucleotide-binding oligomerization domain (NOD)-like receptors (NLRs)[16]. In humans about 10 TLRs, and in mouse 12 functional TLRs (TLR1-9 and TLR11-13), have been described[17]. All TLRs share an extracellular leucin-rich repeat (LRR) domain for ligand recognition, a trans-membrane domain and a cytoplasmatic Toll-interleukin-1 receptor (TIR), which recruits adaptor proteins, including myeloid differentiation factor 88 (MyD88) or TIR-domain containing adaptor inducing interferon-β (IFN-β) (TRIF)[18]. Except TLR3, all TLRs engage MyD88, which leads to an activation of transcription factors, such as nuclear factor-kappa B (NF-κB) and activator protein-1 (AP-1). Furthermore, TRIF engagement is unique for TLR3 and endocytosed TLR4, which leads to type I IFN production and late NF-κB activation[18]. TLR4 is a well-studied TLR family member, which recognizes DAMPs, among

others S100A8/S100A9 and PAMPs, including lipopolysaccharide (LPS) of gram-negative bacteria[19].

1.2.2. RAGE

The receptor for advanced glycation end products (RAGE) is a PRR[20], and like TLR4, it is expressed on cell types which are critical for immune surveillance, including vascular endothelium, monocytes and dendritic cells[21]. RAGE and TLR4 have overlapping ligands, such as high mobility group box 1 protein (HMGB1) and S100A8/S100A9, whereby both receptors share the adaptor MyD88 to initiate downstream signaling[22]. RAGE is composed of an extracellular region, a hydrophobic transmembrane domain and a short cytoplasmatic domain[23]. Multiple signaling pathways can be initiated via RAGE, which are also initiated by TLR4, which activate various transcription factors such as NF-κB[22] and early growth response protein 1, which is activated via RAGE[24]. Besides the transduction pathway via MyD88, RAGE initiates signaling pathways via a newly discovered binding partner Diaphanous-1 (Dia-1), which controls cellular migration[25] and the production of reactive oxygen species (ROS), via activation of nicotinamide adenine dinucleotide phosphate (NADPH) oxidase[26].

1.2.3. Damage-associated molecular patterns

DAMPs are similar to PAMPs, but are endogenous molecules, so called alarmins and are also recognized by PRRs[19, 27]. They share several characteristics; 1) they are released via an active nonclassical secretion, which involves the activation of protein kinase C (PKC) and an intact microtubule network[28]; 2) they recruit and activate innate immune cells and indirectly lead to stimulation of adaptive immunity; and 3) they restore the homeostatic state of damaged tissue[27]. HMGB1, uric acid, heat shock proteins (HSPs), hepatoma-derived growth factor and S100 proteins represent some of the DAMPs[27]. The designation “S100” is a consequence of their solubility in 100% ammonium sulphate[29]. The S100A family includes more than 20 members and some of them are directly linked to the innate immune system, such as S100A7, S100A15, S100A12, S100A8 and S100A9[19].

1.2.4. S100A8 and S100A9 damage-associated molecular patterns

S100A8 and S100A9 are calcium binding cytosolic proteins defined by two calcium-binding sites which are referred to as EF-hands. The EF-hand motif, which is a classical helix-loop-helix structural motif, consists of two α-helices and a central calcium-binding loop[28, 30] **(Figure 1.2.4.)**. Murine S100A8 and S100A9 form noncovalently-associated homodimers and heterodimers[19]. In humans, S100A8 and S100A9 form heterodimers and higher oligomers[31], whereby a functional involvement of S100A8 and S100A9 homodimers in human inflamed upper airway tissue has been shown[32]. Vogl *et al.*[33] demonstrated that S100A8/S100A9 is an endogenous TLR4 ligand in LPS-induced sepsis, where interaction of S100A8 with the TLR4/MD2 complex leads to an activation of NF-κB and mitogen-activated protein kinase (MAPK) p38, extracellular-signal regulated kinase (ERK) and PKC[19] **(Figure 1.2.4.)**. Furthermore, they showed that S100A8/S100A9, the predominant form[19], develops its pro-inflammatory character only in the presence of LPS[33]. This circumstance emphasises the fact that the heterodimer S100A8/S100A9 has physiological functions under normal conditions, including physiological homeostasis[19], whereas S100A8 and S100A9 homodimers are pro-inflammatory *per se*[32-34]. Furthermore, S100A9/S100A9 homodimer activates NF-κB via TLR4 in THP-1 cells and periodontal ligament cells[35, 36], whereas in lung fibroblasts, it activates the RAGE axis[37]. For endothelial cells, S100A8/S100A8 showed prevalence for TLR4 activation, S100A9/S100A9 for RAGE and S100A8/S100A9 for both receptors[38]. In summary, the specific receptor and pathway for all three combinations depends on the cell type[36] and probably on the disease. S100A8 and S100A9 are abundantly expressed in neutrophils and monocytes[19]. During inflammatory conditions, these proteins are released from phagocytes, which are activated by inflammatory cytokines[19]. S100A8, S100A9 and S100A8/S100A9 are associated with autoimmune and inflammatory disorders, such as arthritis[39], systemic lupus erythematosus[40] and Crohn's disease[41]. Furthermore, S100A8/S100A9 serves as an excellent biomarker in rheumatoid arthritis, juvenile idiopathic arthritis and inflammatory bowel disease[42].

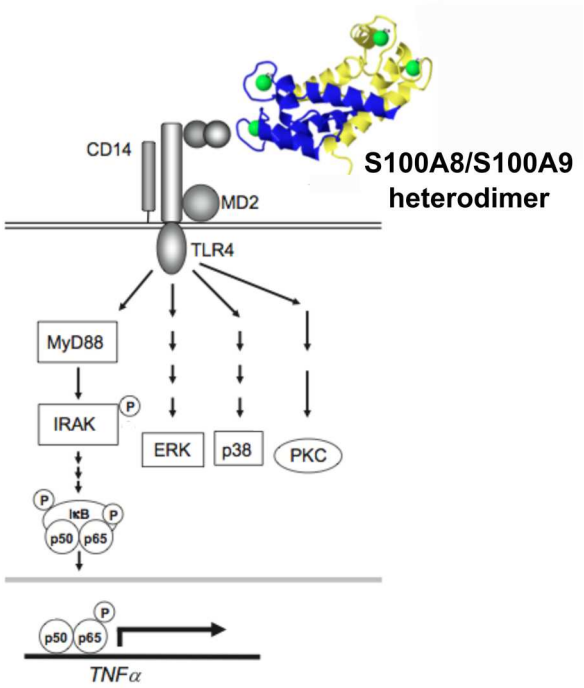

Figure 1.2.4. S100A8/S100A9 as a TLR4 ligand. S100A8, as the active form of S100A8/S100A9, binds to TLR4 and initiates distinct signaling pathways. IκB=Inhibitor of NF-κB; P=Phosphorylated form; p50 and p65=NF-κB subunits (adapted from 'The endogenous Toll-like receptor 4 agonist S100A8/S100A9 (Calprotectin) as innate amplifier of infection, autoimmunity and cancer'; Ehrchen *et al.* Journal of Leukocyte Biology 2009 86: 557-566). S100A8/S100A9 displayed as a crystal form, where S100A8 is displayed in sea-blue, S100A9 in yellow and bound Ca^{2+} ions in green (adapted from 'Pro-Inflammatory S100A8 and S100A9 Proteins: Self-Assembly into Multifunctional Native and Amyloid Complexes'; Vogl *et al.* International Journal of Molecular Sciences 2012 13: 2893-2917).

1.2.5. NOD-like oligomerization domain receptors

The function of NLRs is to sense intracellular microbial, viral and endogenous molecules (PAMPs and/or DAMPs), which include for example peptidoglycan, flagellin, virus RNA and DNA, uric acid and adenosintriphosphate[16, 43]. Twenty-two members of NLRs are found in humans and more than 30 in mice[44]. Five subfamily classifications have been made based on the N-terminal domain; 1) NLR family, acidic domain containing (NLRA); 2) NLR family, BIR domain containing (NLRB); 3) NLR family, caspase-recruiting domain (CARD) containing (NLRC); 4) NLR family, pyrin domain containing (NLRP) and the mitochondria- localized NLRX1[43].

1.2.6. NOD2

NOD2 is one of the best-characterized members of the NLR family and is characterized by two N-terminal CARDs, a central nucleotide-binding oligomerization domain (NACHT), and an LRR segment at the C-terminal end. NOD2 can recognize the peptidoglycan muramyl dipeptide (MDP), a component in both gram-negative and gram-positive bacteria[45]. MDP sensing leads to an auto-oligomerization of NOD2, followed by exposure of the CARD domain and a subsequent recruitment and activation of receptor-interacting protein kinase 2 (RIPK2) via CARD-CARD interactions[45]. Active RIPK2 directly ubiquitinises the NF-κB essential modulator (NEMO) and thus activates the inhibitor kappa B (IκB) kinase complex (IKKα, IKKβ), inducing the activity of NF-κB by phosphorylation of the NF-κB inhibitor (IκB). RIPK2-dependent transforming growth factor beta-activated kinase 1 (TAK1) activation affects the IKK complex and can activate three MAPKs; p38 MAPK, c-jun N-terminal kinase (JNK) and ERK[45] **(Figure 1.2.6.)**. Furthermore, it has been described that NOD2 activates MAPK p38 and JNK via CARD9[46]. Further investigation into NOD2-mediated MAPK activation is necessary. Moreover, NOD2 initiates the autophagy pathways[47]. The control of the type I IFN signaling completes the NLRs repertoire of multiple cellular processes[16].

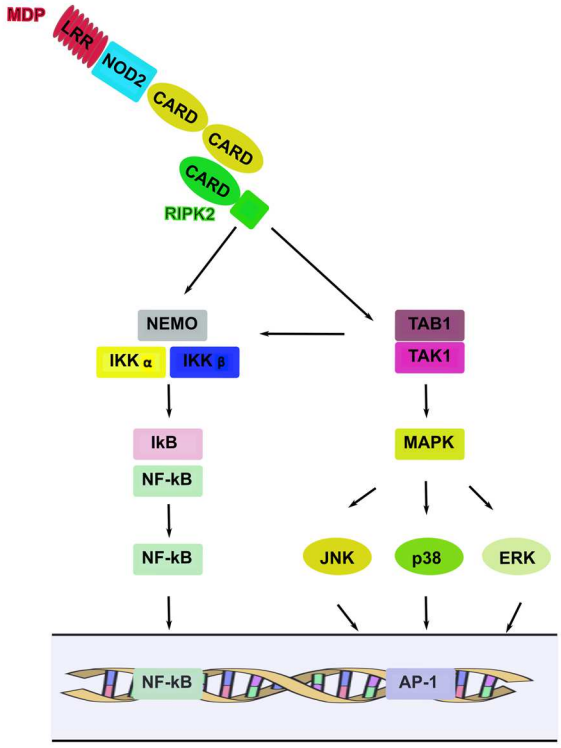

Figure 1.2.6. NOD2 signaling pathway (based on Antosz *et al.* Acta Biochimica polonica 2013 60: 351-360).

1.3. NOD2, TLR4, and S100A8/S100A9 in cardiac diseases and viral infection

1.3.1. Role of NOD2 in cardiac diseases

Three functional polymorphisms in the *NOD2/CARD15* gene are associated with an increased risk for Crohn's disease, which leads to an excessive immune response[48]. The relevance of the innate immune system and inflammation in the pathogenesis of cardiovascular diseases supports a potential role of NOD2 in cardiovascular disorders[48]. In agreement, an up-regulation of NOD2 in atheroma lesions was found in patients with coronary heart disease[49]. Furthermore, NOD2 depletion in mice led to the proliferation of vascular smooth muscle cells after vascular injury[50]. Finally, NOD2 deficiency in mice has been shown to be protective against cardiac remodeling after myocardial infarction[51]. Overall, the research of NOD2 and cardiac diseases has just emerged and needs more investigation.

1.3.2. Role of NOD2 in viral infection

Recently, Sabbah *et al.*[52] found that NOD2 was activated after cells were infected *in vitro* with viruses containing a negative (-) ssRNA genome, including respiratory-syncytial virus (RSV), vesicular stomatitis virus, or influenza virus. Activation of NOD2 leads to an antiviral immunity facilitated by IFN regulator factor 3 (IRF3)-dependent IFN-β secretion. The investigators found that $NOD2^{-/-}$ mice were accompanied with lower IFN-β production and were more susceptible to the RSV infection. Further, Sabbah *et al.*[52] demonstrated that depletion of the mitochondrial antiviral signaling protein (MAVS) impaired NOD2-dependent IFN-β production after RSV infection. Collectively, the mitochondrial adaptor MAVS might play an important role in NOD2-dependent IFN-β production in response to ssRNA, by recruiting signaling complexes for IRF7, IRF3 and NF-κB activation[16, 52]. Additionally, type I IFN production (IFN-α and IFN-β) can be triggered by stimulation of NOD2 upon *Mycobacterium tuberculosis* infection, whereby this NOD2 stimulation leads to RIPK2 activation and IRF5 dependent signaling[16]. In the case of the positive stranded (+) ssRNA porcine reproductive and respiratory syndrome virus, the NOD2-RIPK2 signaling pathway is activated, leading to a pro-inflammatory response, however NOD2 and RIPK2 knockdown diminished this pro-

inflammatory response[53]. The role of NOD2 in viral infection has only just emerged and is subject to ongoing research.

1.3.3. Role of TLR4 in cardiac diseases

All human TLRs have been found in the human heart, whereby TLR4 is the best described receptor in cardiovascular diseases[54]. Studies on the role of TLR4-deficiency in myocardial infarction showed a beneficial effect of its depletion with respect to better outcomes and decreased inflammation[55]. In doxorubicin-induced cardiomyopathy, TLR4 knockout improved cardiac function and attenuated pathophysiological doxorubicin-induced mechanisms[56]. In addition, inhibition of TLR4 with the pharmacological antagonist eritoran resulted in reduced murine cardiac hypertrophy[57]. A protective effect of TLR4 knockout was also evident after ischemia/reperfusion injury in mice[58].

1.3.4. Role of TLR4 in viral infection

TLR4 harbours both cardiotropic and cardioprotective signaling pathways. For example, TLR4 knockout mice display higher CVB3 levels after two days of infection, but 12 days post infection, the viral titers and the myocarditis score decreased. Concomitantly, the interleukin (IL)-1β and IL-18 levels decreased, whereupon TLR4 seems to play an important role in CVB3-induced myocarditis[59]. A further study demonstrated that MyD88 depletion protects mice from CVB3 infection[60]. In contrast, a TRIF knockout led to higher susceptibility to CVB3 infection compared to non-infected mice[61], pointing out the complexity and diversity of TLR4-downstream pathways.

1.3.5. Role of S100A8 and S100A9 in cardiac diseases

The expression of S100A8 and S100A9 has been reported to be increased in acute coronary syndromes[62] and to act via TLR4[63]. These molecules are also elevated in atherosclerosis[64] and overall correlate with cardiovascular risk factors and cardiovascular disease in middle-aged healthy individuals[65]. The alarmins S100A8 and S100A9 have been identified as a

potential tool to distinguish between stable and un-stable coronary artery plaque[62] and myocardial infarction in acute coronary syndrome[66].

1.3.6. Role of S100A8 and S100A9 in viral infection

Elevated systemic S100A8/S100A9 levels are associated with viral infection, such as papillomavirus[67] and in patients with acute respiratory syndrome caused by a coronavirus[68]. Additionally, patients infected with lentivirus or HIV-1 show a positive correlation between high S100A8/S100A9 levels and disease progression[69]. Further, S100A8, S100A9 and S100A8/S100A9 promote viral replication in human cluster of differentiation (CD) 4^+ T-lymphocytes latently infected with HIV-1[70]. An infection with a double stranded (ds) RNA mimetic polyinosinic:polycytidylic acid, in murine macrophages leads to high S100A8 and in human monocytes and macrophages to enhanced S100A8 and S100A9 levels suggesting that S100A8/S100A9 leads to viral persistence[69]. In the same study, S100A8 levels elevated to a maximum at day 8 in the lungs of influenza virus-infected mice and decreased in the recovery phase[69]. Overall, S100A8 and S100A9 are regulated during viral infection[69]. The roles of S100A8 and S100A9 after Coxsackievirus infection and thus in viral myocarditis are unclear and require further investigation.

1.4. The inflammasome

1.4.1. The NLRP3 inflammasome

In the past ten years, the inflammasome has been recognized as a regulator in the host defense against invading pathogens and for its role in development of auto-inflammatory, metabolic and oncological diseases[71]. Inflammasome activation occurs via three of the 22 described in human NLRs: NLRP1 inflammasome, NLRP3 inflammasome and NLRC4 inflammasome (Ipaf), along with pyrin and HIN domain-containing (PYHIN) family absent in melanoma 2 (AIM2)[71]. The subsequent inflammasome assembly requires in most cases the apoptosis-associated speck-like protein containing a CARD (ASC), which is responsible for pro-caspase-1 recruitment[71]. In this complex, autocatalytic activated caspase-1 cleaves pro-

IL-1β and pro-IL-18 in its mature form[72]. Caspase-1 activity can result in plasma membrane rupture and release of inflammatory IL-1β and IL-18: pyroptotic cell death[73]. There are first reports, that NLRP6 inflammasome, NLRP7 inflammasome, retinoic acid inducible gene I (RIG-I), pyrin and IFNγ-inducible protein 16 (IFI16) form inflammasome complexes[72]. The NLRP3 inflammasome is the best-studied inflammasome and is implicated in the pathogenesis of many diseases such as gout[74, 75], type II diabetes[74, 76], and atherosclerosis[74, 77]. NLRP3 responds to a vast range of DAMPs and PAMPs, such as ROS[78], mitochondrial DNA, ionic in- and efflux, mitochondrial damage[72], ATP, bacterial messenger (m) RNA, bacterial DNA:RNA hybrids, MDP, fungi and protozoa[71].

1.4.2. Priming and activation of the NLRP3 inflammasome

It is generally accepted, that the assembly of a functional NLRP3 inflammasome depends on priming, which occurs prior to or coincident with activating signals[72]. The priming step represents a regulatory checkpoint at the transcriptional level. Ligands of TLRs, such as TLR4, NLRs including NOD2, IL-1R1 and tumor necrosis factor (TNF) receptors TNFR1 and TNFR2, activate downstream NF-κB and initiate the transcription and translation of pro-IL-1β and NLRP3. In contrast, NLRP3 inflammasome components ASC, pro-caspase-1 and IL-18, are constitutively expressed, thus a transcriptional activation is not necessary for an inflammasome activation[72]. Subsequently, HSP and its co-chaperone SGT1, an ubiquitin ligase-associated protein, dissociate from NLRP3[79]. Additionally, the JAMM domain-containing Zn^{2+} metalloprotease deubiquitinating enzyme BRCC3, deubiquitinizes NLRP3, while ASC is ubiquitinated via LUBAC and phosphorylated by spleen tyrosine kinase (SYK) and JNK[72, 80] **(Figure 1.4.2.1.)**.

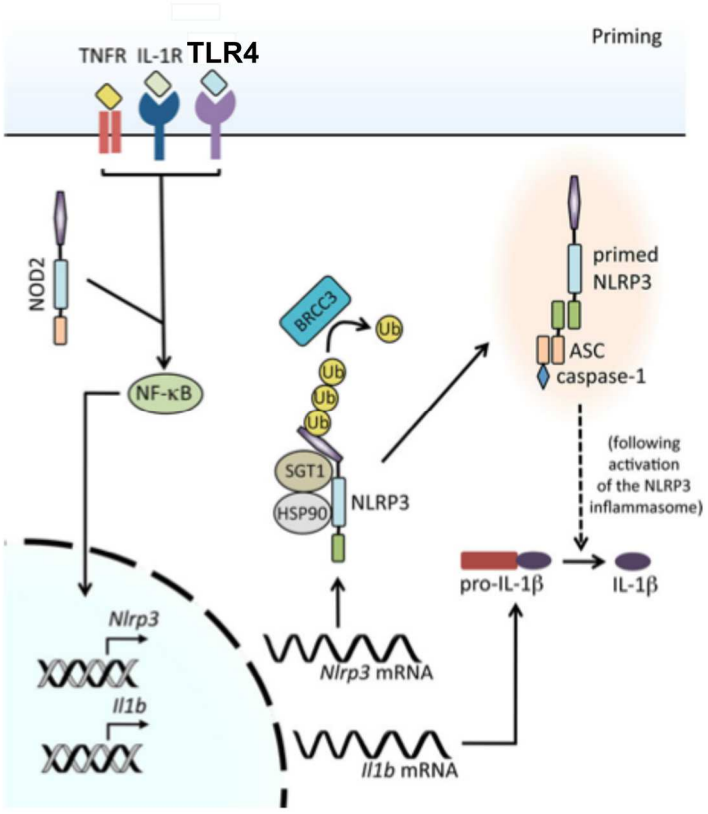

Figure 1.4.2.1. Priming of NLRP3 via NOD2 and the TLR4 receptor (adapted from 'Mechanism of NLRP3 inflammasome activation'; Sutterwala *et al.* Annals of the New York Academy of Sciences 2014 1319: 82-95).

Interestingly, the TLR4/MyD88 axis skips transcriptional priming and leads to a deubiquitination of NLRP3, which represents transcriptional-independent priming[81]. Interestingly, two other groups showed that via TLRs/MyD88/IL-1 receptor associated kinase 1 (IRAK1), a direct and priming-independent activation of the NLRP3 inflammasome is possible, by direct interaction of IRAK1 with ASC[82, 83]. As previously described, the NLRP3 activators are structurally dissimilar and act on cell pathways in diverse ways. An explanation for their similar activity with different structures has been suggested whereby downstream of these unrelated activators, there is a common pathway that could activate the NLRP3 inflammasome[72]. Upon activation, NLRP3 forms a homo-oligomer via its NACHT domain and interacts directly through its pyridine with the adaptor protein ASC. ASC interacts via its CARD domain with pro-caspase-1. This complex activates caspase-1, which cleaves pro-IL1β and pro-IL-18 in its mature forms[84]. Collectively, competing models of NLRP3 inflammasome complex assembly exist, and are summarized in **Figure 1.4.2.2**. The physical architecture and molecular composition of the activated NLRP3 inflammasome needs further investigation[80].

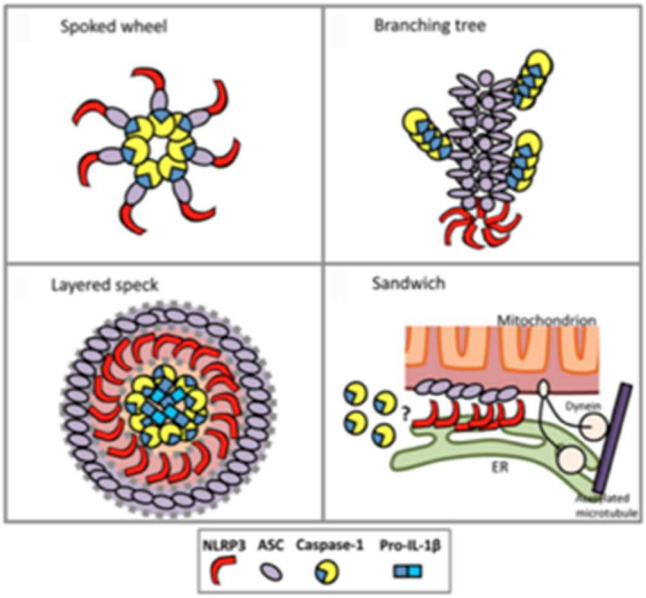

Figure 1.4.2.2. Models of NLRP3 inflammasome assembly. The apoptosome served as an example for the ***Spoked wheel*** model, which consists of NLRP3 spokes interacting indirectly with caspase-1 through the adaptor ASC. In the ***Branching tree*** model, the NLRP3 inflammasome assembles as a tree, where NLRP3 builts a heptameric root, which nucleates the ASC-stem. Caspase-1 polymerizes laterally as branches. The ***Layered Speck*** model consists of aggregated ASC, which contains the NLRP3 molecules. Caspase-1 and IL-1β are accumulated in the core of the complex. In the ***Sandwich*** model, the ASC associated NLRP3 complex forms a sandwich-like complex, by associating with endoplasmatic reticulum (ER) and the outer membrane of the mitochondrion (Elliot *et al.* Immunological Reviews 2015 265: 35-52).

1.4.3. NLRP3 inflammasome in cardiac diseases and viral infection

Growing evidence suggests an important role of the inflammasome in the development of HF. Marchetti *et al.*[85] showed *in vivo* that NLRP3 inflammasome inhibition preserved cardiac dysfunction after ischemic and non-ischemic injury. In biopsies of patients with lymphocytic acute myocarditis, the formation of the inflammasome was significantly higher compared to control patients[86]. Furthermore, there was a positive correlation between increased inflammasome activity and severe HF[86]. Additionally, this group showed recently that NLRP3 priming is essential for inflammasome activation to induce caspase-1 activation and to induce LV dysfunction[87]. NLRP3 is activated by dsRNA and ssRNA viruses, including influenza virus, encephalomyocarditis virus, sendai virus, RSV and CVB3 virus[74, 88]. Double stranded DNA viruses, such as adenovirus are likewise recognized via NLPR3[89]. However, the activating mechanism of the NLRP3 inflammasome, how the ligands are recognized and

how the complex assembly functions, is still unclear[74]. Recently, it has been shown by Wang *et al.*[88] that the NLRP3 inflammasome plays an important role in CVB3-induced myocarditis. In this study, a caspase-1 inhibitor as well as an IL-1β antibody reduced the CVB3-myocarditis damage *in vivo*. With respect to NLRP3 itself, only *in vitro* experiments were performed showing a reduction of caspase-1 activity and IL-1β levels after a NLRP3 knockdown[88].

1.4.4. Role of NOD2, TLR4, S100A8, and S100A9 in inflammasome

Besides the fact that TLR4 and NOD2 prime the NLRP3 inflammasome[72], it has been shown that NOD2 is able to activate the NLRP3 inflammasome by interacting directly with NLRP3[90]. Another group proposed that NOD2 is a part of the NLRP3 inflammasome[91]. In addition, a direct interaction between NOD2 and caspase-1 has been described[92]. Interestingly, TLR4 can overcome the transcriptional priming and directly induce the NLRP3 deubiquitination via MyD88[81]. Since monocytes and macrophages control IL-1β secretion predominantly by the NLRP3 inflammasome[93] and S100A8 and S100A9 are mainly expressed in monocytes[33] and are released via activated phagocytes after TLR4 sensing[19], a connection between S100A8/S100A9 and the NLRP3 inflammasome is likely. Indeed, there seem to be two ways by which these alarmins regulate the NLRP3 inflammasome. Simard *et al.*[93] showed that S100A8 and S100A9 enhance the NLRP3 and IL-1β expression via a ROS-dependent NF-kB activation. Additionally, Nagareddy *et al.*[94] demonstrated, that this pathway occurs via TLR4. In contrast, Koy *et al.*[95] showed that S100A8 and S100A9 influence the inflammasome in a TLR4-independent way, which is favored by a T helper cell type 1 environment. The fact that S100A8 and S100A9 enhance ROS production and that this oxidative species is an NLRP3 inflammasome activator[72, 78], leads to the assumption that S100A8 and S100A9 activate NLRP3 via ROS[93, 96].

1.5. Pharmacological targets

DCM patients have only a 5-year survival rate of 55% under current HF treatment, emphasising the need for target-specific strategies[97]. In patients with virus-negative DCMi, an immunosuppressive therapy has been shown to exert beneficial effects[11]. With respect to chronic viral myocarditis, however, no target-specific therapeutical strategies which have been investigated in large and placebo-controlled trials exist so far[97]. For the treatment of early stages of viral myocarditis, several small molecules and biologicals have been developed and screened in the last 25 years, but none of them are in routine clinical use[98]. Low molecular weight substances can prevent viral replication, including inhibiting Coxsackievirus[98]. Since besides viral aspects, particularly the immune processes play a crucial role in the pathophysiology of viral myocarditis, it is necessary to search for novel potential targets[98].

The inflammasome is associated with several inflammatory disorders, including HF[85] and myocarditis[86]. Different pharmacological agents are available counteracting inflammasome activity; 1) the drug Colchicine reduces NLRP3 activation[99]. Clinical studies have supported the application of Colchicine as a strategy to improve the outcome in patients with coronary artery disease[99] and have shown a better clinical outcome in severe myocarditis patients[100]. A further pharmacological inhibitor of the NLRP3 inflammasome showed beneficial effects in myocardial injury after ischemia-reperfusion[85]; 2) targeting caspase-1 via the inhibitor pralnacasan showed effects in rheumatoid arthritis[101]; 3) targeting IL-1β, which is downstream of the inflammasome, via the IL-1β receptor antagonist Anakinra, showed effective reduction of post-infarct inflammation and incidence of HF[102]. Additionally, inhibition of S100A8/S100A9 via icariin reduced cytokine production and showed anti-inflammatory effects[96]. Collectively, these are potential therapeutical agents that require further investigation to confirm their probable relevance in the context of (CVB3-induced) myocarditis.

2. RATIONALE

CVB3 infection induces cardiac damage via direct CVB3-mediated cardiomyocyte damage[135, 136] and results in an elevated inflammatory[103] and oxidative response[104]. The literature record shows accumulating evidence that particularly the inflammatory and oxidative arms exacerbate CVB3-induced myocarditis[103, 104]. Prevailing pharmacological treatment of myocarditis-associated cardiomyopathy targets mainly the neuroendocrine system, but does not directly influence virus-induced inflammation and oxidative stress[11]. NOD2 senses ssRNA[52] and thus CVB3 virus. Furthermore, the NLRP3 inflammasome plays an important role in CVB3 myocarditis[88], whereby a relation between NOD2 and NLRP3 has been described[72]. S100A8/A9 plays a pivotal role in cardiovascular[62, 65] and inflammatory diseases[105], and acts as an inducer of ROS production, which is an NLRP3 activator[78]. Based on these facts, we wanted 1) to confirm our previous NOD2$^{-/-}$ *in vivo* findings with further *in vitro* experiments; 2) to investigate the link between NOD2 and NLRP3 in patients, *in vivo* and *in vitro*; 3) to examine the role of S100A8 and S100A9 in a CVB3-positive patient collective, in an experimental CVB3-induced myocarditis model by utilizing S100A9$^{-/-}$ mice, and finally by *in vitro* experiments; and 4) to investigate the link between S100A8, S100A9, and NLRP3 in CVB3-infected S100A9$^{-/-}$ mice and also in *in vitro* experiments.

3. MATERIALS AND METHODS

3.1. Materials

3.1.1. Laboratory equipment

Balance	Precisa Gravimetrics, Dietikon, Switzerland
BD FACSCalibur System	BD Biosciences, Heidelberg, Germany
Centrifuge, 5415D, 5415R, 5810R	Eppendorf AG, Hamburg, Germany
Centrifuge Allegra x-15R	Beckman Coulter, Krefeld, Germany
CO_2 Incubator	Thermo Fisher Scientific, Dreieich, Germany
FACSCanto II System	Thermo Fisher Scientific, Dreieich, Germany
Freezer, -80°C	Thermo Fisher Scientific, Dreieich, Germany
Heating block	Labnet international, Edison, USA
Laboratories Flow Hood	Thermo Fisher Scientific, Dreieich, Germany
LB 940 Multimode Reader Mithras	Berthold Technologies, Bad Wildbad, Germany
Leica light microscope	Leica Microsystems, Wetzlar, Germany
Light microscope	Carl Zeiss, Berlin, Germany
MACSQuant Analyzer, MACSQuantify™ Software	Miltenyi Biotec, Bergisch Gladbach, Germany
Magnetic stirrer/heating plate	Heidolph, Schwabach, Germany
Microcentrifuge	Thermo Fisher Scientific, Dreieich, Germany
NanoDrop™ 1000	Thermo Scientific, Wilmington, USA
Odyssey® infrared imaging system	LI-COR® Biosciences GmbH, Lincoln, USA
Orbital shaker	Schmidt Laborgeräte, Vienna, Austria
pH-meter	Sartorius, Göttingen, Germany
Pipettes, adjustable	Eppendorf AG, Hamburg, Germany
PowerPac 1000	BioRad Laboratories, München, Germany
Quant Studio 6 Flex TaqMan	Life Technologies GmbH, Darmstadt, Germany
Rotating Mixer	IKA, Staufen, Germany
SpectraMax Gemini microplate reader	Molecular Devices, Biberach an der Riss, Germany
Table centrifuge	Beckman Coulter, Krefeld, Germany
Thermocycler	Eppendorf AG, Hamburg, Germany
Tank Blot chambers	BioRad Laboratories, München, Germany
ViiA 7 real-time PCR	Life Technologies GmbH, Darmstadt, Germany
Vortexer	Scientific Industries, Bohemia, USA
Water bath	GFL, Burgwedel, Germany
7900HT real-time system	Applied Biosystems, Darmstadt, Germany

3.1.2. Chemicals

Acetone	Sigma, Deisenhofen, Germany
Ammonium persulfate (APS)	Sigma, Steinheim, Germany
Ascorbic acid	Sigma, Steinheim, Germany
BD FACSFlow™	BD Biosciences, San Jose, USA
Bovine serum albumin (BSA)	Sigma, Steinheim, Germany
Bromophenol blue	Sigma, Steinheim, Germany
Cell extraction buffer	Invitrogen, Karlsruhe, Germany
Cellulose membrane	GE Healthcare Lifesciences Amersham, Freiburg, Germany
Chloroform	Merck, Darmstadt, Deutschland
Crystal Violet Solution	Sigma, Steinheim, Germany
Ethanol, 100%	Sigma, Deisenhofen, Germany
FITC antibody	Invitrogen, Karlsruhe, Germany
FITC-LPS	Sigma, Steinheim, Germany
FITC-TLR4 antibody	IMGENEX, San Diego, USA
Glycerol	Sigma, Steinheim, Germany
Glycine	AppliChem, Darmstadt, Germany
HCl 4 N	Carl Roth, Karlsruhe, Germany
HEPES sodium salt	Sigma, Steinheim, Germany
Isopropanol	Merck, Darmstadt, Germany
Methanol	Sigma, Deisenhofen, Germany
Milk powder	AppliChem, Darmstadt, Germany
Phosphatase inhibitor	Sigma, Steinheim, Germany
Polyacrylamide 30%	Carl Roth, Karlsruhe, Germany
Polyformaldehyde 35%	Carl Roth, Karlsruhe, Germany
Protease inhibitor	Sigma, Steinheim, Germany
Proteinlysis buffer	Cell Signaling, Frankfurt am Main, Germany
RAGE antibody	Millipore, Darmstadt, Germany
Sodium Dodecyl Sulfate (SDS)	Sigma, Steinheim, Germany
TEMED	BioRad Laboratories, München, Germany
Tris	AppliChem, Darmstadt, Germany
Trizol®	Invitrogen, Heidelberg, Germany
Tween® 20	Sigma, Steinheim, Germany
β-Mercaptoethanol	Sigma, Deisenhofen, Germany

TEMED=tetramethylethylenediamine

3.1.3. Kits, assays, and stimulation agents

BD Cytofix/Cytoperm® plus Fixation/Permeabilization Kit	BD Biosciences, San Jose, USA
Caspase-Glo 3/7 assay Kit	Promega, Mannheim, Germany
DeadEnd® Fluorometric TUNEL System	Promega, Mannheim, Germany
Envision	Dako, Hamburg, Germany
High Capacity cDNA Archive Kit	Applied Biosystems, Darmstadt, Germany
High Capacity cDNA Kit	Life Technologies GmbH, Darmstadt, Germany
IL-1β ELISA assay Kit	Affymatrix eBiosciences, Frankfurt am Main, Germany
MPO ELISA assay Kit	Cloud-Clone Corp., Houston, USA
NucleoSpin RNA II Kit	Macherey-Nagel, Düre, Germany
RNeasy Mini Kit	Qiagen, Hilden, Germany
S100A8/S100A8 P44 (c=0.84 mg/ml in HBS)	Thomas Vogl, Department for Immunology, University Münster, Germany
S100A9 /S100A9 P13 (c=0.83 mg/ml in HBS)	Thomas Vogl, Department for Immunology, University Münster, Germany

c=concentration; HBS=hepes buffered saline; MPO=myeloperoxidase; P=passage

3.1.4. Small interference RNA and agents

Lipofectamine® RNAiMAX	Invitrogen, Karlsruhe, Germany
NOD2 siRNA (c=20 µM)	Life Technologies GmbH, Darmstadt, Germany
Opti-MEM®	Life Technologies GmbH, Darmstadt, Germany
scr siRNA (c=50 µM)	Life Technologies GmbH, Darmstadt, Germany
S100A8 siRNA (c=20 µM)	Life Technologies GmbH, Darmstadt, Germany

c=concentration, scr=scrambled; siRNA=small interference RNA

3.1.5. Cell culture

3.1.5.1. Cell types

Cell type	Medium composition
Murine cardiac adult fibroblasts derived from LVs of C57BL/6 J male mice (Charles River, Sulzfeld, Germany)	Full DMEM high glucose 4.5 g/l
HL-1 cardiomyocytes	Full Claycomb medium
RAW macrophages 247.6	Full RPMI 1640 medium

LV=left ventricle; composition of cell appropriate full medium is further explained in paragraph 3.1.5.3.

3.1.5.2. Cell culture media and substances

Ascorbic acid	Sigma, Steinheim, Germany
Claycomb medium	Sigma, Steinheim, Germany
DMEM high glucose 4.5 g/l	Gibco, Karlsruhe, Germany
DMEM high glucose 4.5 g/l	PAA, Pasching, Austria
DMSO Cryosure	WAK-Chemie Medical, Steinbach/Ts, Germany
Fetal bovine serum (FBS)	Biochrom, Berlin, Germany
Fibronectin from bovine skin (c=1 mg/ml)	Sigma, Steinheim, Germany
Gelatin from bovine skin	Sigma, Steinheim, Germany
L-glutamine (c=200 mM)	Biochrom, Berlin, Germany
Norepinephrine	Sigma, Steinheim, Germany
Penicillin/Streptomycin (P/S)	Biochrom, Berlin, Germany
Penicillin/Streptomycin	PAA, Pasching, Austria
Phosphate-buffered saline (PBS) 1x	Biochrom, Berlin, Germany
RPMI 1640	Gibco, Karlsruhe, Germany
Trypsin/EDTA	Biochrom, Berlin, Germany

c=concentration; DMSO=dimethylsulfoxide; EDTA=ethylenediaminetetraacetate

3.1.5.3. Composition of cell culture media and substances

Full DMEM high glucose 4.5 g/l	Outgrowth medium DMEM high glucose 4.5 g/l, 20% (v/v) FBS and 1% (v/v) P/S Culture medium DMEM high glucose 4.5 g/l, 10% (v/v) FBS and 1% (v/v) P/S
Full Claycomb medium	Culture medium Claycomb medium, 10% (v/v) FBS, 1% (v/v) P/S, 1% (v/v) L-glutamine final 2 mM and 1% (v/v) norepinephrine final 0.1 mM
Ascorbic acid 30 mM	0.59 g ascorbic acid in 100 ml water Filter
Norepinephrine 10 mM	0.08 mg norepinephrine in 25 ml 30 mM ascorbic acid Filter
Gelatin 0.02%	0.1 g gelatin in 50 ml PBS microwave and subsequently dilute 1:10 in 1x PBS Filter
Gelatin/fibronectin solution	5 ml of 0.02% gelatin + 44.374 ml 1x PBS + 625 µl fibronectin final c=1 mg/80 ml
Full RPMI 1640 medium	Culture medium RPMI 1640 medium, 10% (v/v) FBS and 1% (v/v) P/S

c=concentration; FBS=fetal bovine serum; PBS=phosphate-buffered saline; P/S=penicillin/streptomycin

3.1.6. Reagents and antibodies for Western Blot

3.1.6.1. Reagents for Western Blot

Proteinlysis buffer	10% (v/v) 10x Cell Signaling lysis buffer, 1% (v/v) phosphatase inhibitor, 1% (v/v) protease inhibitor
Stock sample buffer	(0.312 M Tris-HCl, 0.346 M SDS, 50% glycerol, pH 6.8) 3.03 g Tris, 8.0 g SDS, 40 ml glycerol, titrate to pH 6.8 with HCl and add water to 80 ml
Sample buffer 4x	(0.24 M Tris-HCl, 0.24 M SDS, 40% glycerol, 20% β-Mercaptoethanol, pH 6.8, 0.008% bromophenol blue) 8 ml stock sample buffer, 2 ml β-Mercaptoethanol, 0.8 mg bromophenol blue
4x Stacking gel buffer pH 6.8	6.03 g Tris, 2 ml SDS (20%), titrate pH to 6.8 with 4N HCl and add water to 100 ml
4x Seperating gel buffer pH 8.8	18.1 g Tris, 2 ml SDS (20%), titrate pH to 8.8 with 4N HCl and add water to 100 ml
1 Stacking gel 4.5%	2.055 ml water, 0.875 ml 4x stacking gel buffer, 0.525 ml 30% Polyacrylamide, 40 µl 10% APS and 3 µl TEMED
1 Separating gel 15%	1.945 ml water, 2 ml 4x separating gel buffer, 4 ml 30% Polyacrylamide, 54 µl 10% APS and 2.7 µl TEMED
10x Electrophoresis buffer	30.2 g (0.25 M) Tris, 142.5 g (1.9 M) Glycine, 10 g (1%) SDS and add water to 1 l
1x Electrophoresis buffer	100 ml 10x electrophoresis buffer and 900 ml water
10x Transfer buffer	30.2 g (0.25 M) Tris, 142.5 g (1.9 M) Glycine and add water to 1 l
1x Transfer buffer	700 ml water, 200 ml methanol and 100 ml 10x transfer buffer
PBS-T	0.1% (v/v) Tween® 20 in 1x PBS
5% blocking buffer	5% (w/v) milk powder in 1x PBS
Antibody buffer	5% (w/v) BSA in 1x PBS-T
Chameleon protein ladder	Li-Cor Biosciences, Bad Homburg von der Höhe, Germany

APS=ammonium persulfate; BSA=bovine serum albumine; PBS=phosphate-buffered saline; PBS-T=PBS-tween; SDS=sodium dodecyl sylfate; TEMED=tetramethylethylenediamine

3.1.6.2. Antibodies for Western Blot

1st antibody caspase-1 p10 anti-mouse rabbit	1:100 in AB; Santa Cruz Biotechnologies, Heidelberg, Germany
2nd IRdye 680LT anti-rabbit	1:5000 in AB; Li-Cor Biosciences, Bad Homburg von der Höhe, Germany
1st S100A8 anti-mouse rabbit	1:250 in AB; Thomas Vogl, Department for Immunology, University Münster, Germany
2nd IRdye 680LT anti-rabbit	1:5000 in AB; Li-Cor Biosciences, Bad Homburg von der Höhe, Germany
1st S100A9 anti-mouse rabbit	1:1000 in AB; Thomas Vogl, Department for Immunology, University Münster, Germany
2nd IRdye 680LT anti-rabbit	1:5000 in AB; Li-Cor Biosciences, Bad Homburg von der Höhe, Germany
1st GAPDH anti-mouse mouse	1:1000 in AB; BPS Bioscience, San Diego, USA
2nd IRdye 800CW anti-mouse	1:5000 in AB; Li-Cor Biosciences, Bad Homburg von der Höhe, Germany

AB=antibody buffer

3.1.7. Master mix for reverse transcription

Components of High capacity (HP) cDNA kit	**Initial concentration**	**Final concentration**	**Volume (µl) *In vivo* left ventricles**	**Volume (µl) *In vivo and in vitro* spleen + cell culture**
RT buffer (HP)	10x	2x	2	2
dNTPs mix (HP)	25x	2x	0.8	0.8
Random primers (HP)	10x	2x	2	2
MultiScribe RT (HP)	50 U/µl	50 U	1	1
RNase free water			4.2	3.2
Total volume			10	9

RT=reverse transcriptase; U=units

3.1.8. Master mix for real-time PCR and primers

3.1.8.1. Master mix for real-time PCR

Components	Volume (µl) for 1 reaction with 1 µl cDNA	Volume (µl) for 1 reaction with 3 µl cDNA	Volume (µl) for 1 reaction with 2 µl cDNA
TaqMan® *Gene expression assay*			
*TaqMan Gene expression assay (20x)	0.5	0.5	
*TaqMan Gene expression master mix (2x)	5.0	5.0	
Nuclease free water	3.5	1.5	
cDNA	**1.0**	**3.0**	
Total volume	10.0	10.0	
CVB3 copy number			
Forward primer (final c=60 ng/µl)			0.5
Reverse primer (final c=60 ng/µl)			0.5
FAM-labelled MGB probe (final c=5 pM)			0.5
*TaqMan Gen expression master mix (2x)			5.0
Nuclease free water			1.5
cDNA			**2.0**
or CVB3 standard (10-10^6 copy number)			**2.0**
Total volume			10.0

c=concentration; CVB3=Coxsackievirus B3; *acquired by Life Technologies GmbH, Darmstadt, Germany; the murine CVB3 probe and primers were acquired by TIB Molbiol, Berlin, Germany; CVB3 standard was kindly provided by the IKDT (Institute for Cardiac Diagnostics and Therapy)

3.1.8.2. Primers

Human primers	Ordering number	Volume cDNA (µl)
CDKN1b	Hs0099999909_m1	1
HPRT	Hs99999909_m1	1
IL-1β	Hs00174097_m1	1
NLRP3	Hs00918082_m1	1
NOD2	Hs01550736_m1	1
S100A8	Hs00374264_g1	1
S100A9	Hs00610058_m1	1
18S	Hs99999901_s1	1
Murine primers		
ASC	Mm00445747_g1	1
α-SMA	Mm00725412_s1	1
MIP-2	Mm00436450_m1	1
CAR	Mm00438361_m1	1
CDKN1b	Mm00438167_g1	1
Col1a1	Mm01302043_g1	1
Col3a1	Mm00802331_m1	1
Dia-1 (Cyb5r3)	Mm00504077_m1	1
GAPDH	Mm99999915_g1	1
IFN-β	Mm00439546_s1	3
IL-1β	Mm00434228_m1	1
IL-6	Mm00446190_m1	1
Ly6c	Mm03009946_m1	1
Ly6g	Mm00439154_m1	1
MyD88	Mm00440338_m1	1
NLRP3	Mm00840904_m1	1
NOD2	Mm00467543_m1	1
Nox1	Mm00549170_m1	1
RAGE	Mm001134790_g1	1
S100A8	Mm00496696_g1	1
S100A9	Mm00656925_m1	1
TGF-β	Mm00441724_m1	1
Ticam-1 (TRIF)	Mm00844508_s1	1
TLR4	Mm00445274_m1	1
TNF-α	Mm00443258_m1	1

Murine CVB3 primers and standard		Volume (µl)
Forward primer (c=3.028 µg/µl)	5'-CCCTG AATGCGGCTAATCC-3'	0.5
Reverse primer (c=3.197 µg/µl)	5'-ATTGTCACCA TAAGCAGCCA-3'	0.5
FAM-labelled MGB probe (c=100 µM)	5'-FAM-TGCAGCGGAACCG-3'	0.5
CVB3 standard ($10-10^6$ copy number)		2

c=concentration; CVB3=Coxsackievirus B3; all reporter assays were acquired by Life Technologies GmbH, Darmstadt, Germany

3.1.9. Fluorescence activated cell sorting antibodies and reagents

CM-H_2DCF-DA	Invitrogen, Heidelberg, Germany
FAM-YVAD anti-mouse caspase-1 inhibitor	Immunochemistry technologies/Biomol, Hamburg, Germany
PE anti-mouse ASC (TMS-1)	BioLegend, Fell, Germany
PE anti-mouse IL-1β pro-form	eBioscience, San Diego, USA
PerCP anti-mouse IL-1β/IL-1F2	R&D Systems, Wiesbaden-Nordenstadt, Germany

3.1.10. Software

BDB FACSDiva Software version 6.1.3	BD Biosciences, San Jose, USA
FlowJo 8.7. software	Tree Star, Ashland, USA
GraphPad Prism 5.0 software	GraphPad Software, La Jolla, USA
LI-COR Image Studio™ Lite	Li-Cor Biosciences, Bad Homburg von der Höhe, Germany
Lucia software	Nikon, Düsseldorf, Germany

3.2. Methods

3.2.1. Patients

3.2.1.1. Patient characteristics

The patient groups for the NOD2 and alarmin studies comprised; 1) patients with an EMB-proven cardiac infection of CVB3 including for the NOD2 study, patients presented with an acute myocarditis (AMC), a chronic DCMi and DCM, and for the alarmin study: patients presented with AMC and a chronic DCMi; 2) CVB3-positive patients who eliminated cardiac CVB3 over time, proven by follow-up EMBs; 3) patients with a CVB3-negative AMC, only for the NOD2 study; 4) CVB3-negative DCM; and 5) controls. Patients served as controls where a cardiac cause for exercise limitation and/or chest complaints could be excluded after several investigations including regular findings in their EMBs. Coronary artery disease was angiographically excluded in all patients. All diagnostic procedures and evaluation were obtained by using standardized protocols[106]. All patients provided written consent for the procedures.

3.2.1.2. Clinical definition of disease entities

Cardiac inflammation was defined according to the ESC recommendations[107, 108], including the evidence of infiltrating lymphocytes (CD3) > 7.0 cells/mm^2 (median cell count), macrophages > 35.0 cells/mm^2 (median cell count), and/or detection of viral genomes, and/or positive/negative Dallas criteria in the EMB analysings. Patients with AMC clinically presented with acute onset angina, ST-segment elevation, elevated creatine kinase or Troponin T, or sudden onset of HF or arrhythmias mimicking acute myocardial infarction. Predominantly focal inflammatory cell infiltrates were confirmed histologically and/or immunohistologically. In the DCMi group, biopsy analyses confirmed infiltrates of lymphocytes or macrophages in patients with a DCM phenotype. DCM patients presented symptoms of HF, left ventricular enlargement and global wall motion abnormalities of unknown origin with a documented reduced systolic left ventricular ejection fraction (EF) below 45% without any history or clinical signs of myocarditis or myocardial inflammation in EMB. In the controls, EMB failed to elucidate any specific reason for cardiac complaints such as atypical angina, unspecific exercise intolerance or palpitations.

3.2.1.3. Endomyocardial biopsy

After routine non-invasive diagnostic work-up and angiography had failed to elucidate any specific cause of HF, all patients underwent EMB and right heart catheterization in a standardized manner, as previously described. All invasive cardiac procedures were performed after written informed patient consent. A minimum of eight EMBs were obtained from the right side of the ventricular septum with a flexible bioptome (Westmed, Germany). One specimen was fixed in 5% buffered formalin and embedded in paraffin for histologic evaluation while immunohistochemical analyses (1 EMB) were carried out in TissueTec© embedded frozen specimens[109, 110]. Inflammatory cells, including lymphocytes (CD3), macrophages (Mac-1) and cellular adhesion molecules (HLA-1, CD54) were counted by quantitative digital imaging analysis as reported elsewhere[111]. The remaining biopsy specimens were immediately frozen in liquid nitrogen and used for the evaluation of RNA or DNA viruses by nested polymerase chain reaction (nPCR), separately. PCR and reverse transcription PCR (RT-PCR) were performed as previously published[3].

3.2.2. *In vivo* studies

3.2.2.1. NOD2 knockdown mice

$NOD2^{-/-}$ "knockdown" ($^{-/-}$) mice and wild-type (WT) (C57BL/6) mice were provided by the Department of Microbiology and Hygiene, Charité – Universitätsmedizin Berlin (Berlin, Germany)[112]. Male $NOD2^{-/-}$ mice were generated on a genetic background of C57BL/6. The experimental groups included control WT, $NOD2^{-/-}$, WT CVB3, and $NOD2^{-/-}$ CVB3 (n=6 for WT and $NOD2^{-/-}$ and n=9 for WT CVB3 and $NOD2^{-/-}$ CVB3). Six week old WT mice (WT CVB3) and $NOD2^{-/-}$ mice ($NOD2^{-/-}$ CVB3) were randomly divided into test and control groups. Test animals were infected with 5×10^5 plaque forming units (p.f.u.) of CVB3 ("Nancy strain") via intraperitoneal (i.p.) injection at day 0. An identical volume of saline (0.2 ml) was injected into control animals instead of CVB3. Experiments followed the guidelines of the U.S. National Institute of Health, USA, "Guide for the Care and Use of Laboratory Animals", published by the U.S. National Institutes of Health (NIH Publication no. 85-23 revised, 1985) and were approved by the local ethics committee (Landesamt für Gesundheit und Soziales, Tierschutz, Berlin).

3.2.2.2. S100A9 knockout mice

S100A9$^{-/-}$ "knockout" ($^{-/-}$) mice were generated by disrupting the S100A9 gene. Specifically, a targeting vector was constructed by replacing 760 bp of the genomic sequence, containing exon 2 and the adjacent intron region. This mutation led to a deletion of the start codon. Subsequently, the construct was electroporated into embryonic stem cells (ES) line E14-1-1 derived from 129/Ola mice. Resistant colonies were isolated and expanded. Into blastocysts of C57BL/6 mice, four independent ES were microinjected and chimeras were bred against the background of the host blastocyst. Mice which were heterozygous for the S100A9 mutation were interbred and the offspring were genotyped by PCR[113]. Manitz *et al.*[113] demonstrated that these animals are also deficient for S100A8 on the protein level and thus represent a functional double$^{-/-}$ mouse model due to the lack of the binding partner S100A9. The experimental groups included control WT, S100A9$^{-/-}$, WT CVB3, and S100A9$^{-/-}$ CVB3 (n=7 for WT and WT CVB3, n=8 for S100A9$^{-/-}$, and n=10 for S100A9$^{-/-}$ CVB3). Six weeks old WT mice (WT CVB3) and S100A9$^{-/-}$ mice (S100A9$^{-/-}$ CVB3) were randomly divided into test and control groups as in 3.2.2.1 with test animals receiving CVB3, while controls received PBS. A subgroup of S100A9$^{-/-}$ CVB3 mice was additionally treated by i.p. injections of 100 µg S100A8 every two days (300 µg in total). The experiments followed the guidelines of the European legislation (Directive 2010/63/EU) and were approved by the local ethics committee (Landesamt für Gesundheit und Soziales, Tierschutz, Berlin).

3.2.3. Hemodynamic measurements and surgical procedures

Seven days after infection, mice were anesthetized (0.8–1.2 g/kg urethane and 0.05 mg/kg buprenorphine i.p.), intubated and mechanically ventilated. The hemodynamical function of the heart was measured by a 1.2 French-microconductance pressure catheter (Transonic Scisense Inc., London, Canada) in closed-chest animals as described previously[114]. Global heart function was expressed by heart rate (HR; bpm), ejection fraction (EF; %), cardiac output (CO; µl/min), LV end-systolic volume (LVESV; µl) and LV end-diastolic volume (LVEDV; µl), stroke volume (SV; µl), stroke work (SW; mmHg/ml). Parameters of systolic heart function were maximum LV pressure (LVP_{max}; mmHg) and maximal LV pressure rise rate ($dP/dt_{max;}$ mmHg/s). End-diastolic LV pressure (LVEDP; mmHg), minimum LV pressure decay rate (dP/dt_{min}; mmHg/s), Tau (τ, ms), and pressure half time (PHT; ms) exhibited the

diastolic function. Thereafter, all mice were sacrificed. The hearts and spleens were removed and quickly frozen in liquid nitrogen and stored at -80°C for later molecular and immunohistochemical examinations. Serum was stored at -80°C for later molecular examination.

3.2.4. Cell culture experiments

3.2.4.1. Murine primary cardiac fibroblasts

Murine primary cardiac fibroblasts obtained by outgrowth from LV pieces of 12-week-old mice were cultured for two weeks in outgrowth medium, consisting of DMEM (PAA, Pasching, Austria) containing 20% FBS (Biochrom, Berlin, Germany) and 1% penicillin/streptomycin (PAA, Pasching, Austria) in 12-well plates (passage 0). Subsequently, medium was refreshed every 3rd day. Four weeks after the initial placement of the biopsies into 12-well plates, the outgrown fibroblasts were washed 1x with PBS and were detached with 2-times concentrated Trypsin/EDTA (Biochrom, Berlin, Germany) solution. Three minutes later, the reaction was stopped by adding outgrowth medium, and the fibroblasts were transferred into a T75 flask (passage 0) and were cultured further in the outgrowth medium. After reaching confluency of 90%, cells were further passaged as described, or cells from a confluent T75 flask were frozen in 10% DMSO in full medium in a cryovial and stored in liquid nitrogen. For stimulation experiments, fibroblasts were seeded in full DMEM (Gibco, Karlsruhe, Germany) medium, containing 10% FBS and 1% penicillin/streptomycin (Biochrom, Berlin, Germany), into 6-well plates at a cell density of 250,000 cells/well. For knockdown experiments, fibroblasts were also seeded in full DMEM medium into 6-well plates at a cell density of 150,000 cells/well.

3.2.4.2. HL-1 cardiomyocytes

The murine cardiomyocyte cell line HL-1 was cultured in full Claycomb medium consisting of Claycomb medium (Sigma-Aldrich Chemie, Steinheim, Germany) supplemented with 10% FBS, 1% penicillin/streptomycin, 0.1 mM norepinephrine (Sigma-Aldrich Chemie GmbH, Steinheim, Germany) and 2 mM L-glutamine (Biochrom, Berlin, Germany). For stimulation experiments, HL-1 cells were seeded in full Claycomb medium in 6-well plates at a cell density of 270,000 cells/well. For knockdown experiments, cells were also plated in full Claycomb medium into 6-well plates at a density of 200,000 cells/well and in 96-well plates at a cell density of 7,500 cells/well.

3.2.4.3. RAW macrophages

RAW macrophages were cultured in RPMI 1640 full medium consisting of RPMI 1640 medium (Gibco, Karlsruhe, Germany) supplemented with 10% FBS and 1% penicillin/streptomycin. For stimulation experiments, RAW cells were seeded in full RPMI 1640 medium into 6-well plates at a cell density of 600,000 cells/well. For knockdown experiments, RAW cells were plated also in full RPMI 1640 medium into 6-well plates at a cell density of 500,000 cells/well.

3.2.5. NOD2 and S100A8 siRNA transfection in 6-well plates

To determine the knockdown efficiency of NOD2 and S100A8 siRNA in HL-1 cells and of S100A8 siRNA in cardiac fibroblasts, a preliminary comparison of 5, 10, 15 nM of NOD2 and of 1, 2.5, 5 nM of S100A8 was performed versus scr siRNA in HL-1 cells, whereas in fibroblasts, a comparison of 5 and 15 nM of S100A8 siRNA versus scr siRNA was performed **(Figure 3.2.5.)**. In preliminary experiments, we found that HL-1 cells, RAW macrophages, and cardiac fibroblasts do not express S100A9. In brief, the transfection procedure, which was first tested for HL-1 cells and cardiac fibroblasts, was performed as follows. Twenty-four hours prior to transfection, HL-1 cells were plated into gelatin/fibronectin (Sigma-Aldrich Chemie GmbH, Steinheim, Germany) pre-coated 6-well plates at a density of 200,000

cells/well. Also fibroblasts were seeded into 6-well plates in full DMEM medium, which contained 150,000 cells/well. In order to achieve the above described final siRNA concentrations, 3 µl of a siRNA/Opti-MEM® pre-dilution, which contained siRNA concentrations described in Table 3.2.5. (made of respective stock solutions; NOD2 and S100A8 siRNA stock solution c=20 µM; scr siRNA stock solution c=50 µM; all siRNAs were acquired from Life Technologies GmbH, Darmstadt, Germany) were added to 247 µl reduced serum medium Opti-MEM® (Life Technologies GmbH, Darmstadt, Germany). Simultaneously, 5 µl of Lipofectamine RNAiMAX reagent (Invitrogen, Karlsruhe, Germany) was diluted in 245 µl Opti-MEM®. The siRNA/Opti-MEM® and Lipofectamine/Opti-MEM® solutions were combined in a total volume of 500 µl and were incubated for 20 minutes. Meanwhile, cells were washed 2x with PBS, then 1.5 ml/well of Claycomb medium supplemented with 0.1 mM norepinephrine and 2 mM L-glutamine was added to HL-1 cells and the same volume of supplement-free DMEM medium was added to fibroblasts. After the incubation time, 500 µl of the siRNA/Lipofectamine solution was pipetted into each well. Four hours later, the transfection/medium solution was replaced by full Claycomb or full DMEM medium for HL-1 cells and fibroblasts, respectively. Twenty-four hours later, RNA was isolated using the RNeasy Mini Kit as described later **(paragraph 3.2.9)**.

For the subsequent transfection and infection experiments, a final concentration of 5 nM for NOD2, S100A8 and scr siRNA was used in HL-1 cells and fibroblasts, at a cell density of 200,000 or 150,000 cells per well in 6-well plates, respectively. RAW cells were transfected with 15 nM scr and S100A8 siRNA at a cell density of 500,000 cells/well in 6-well plates according to the same transfection procedure as described for HL-1 cells and fibroblasts. Cells transfected and infected in 6-well plates, were lysed in TRIzol® for RNA isolation. An overview of the different concentrations of siRNA, and of the corresponding target genes for each cell type is given in **Table 3.2.5**.

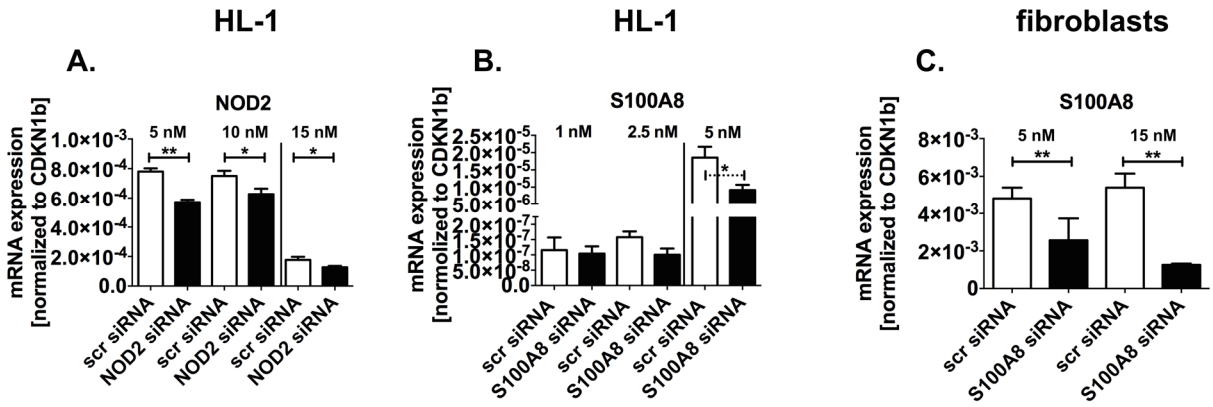

Figure 3.2.5. NOD2 and S100A8 knockdown efficacy in HL-1 cells or cardiac fibroblasts. A. Comparison of the NOD2 knockdown efficiency in HL-1 cells with 5, 10, and 15 nM scr or NOD2 siRNA, expressed as mRNA levels. The line indicates that the experiments with 5 and 10 nM were performed in a seperate experiment compared to those with 15 nM scr and NOD2 siRNA. **B.** Comparison of the S100A8 knockdown efficiency in HL-1 cells with 1, 2.5, or 5 nM scr or S100A8 siRNA, expressed as mRNA levels. The line indicates that the experiments with 1 and 2.5 nM were performed in a seperate experiment compared to those with 5 nM scr and S100A8 siRNA. **C.** Comparison of the S100A8 knockdown efficacy in murine cardiac fibroblasts with 5 and 15 nM scr or S100A8 siRNA, expressed as mRNA levels. Bar graphs represent the mean of ± SEM with n=5-6/group, with *p<0.05 and **p<0.0005. An unpaired t-test was used. NOD2=nucleotide binding oligomerization domain; siRNA=small interference RNA; scr=scrambled.

Table 3.2.5. Overview of different siRNA concentrations for knockdown in 6-well plates

	NOD2 or scr siRNA		**S100A8 or scr siRNA**	
	Final c in V=2 ml (nM)	**c in V=3 µl Opti-MEM®** (µM)	**Final c in V=2 ml** (nM)	**c in V=3 µl Opti-MEM®** (µM)
HL-1 cells	5	3.3	1	0.6
	10	6.6	2.5	1.6
	15	10	5	3.3
Cardiac fibroblasts			5	3.3
			15	10
RAW macrophages			15	10

c=concentration; V=volume

3.2.6. NOD2 and S100A8 siRNA transfection in 96-well plates

To obtain a final concentration of 5 nM per well of scr, NOD2 or S100A8 siRNA, 0.18 µl of previously diluted siRNA stock solutions (in respect to stock solutions, see paragraph 3.2.5.) was added to 9.82 µl reduced serum medium Opti-MEM® **(Table 3.2.6.)**. Additionally, 0.2 µl of Lipofectamine RNAiMAX reagent was diluted in 9.8 µl Opti-MEM®. The siRNA/Opti-MEM® and Lipofectamine/Opti-MEM® solutions were combined in a total volume of 20 µl and were incubated for 20 minutes. Meanwhile, HL-1 cells were washed 2x with PBS and 100 µl Claycomb medium supplemented with 0.1 mM norepinephrine and 2 mM L-glutamine was added per well. After the incubation time, 20 µl of the siRNA/Lipofectamine solution was pipetted into each well. Four hours later, medium was replaced by full Claycomb medium and HL-1 cells were incubated for a further 24 hours, followed by CVB3 infection for 24 hours and a final FITC-LPS or a caspase 3/7 activity assay. Cells, 6 and 8 hours post infection were used for FITC-RAGE or FITC-TLR4 assays, respectively.

Table 3.2.6. Overview of different siRNA concentrations for knockdown in 96-well plates

	NOD2 or scr siRNA		**S100A8 or scr siRNA**	
	Final c in V=120 µl (nM)	**c in V=0.18 µl Opti-MEM®** (µM)	**Final c in V=120 µl** (nM)	**c in V=0.18 µl Opti-MEM®** (µM)
HL-1 cells	5	3.3	5	3.3

c=concentration; V=volume

3.2.7. Stimulation with S100A8 and S100A9 proteins

To asses the impact of S100A8 and S100A9 homodimers on CVB3-infected HL-1 cells, cardiac fibroblasts, and RAW cells, the respective cells were plated into 6-well plates as previously described. Twenty-four hours later, HL-1 cells, cardiac fibroblasts and RAW macrophages designated for RNA isolation were infected with CVB3 at an MOI of 2 for 1 hour in starved DMEM medium supplemented with 0.01% FBS and 5 mM D-glucose, whereas HL-1 cells for flow cytometric measurements were infected at an MOI of 4. Subsequently, cells were stimulated with S100A8 and S100A9 in the cell appropriate full medium at a final concentration of 5 µg/ml 1 hour post-infection. Twenty-four hours later, the 2 MOI-infected HL-1 cells, RAW macrophages and fibroblasts were lysed in TRIzol® for RNA

isolation, whereas the 4 MOI-infected HL-1 cells were submitted to flow cytometric analysis 4 hours post infection and stimulation. It should be noted that S100A8/S100A9 heterodimers were not used for stimulation experiments, due to the lack of function observed in the case of murine *in vitro* experiments (Vogl T., data not published).

3.2.8. Coxsackievirus B3 infection

Overall, for the CVB3 ("Nancy strain") infection, the 6- or 96-well plated cells were washed 2x with PBS. For the stimulation experiments, infection occurred 24 hours after cell plating and in case of transfection experiments cells were infected 48 hours post plating, at an MOI of 2 for 14 or 24 hours and at an MOI of 4 for 4, 6 or 8 hours in starved DMEM supplemented with 0.01% FBS and 5 mM D-glucose. In general, one hour after the addition of the CVB3 virus, cells were washed 2x with PBS and cultured depending on the experiment for the times described above in cell appropriate full medium. Un-infected control cells did not receive CVB3. Finally, cells in 6-well plates were subjected to flow cytometry analysis or were lysed in TRIzol® for RNA isolation. Cells plated in 96-well plates were used for a caspase 3/7 activity assay, FITC-LPS, FITC -TLR4 or FITC-RAGE assays.

3.2.9. RNA isolation

Left ventricular tissues and spleens were homogenized in TRIzol® reagent (Invitrogen, Heidelberg, Germany) and were homogenized with a motorized pellet pestle or homogenizer, respectively. The specimens were then incubated for 10 minutes in a thermomixer. For RNA extraction, chloroform was added, followed by a mixing and centrifugation step for 15 minutes at 4°C with 12,000 g. The upper aqueous phase containing RNA was carefully transferred without disturbing the interphase into a fresh tube, and precipitated using isopropanol. The samples were incubated at room temperature (RT) for 10 minutes and were centrifugated for 15 minutes at 4°C with an acceleration of 12,000 g. The RNA pellets were diluted in 100 µl RNAse-free water. Similarly, cells from cell cultures were lysed with TRIzol® reagent. To extract the RNA, chloroform was added, mixed, incubated at RT and centrifuged at 4°C. The aqueous phase containing the RNA was transferred to a separate tube and isopropanol was added. For precipitation, the RNA solution was centrifuged 10 minutes at

4°C at 14,000 rpm. The RNA pellets were washed with 70% ethanol followed by diluting the pellet in 100 µl RNAse-free water. The dissolved LV, splenic and cell culture RNA pellets were all then further purified using the RNeasy Mini Kit (Qiagen, Hilden, Germany) or the NucleoSpin® RNA mini kit (Macherey-Nagel GmbH, Düren, Germany) according to the manufacturer's protocols. The yield of purified total RNA was determined by measuring the UV absorbance at 260 nm on the Nanodrop ND1000 spectrophotometer. From EMBs, total RNA was isolated with TRIzol® as previously described[115].

3.2.10. cDNA synthesis

One µg of murine LV RNA was reverse transcribed into cDNA in a final reaction mix of 20 µl using the High-Capacity cDNA Archive Kit (Applied Biosystems, Darmstadt, Germany). Therefore, the appropriate amount of RNA was brought to 10 µl with nuclease-free water and was denaturated at 70°C, followed by addition of the master mix in a 1:2 ratio, containing 2 µl random primers, 0.8 µl of dNTP mix, 2 µl of buffer, 1 µl of reverse transcriptase and 4.2 µl of RNase free water **(paragraph 3.1.7.)**. After running the reverse transcription program (10 minutes at 25°C, 2 hours at 37°C and 5 minutes at 85°C) in the Thermocycler (Eppendorf AG, Hamburg, Germany), the cDNA obtained from the NOD2$^{-/-}$ and S100A9$^{-/-}$ CVB3+S100A8 *in vivo* studies was further diluted to a final concentration of 10 ng/µl cDNA, whereas the cDNA of the S100A9$^{-/-}$ CVB3 *in vivo* study was diluted to a final concentration of 5 ng/µl. One µg each of splenic, HL-1 cell, cardiac fibroblast, and RAW cell RNAs were reverse transcribed into cDNA in a final reaction mix of 20 µl using the High Capacity cDNA Kit (Life Technologies, Darmstadt, Germany). For this purpose, the appropriate amount of RNA was brought to 11 µl with nuclease-free water. Additionally, 2.8 µl of the random primers and dNTPs mix at the same ratio as mentioned above, was added to the RNA, followed by a denaturation step at 70°C for 5 minutes. Furthermore, 6.2 µl of a mix of reverse transcriptase, buffer and water (2 µl of 10x buffer, 1 µl of reverse transcriptase and 3.2 µl of RNase free water) was added to the samples **(paragraph 3.1.7)**. After running the reverse transcription program, the cDNA was further diluted to a final concentration of 20 ng/µl cDNA for HL-1 cells, cardiac fibroblasts, RAW cells, or splenic tissue.

Due to amounts of EMB cDNA being limited, a pre-amplification technique was used together with the High-Capacity cDNA Archive Kit (Life Technologies GmbH, Darmstadt, Germany). For the pre-amplification of each designated gene, 6.25 µl cDNA, 6.25 µl TaqMan® Gene

Expression Assay and 12.5 µl TaqMan® Pre-Amp Master Mix (Life Technologies GmbH, Darmstadt, Germany) was used as previously described[115].

3.2.11. Gene expression analysis

To assess the relative mRNA expression of the target genes in human biopsies, as well as from *in vivo* and *in vitro* experiments, real-time PCR was performed on a Viia7 system (Life Technologies GmbH, Darmstadt, Germany), a Quant Studio 6 Flex TaqMan system (Life Technologies GmbH, Darmstadt, Germany) or a 7900HT real-time system (Applied Biosystems, Darmstadt, Germany). A gene expression assay from Life Technologies was used with all systems. Therefore, 5 µl of the gene expression master mix (comprised of TaqMan DNA polymerase, dNTPs and buffer; Life Technologies GmbH, Darmstadt, Germany) and 0.5 µl of the gene expression assay (which includes forward and reverse primers as well as the fluorescently 5' 6'FAM-labelled probe, with the 3' non-fluorescent Quencher NFQ-MGB) from Life Technologies and 1, 2 or 3 µl (depending on the gene and the material origin) of cDNA in a final volume of 10 µl. The real-time PCR program started with 2 minutes at 50°C and an initial denaturating step for 10 minutes at 95°C, followed by a denaturating step for 15 seconds at 95°C and then an annealing and elongation step for 1 minutes at 60°C. The last two steps (15 seconds at 95°C and 1 minutes at 60°C) were repeated 40, 45 or 60 times, depending on the gene and the origin of the material. In all cases, quantification of a housekeeping gene such as 18S, CDKN1b, HPRT or GAPDH was performed for each sample as an internal endogenous control. Data were normalized to 18S, CDKN1b, HPRT or GAPDH mRNA levels and are expressed using the formula $2^{-\Delta Ct}$. CVB3 copy numbers were detected using the forward primer (5'-CCCTG AATGCGGCTAATCC-3') and the reverse primer (5'-ATTGTCACCA TAAGCAGCCA-3') at a final concentration of 60 ng/µl and the FAM-labelled MGB probe (5'-FAM-TGCAGC GGAACCG-3') was used at a final concentration of 5 pM. The CVB3 copy numbers in murine LVs of the $S100A9^{-/-}$ CVB3 *in vivo* study were determined per 10 ng cDNA, in the $NOD2^{-/-}$ and $S100A9^{-/-}$ CVB3+S100A8 *in vivo* studies per 20 ng cDNA, and in murine spleens and HL-1 cells per 40 ng cDNA.

3.2.12. Left ventricle protein isolation

Murine LVs were homogenized in protein lysis buffer supplemented with protease and phosphatase inhibitors (Cell Signaling, Frankfurt am Main, Germany; Sigma-Aldrich Chemie GmbH, Steinheim, Germany, respectively) with a motorized pellet pestle, followed by incubation in a thermomixer at 4°C for 10 minutes. Subsequently, samples were centrifuged for 30 minutes at 4°C with 16,000 g acceleration. The supernatants were transferred into a fresh eppendorf tube and frozen at -80°C.

3.2.13. Bicinchoninic acid-protein assay

To determine the total protein yield after protein isolation from LV tissue, the colorimetric bicinchoninic acid (BCA)-protein assay from Thermo Fisher Scientific (Dreieich, Germany) was used. In this method, Cu^{2+} ions are reduced through the proteins, and the reaction is especially influenced by cysteine, tyrosine and tryptophane amino acid residues. Subsequently, two BCA molecules form a purple coloured complex with one Cu^{+} ion. The amount of the reduction is proportional to the protein amount. For all samples, the proteins were diluted directly in a microtiter 96-well plate with PBS at a ratio of 1:5 in a final volume of 10 µl. Additionally, 190 µl of BCA-solution per well (containing 1x solution B and 50x solution A) was added. Bovine serum albumin (BSA) served to generate a standard curve, whereby BSA was diluted in PBS, starting at 2000 µg/ml continuing with 1500 and 1000 µg/ml and followed by 1:2 dilution steps until a concentration of 62.5 µg/ml was reached. Ten microliters of each standard was applied per well followed by the addition of 190 µl of BCA-solution. The plate was incubated 30 minutes at 37°C and then measured at a wavelength of 562 nm in a SpectraMax 340PC384 plate reader (Molecular Devices, Biberach an der Riss, Germany). The protein content was calculated by utilizing the standard curve to interpolate from the absorbance values measured.

3.2.14. Western Blot

To determine the protein expression of certain proteins of *in vivo* LV homogenates, the samples were separated via a denaturating sodium dodecyl sulphate polyacrylamide gel electrophoresis (SDS-PAGE). The SDS-PAGE consists of two different gels with different pore size and ionic strength using a stacking gel with a pH-value of 6.8 with 4.5% acrylamide together with a separating gel with a pH-value of 8.8 with 15% acrylamide. This method offers the opportunity to separate proteins depending on their molecular weight, whereby the proteins migrate in an electrical field and form specific bands, regardless of their loading properties and their tertiary structures. Subsequently, the protein bands were transferred onto a nitrocellulose membrane using the tank-blot method. The cell lysates were dissolved in PBS and were supplemented with an SDS-containing sample buffer at a ratio of 1:4 followed by a denaturating step at 95°C for 5 minutes. Thus, the proteins were negatively and equally loaded, via SDS intercalations. Twenty-two microliters per slot of each sample containing 65 µg total protein, was applied on the stacking gel. The negatively charged proteins were allowed to migrate towards the positive anode at 180 V for 1 hour. Additionally, on each gel a protein marker with defined molecular weights was applied. Subsequently, the separated proteins were transferred onto a nitrocellulose membrane by using the tank-blot technique at 350 mA for 1 hour and 20 minutes. Afterwards, the membranes were blocked with a 5% milk powder solution for 1 hour to avoid nonspecific antibody interactions and were washed 1x with PBS-T. The membranes were then incubated with a primary antibody, which was diluted at an appropriate ratio in an antibody buffer **(paragraph 3.1.6.2.)** overnight at 4°C. The next day, the membranes were washed 4x for 5 minutes each with PBS-T to remove the remaining antibody and were incubated with a near infrared (NIR) fluorescent dye conjugated secondary antibody **(paragraph 3.1.6.2.)** for 45 minutes in the dark at RT. Afterwards, membranes were washed 4x for 5 minutes with PBS-T, and 1x with PBS, and were dried for 30 minutes in the dark. The specific proteins were visualized using the Odyssey® infrared imaging system from LI-COR® Biosciences. The LI-COR Image Studio™ Lite (Li-Cor Biosciences, Bad Homburg von der Höhe, Germany) was used for the quantification of band intensities and the values were then normalized to the GAPDH expression.

3.2.15. Enzyme-linked immunosorbant assay

The enzyme-linked immunosorbant assay (ELISA) is a plate-based assay technique, in which peptides and proteins can be detected and quantified due to the highly specific antibody-antigen interaction. Therefore, a specific antibody is immobilized on the solid surface of a 96-well microtiter plate, to which the appropriate antigen binds. In the next steps, a biotin-conjugated detection antibody binds the antigen and an avidin or streptavidin horseradish peroxidase (HRP) conjugate reacts covalently with the biotin. Between each step, the microtiter plate is subjected to washing steps, to remove unbound material. Finally, through addition of a substrate, such as tetramethylbenzidine (TMB), HRP oxidizes the chromogenic substrate, which results in a blue coloured product. After stopping the reaction with an acid solution, the plate can be read at 450 nm. In order to detect target proteins in murine LV homogenates or sera, two different ELISA assays have been used: one ELISA for the myeloperoxidase (MPO) activity and one for IL-1β.

3.2.16. Enzyme-linked immunosorbant assay of myeloperoxidase activity on left ventricles

MPO protein levels in LVs were analyzed by applying a total protein amount of 2.5 µg per 100 µl PBS to each microtiter well of the tissue homogenate specific ELISA kit of Cloud-Clone Corp., (Houston, USA). The standards were diluted in the standard diluent supplied. The standard curve range was made using 1:2 dilution steps from 5000 pg/ml - 78 pg/ml. To enable the binding of the designated protein to the immobilized antibody, the plate was incubated for 2 hours at 37°C. Afterwards, the fluid was flicked out of the well, without a further washing step. In order to detect the specifically bound antigen, 100 µl of biotinylated antibody “Detection-Reagent A” was added to each well, followed by an incubation for 1 hour at 37°C. To remove all unbound Detection-Reagent A, the plate was washed 3x with a 1x wash solution. Subsequently, 100 µl of avidin-conjugated HRP was pipetted into the wells. After thirty minutes of incubation at 37°C in the dark, the microtiter plate was washed 5x with the 1x wash solution, followed by the addition of 90 µl TMB substrate. The reaction was stopped after 10-15 minutes. The absorbance was immediately measured at 450 nm in a SpectraMax 340PC384 plate reader.

3.2.17. Enzyme-linked immunosorbant assay of IL-1β on murine serum

To detect IL-1β in sera, the instant ELISA assay from Affymatrix eBiosciences (Frankfurt am Main, Germany) was used. Microtiter wells provided in strips were activated with 100 µl distilled water, followed by the addition of 50 µl undiluted sera samples. The standards and blanks were already in the microwell strips, present as lyophilisates in the range of 250 pg/ml – 3.9 pg/ml at a 1:2 dilution ratio. Standard and blank wells each received 180 µl distilled water. After 3 hours of incubation at RT, the wells were emptied and were washed 6x with 400 µl of 1x concentrated wash buffer. Due to the fact that all wells already contained the biotin-conjugated detection antibody as well as the streptavidin-conjugated HRP, the next step was the addition of 100 µl TMB substrate. After an incubation time of 30 minutes at RT, the reaction was stopped by adding 100 µl of 1 M phosphoric acid and read in the plate reader.

3.2.18. Caspase 3/7 activity assay

Prior to the application of the caspase-Glo 3/7 assay kit (Promega, Mannheim, Germany) HL-1 cells were plated in a fibronectin/gelatin coated 96-well plate for transfection experiments as described previously, and were incubated for 24 hours. HL-1 cells were transfected with 5 nM of scr siRNA or NOD2 siRNA and infected 24 hours later with CVB3 at an MOI of 2 for 24 hours. Finally, 100 µl of the caspase-Glo 3/7 reagent was added per well, at a 1:2 ratio of medium versus caspase-Glo 3/7 reagent. The plate was incubated in the dark at RT. The luminescence, expressed as relative light units (RLU), was measured after 1, 2 and 3 hours of incubation, on a Berthold Mithras LB 940 reader (Berthold Technologies, Bad Wildbad, Germany). Caspase 3/7 activity was normalized to the cell amount. Therefore, crystal violet (Sigma-Aldrich Chemie GmbH, Steinheim, Germany) staining was performed. Subsequently, the optical density (OD), which increases linearly with the cell amount, was measured at a wavelength of 595 nm in a Spectramax reader. Data are expressed as the ratio of caspase 3/7 activity (RLU) to the respective cell number calculated.

3.2.19. FITC-Lipopolysaccharide assay

To evaluate the impact of NOD2 knockdown on TLR4 receptor expression, FITC-LPS (Sigma-Aldrich Chemie GmbH, Steinheim, Germany) was applied on NOD2 siRNA and scr siRNA transfected HL-1 cells, 24 hours post CVB3 infection. Overall, the FITC-LPS binding to TLR4 was determined by measuring the fluorescence at excitation and emission wavelengths of 485 nm and 530 nm. FITC-LPS was then normalized to the cell amount as determined by crystal violet staining. Subsequently, the OD was measured at a wavelength of 595 nm in a Spectramax plate reader. Data are expressed as the ratio of fluorescence to the respective cell number calculated.

3.2.20. FITC-TLR4 and FITC-RAGE assay

To evaluate the impact of S100A8 knockdown on TLR4 and RAGE receptor expression, FITC-TLR4 (IMGENEX, San Diego, USA) or FITC-RAGE (FITC: Invitrogen, Karlsruhe, Germany and RAGE: Millipore, Darmstadt, Germany) were applied on S100A8 siRNA and scr siRNA transfected HL-1 cells, 8 or 6 hours post CVB3 infection, respectively. Overall, the FITC-TLR4 (final concentration 5 µg/ml) and FITC-RAGE (final concentration FITC 5 µg/ml and RAGE 1 µg/ml) binding to TLR4 or RAGE was determined by measuring the fluorescence at excitation and emission wavelengths of 485 nm and 530 nm. FITC-TLR4 and FITC-RAGE was next normalized to the calculated cell amount determined with crystal violet staining. Subsequently, the OD was measured at a wavelength of 595 nm in a Spectramax plate reader. Data are expressed as the ratio of fluorescence to the respective cell number calculated.

3.2.21. Crystal violet staining

To normalize the caspase 3/7 activity assay, FITC-LPS or FITC-TLR4, and FITC-RAGE assay values to the cell amount, duplicate 96-well plates were plated, transfected and infected, and then subjected to crystal violet staining rather than the activity assay. The crystal violet method represents a rapid technique to determine the cell amount in monolayer cultures. The supernatant was removed and 100 µl of 4% paraformaldehyde was added to

the wells overnight at 4°C to enable cell fixation and permeabilization. Afterwards, the plate was washed 1x with distilled water and 100 µl of staining solution (crystal violet diluted 1:10 in distilled water) was added and allowed to incubate for 30 minutes in each well at RT to stain the cell nuclei. The unbound material was removed by washing the plate 3x with distilled water. Quantification was enabled by solubilizing the bound crystal violet into 100 µl of 1% SDS after an incubation time of 1 hour. Subsequently, the OD was measured at a wavelength of 595 nm in a Spectramax plate reader and used to calculate the cell amount.

3.2.22. Fluorescence activated cell sorting

For the determination of the effect of $NOD2^{-/-}$ on intracellular ASC, pro-IL-1β, IL-1β, and caspase-1 activity in HL-1 cells, flow cytometry was performed. To examine the effect of S100A8 and S100A9 stimulation on ROS production in HL-1 cells, a CM-H_2DCF-DA dye was used. Fifty-two hours prior to ASC, pro-IL-1β, and IL-1β, staining and FAM-YVAD caspase-1 inhibitor application, HL-1 cells were plated in a fibronectin/gelatin coated 6-well plate at a density of 200,000 cells per well in full Claycomb medium and were incubated for 24 hours in appropriate cell culture conditions. Subsequently, cells were transfected with scr siRNA or NOD2 siRNA at a final concentration of 5 nM. Twenty-four hours later, cells were CVB3 infected at a MOI of 4. After 1 hour of infection, the virus was removed, cells were washed 2x with PBS, followed by addition of 1 ml of full Claycomb medium per well. Four hours later, cells were washed with 1 ml of PBS, followed by a detachment step with Trypsin/EDTA at 37°C. Trypsin was neutralized by adding FBS. Subsequently, cell pellets for ASC, pro-IL-1β, and IL-1β staining were centrifuged 5 minutes at 2,500 rpm and 4°C. For the measurement of caspase-1 activity measurement, 1x FAM-YVAD caspase-1 inhibitor was added to the cell pellets followed by incubation for 30-60 minutes at 37°C and 2 washing steps with 1x Apoptosis Wash Buffer and centrifugation steps at 200x g for 5 minutes. Finally, cells were resuspended in 1x Apoptosis Wash Buffer and were subjected to fluorescence determination. To enable intracellular staining with ASC, pro-IL-1β and IL-1β, HL-1 cells were incubated for 20 minutes in 500 µl of Fixation/Permeabilization solution at 4°C, followed by a washing step with 1x BD Perm/Wash buffer™. After a centrifugation step, cell pellets were dissolved in 1x BD Perm/Wash buffer™ and 2 µl (in a 1:50 dilution) of IL-1β, IL-1β pro-form, or ASC antibody was added, followed by incubation for 30-45 minutes at RT. Subsequently, pellets were resuspended in 200 µl PBS.

With respect to ROS, twenty-eight hours prior to staining, HL-1 cells were plated into 6-well plates at a cell density of 270,000 cells/well. Twenty-four hours later, cells were CVB3 infected and stimulated with S100A8 and S100A9. Four hours later, cells were detached and pelleted. Finally, cell pellets were incubated in 200 µl PBS containing 5 µM CM-H_2DCF-DA per sample for 30 minutes at 37°C.

The fluorescence of FAM-YVAD caspase-1 inhibitor, IL-1β, pro-IL-1β, and ASC antibodies and the CM-H_2DCF-DA dye was measured using the MACSQuant Analyzer 10 (Miltenyi Biotec, Bergisch Gladbach, Germany). Re-analysis of flow cytometry data was performed using FlowJo software version 8.8.6. (Tree Star Inc.). Data are expressed as ASC^+, pro-IL-$1\beta^+$, IL-$1\beta^+$, caspase 1^+, and ROS^+ cells (% gated cells).

3.2.23. Immunohistological measurements

The tissue samples obtained of the heart were embedded in Tissue-Tek OCT compound (Sakura, Zoeterwoude, NL). Immunohistochemistry of the 5 µm thick tissue slides was performed with specific antibodies directed against CD68 (rabbit anti-CD68, Bioss, Freiburg, Germany), collagen I (rabbit anti-Col I, Chemicon, Nürnberg, Germany) and collagen III (rabbit anti-Col III, Calbiochem, Darmstadt, Germany). For CD68, collagen I and collagen III, a secondary swine anti-rabbit dextran-conjugated antibody was used and was visualized by the Envision peroxidase technique (Dako, Hamburg, Germany). Quantification was performed by digital image analyses using a 200x magnification. Briefly, the ratio between the heart tissue area and the specific chromogen-positive area was calculated for collagen I, collagen III (area fraction mean). The amount of infiltrating $CD68^+$ cells was calculated by measuring the number of cells per area of heart tissue (cells/mm^2).

3.2.24. Ca^{2+} diastolic signal in adult rat ventricular cardiomyocytes

Measurement of intracellular Ca^{2+} signal was performed as described previously[116] in cooperation with Dr. David Rhode and Prof. Patrick Most (Center for Molecular and Translational Cardiology, Department of Internal Medicine III, University of Heidelberg, Heidelberg, Germany). In brief, adult rat ventricular cardiomyocytes were incubated with PBS (control) or S100 proteins for 24 hours and then loaded with 2 µM Fura2-AM for 20 minutes

at 37°C in order to allow complete de-esterification of the dye. Ca^{2+} measurements were carried out using an inverse Olympus microscope (IX81) with a UV filter connected to a monochromator (Polychrome II, TILL Photonics GmbH, Gräfelfing, Germany). Cells were electrically stimulated with a biphasic pulse to contract at 1 Hz and excited at 340/380 nm. After 15 minutes of electrical stimulation, epifluorescence emission was detected at 510 nm, digitized, and analyzed off-line with TILLVision software version 3.3.4. Consecutive steady-state transients from one cardiomyocyte were averaged for analysis with 20 cells pooled per group.

3.2.25. Statistical analysis

Statistical analysis was performed using GraphPad Prism 5.0 software (GraphPad Software, La Jolla, CA). Data are expressed as the mean ± SEM. The standard one-way ANOVA test was performed for data comparison, of *in vitro*, *in vivo* experiments, and EMBs measurements, unless stated differently. For the pairwise comparison of EMB NOD2, NLRP3, IL-1β, S100A8, and S100A9 mRNA expression in CVB3 patients who eliminated the virus over time, the parametric, paired t-test was used. Differences were considered statistically significant when $p<0.05$.

4. RESULTS

4.1. NOD2, S100A8, and S100A9 expression in patients

4.1.1. Expression of NOD2, S100A8, and S100A9 in endomyocardial biopsies of control, AMC, DCM, and CVB3+ patients

Our investigations were focused on the analysis of mRNA expression of NOD2, S100A8, and S100A9 in EMBs of control, AMC, DCM, and CVB3-positive patients. NOD2 mRNA expression was 2.1-fold ($p<0.01$) induced in EMBs of CVB3-positive patients versus controls, and was not induced in AMC and DCM patients compared to controls **(Figure 4.1.1. A)**. Analysis of endomyocardial S100A8 and S100A9 mRNA levels showed a 13.0-fold ($p<0.05$) and 5.1-fold ($p<0.05$) increase in biopsies of CVB3-positive patients versus controls, respectively **(Figure 4.1.1. B-C)**. DCM patients showed no elevation of S100A8 and S100A9 mRNA expression versus controls **(Figure 4.1.1. B-C)**.

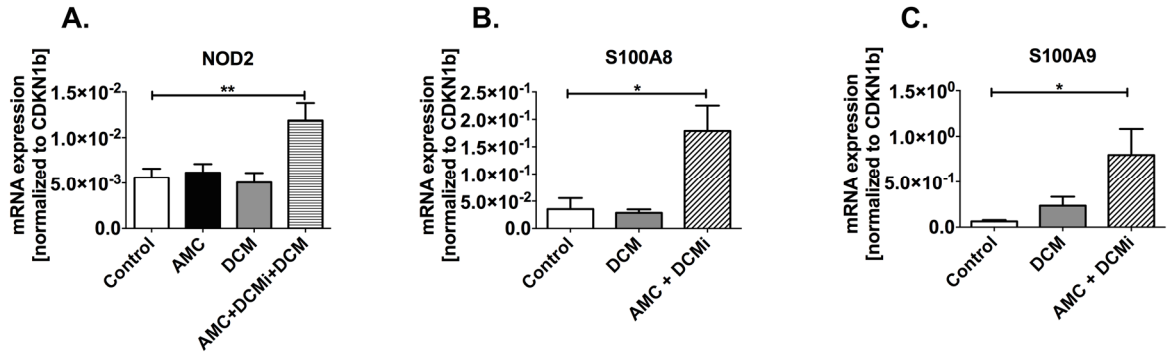

Figure 4.1.1. NOD2, S100A8, and S100A9 mRNA expression in endomyocardial biopsies of control, AMC, DCM, and Coxsackievirus B3-positive patients. A. NOD2 in endomyocardial biopsies (EMBs) of control (open bar), acute myocarditis (AMC; black bar), dilated cardiomyopathy (DCM; gray bar), and Coxsackievirus B3 (CVB3)-positive patients (AMC, inflammatory dilated cardiomyopathy (DCMi), and DCM patients; transversely striped bar), **B.** S100A8, and **C.** S100A9 mRNA expression in EMBs of control (open bar), DCM (gray bar), and CVB3-positive patients (AMC and DCMi; diagonally striped bar). All data are reported as the mean ± SEM for NOD2 with n=12 in controls, n=13 in AMC, n=8 in DCM, and n=13 in CVB3-positive (AMC, DCMi, and DCM) patients. For S100A8 and S100A9, there were n=10 in both control and DCM patient collectives, and n=14 in CVB3-positive patients (AMC and DCMi), with *$p<0.05$ and **$p<0.01$.

4.1.2. Expression of NOD2, NLRP3, IL-1β, S100A8, and S100A9 in endomyocardial biopsies of CVB3+ patients who eliminated the virus over time

Further, mRNA levels of NOD2, NLRP3, IL-1β, S100A8, and S100A9 were determined in CVB3-positive patients (timepoint 1 (T1)), who eliminated the CVB3 virus over time (T2). Results showed a 2.5-fold ($p<0.05$) decrease of NOD2 mRNA levels between time point 1 and 2, which was accompanied by a 2.2-fold ($p<0.05$) and 4.5-fold drop of ($p=0.0592$) NLRP3 and IL-1β, respectively **(Figure 4.1.2. A-C)**. Furthermore, S100A8 and S100A9 mRNA levels decreased significantly over time, as shown by 5.2-fold ($p<0.05$) and 4.5-fold ($p<0.05$) lower expression at time point 2 compared to time point 1, respectively **(Figure 4.1.2. D-E)**.

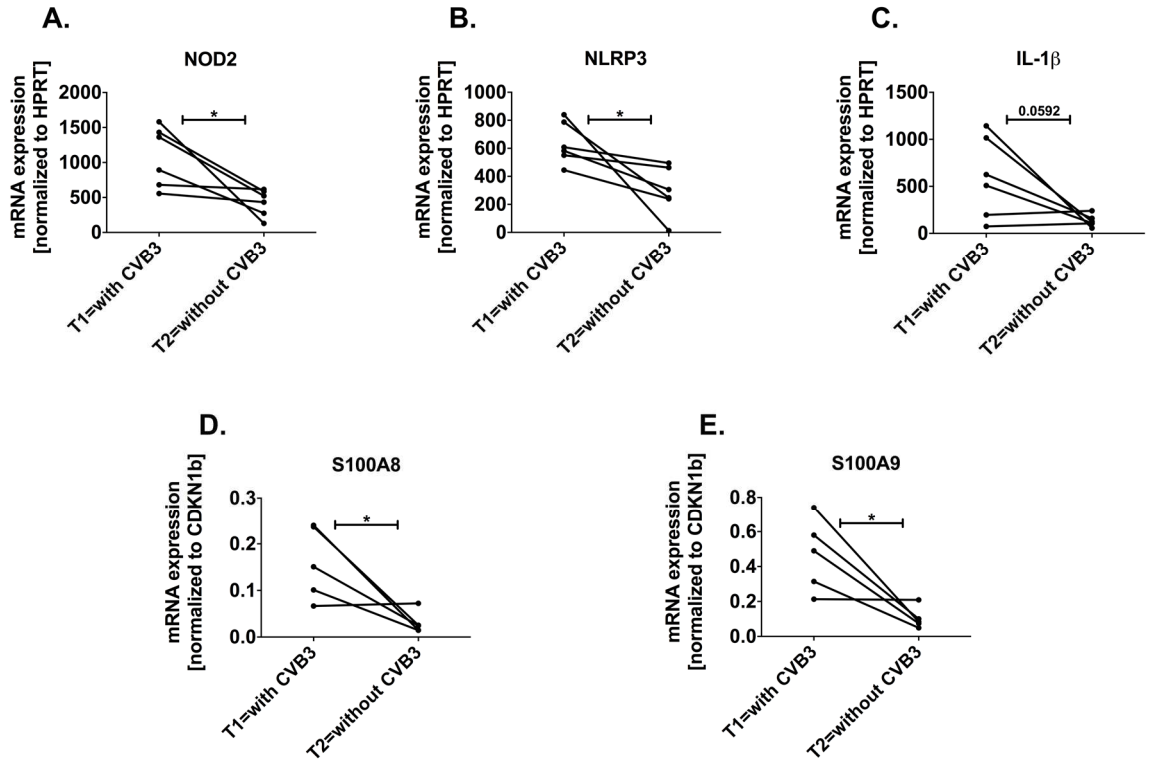

Figure 4.1.2. NOD2, NLRP3, IL-1β, S100A8, and S100A9 mRNA expression in endomyocardial biopsies of Coxsackievirus B3-positive patients, who recovered over time. A. NOD2, **B.** NLRP3, **C.** IL-1β, **D.** S100A8, and **E.** S100A9 mRNA expression in endomyocardial biopsies of recovered Coxsackievirus B3 (CVB3)-positive patients depicting NOD2, NLRP3, IL-1β, S100A8, and S100A9 mRNA expression at timepoint 1 (T1) and 2 (T2). All data are reported as the mean ± SEM with n=6 for T1=with CVB3 and T2=without CVB3 for NOD2, NLRP3, and IL-1β mRNA levels, and with n=5 for T1=with CVB3 and T2=without CVB3 for S100A8 and S100A9 mRNA levels, with *$p<0.05$. CVB3=Coxsackievirus B3.

4.2. NOD2, S100A8, and S100A9 expression *in vivo*

4.2.1. Left ventricular expression of NOD2, S100A8, and S100A9 in Coxsackievirus B3-infected mice

To gain more insight into the expression of NOD2 in the left ventricles of WT and CVB3-infected mice, LV mRNA expression was determined by using real-time PCR. CVB3-infected mice displayed 2.3-fold ($p<0.005$) higher NOD2 mRNA expression compared to WT mice **(Figure 4.2.1. A)**. LV mRNA expression of S100A8 and S100A9 was induced in WT CVB3 mice in a 13.4-fold ($p<0.0005$) and 12.1-fold ($p<0.0005$) manner compared to WT mice, respectively **(Figure 4.2.1. B-C)**.

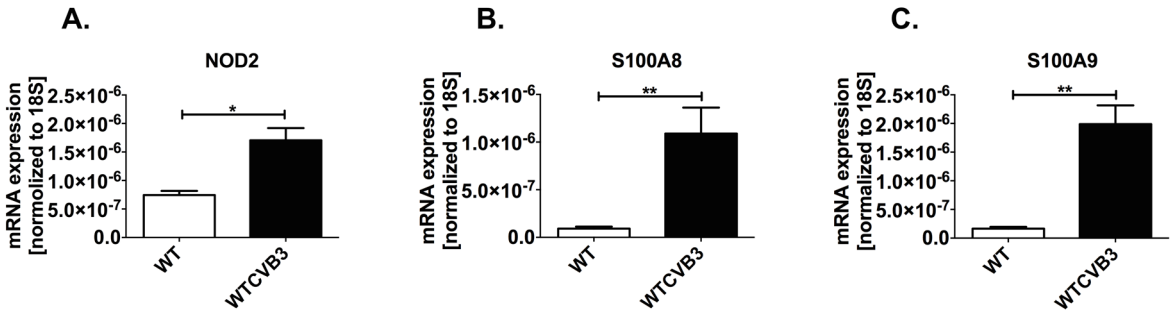

Figure 4.2.1. Left ventricular NOD2, S100A8, and S100A9 mRNA expression in Coxsackievirus B3-infected mice. Left ventricular (LV) mRNA expression of **A.** NOD2, **B.** S100A8, and **C.** S100A9 in WT CVB3 mice compared to non-infected mice. All data are reported as the mean ± SEM with n=7-9/group, with *$p<0.005$ and **$p<0.0005$. The unpaired t-test was used. WT=wild-type; CVB3=Coxsackievirus B3.

Based on these clinical and experimental *in vivo* data, we wanted to further investigate the role of NOD2, S100A8, and S100A9 in mice with experimental CVB3-induced myocarditis, HL-1 cells, murine cardiac fibroblasts and RAW macrophages. For the investigation of NOD2 in CVB3-induced myocarditis, a $NOD2^{-/-}$ *in vivo* mouse model was characterized. The role of NOD2 in CVB3-induced myocarditis was partially investigated within the scope of the medical doctorate thesis of *Xia Yu*. Briefly, it has been shown that $NOD2^{-/-}$ CVB3 mice displayed an improved cardiac LV function, reduced cardiac inflammation and fibrosis, a lower CVB3 copy number and lower apoptosis in comparison to the WT CVB3 group. To further understand the signaling pathways which led to the improvements described above for $NOD2^{-/-}$ CVB3 versus WT CVB3 mice, we characterized the mice in further detail. *In vitro*

experiments with HL-1 cells were performed to better understand the findings of the *in vivo* experiments **(see paragraph 4.3.)**.

Additionally, in a S100A9$^{-/-}$ *in vivo* mouse model, we investigated the role of S100A8 and S100A9 in detail. Of note, S100A9$^{-/-}$ mice are also deficient in S100A8 on the protein level, therefore representing functional double-knockout mice[113]. Also here, *in vitro* experiments were performed to confirm the *in vivo* experiments **(see paragraph 4.4.)**.

4.3. Characterization of the effect of NOD2$^{-/-}$ in experimental Coxsackievirus B3 myocarditis models

4.3.1. NOD2$^{-/-}$ in left ventricles of Coxsackievirus B3-infected mice and HL-1 cells

NOD2 knockdown *in vivo* resulted in a 52% ($p<0.005$) reduction of NOD2 mRNA expression in NOD2$^{-/-}$ mice compared to WT animals **(Figure 4.3.1**. **A)**. Further confirmation for a successfull NOD2 knockdown *in vivo* is given by the forthcoming investigations into NOD2 downstream signaling pathways **(Figure 4.3.2. A and 4.3.4. A-C)**. *In vitro*, NOD2 knockdown efficiency was confirmed by a 81.1% ($p<0.0005$) reduction of NOD2 mRNA levels in NOD2 siRNA cells compared to scr siRNA cells **(Figure 4.3.1**. **B)**.

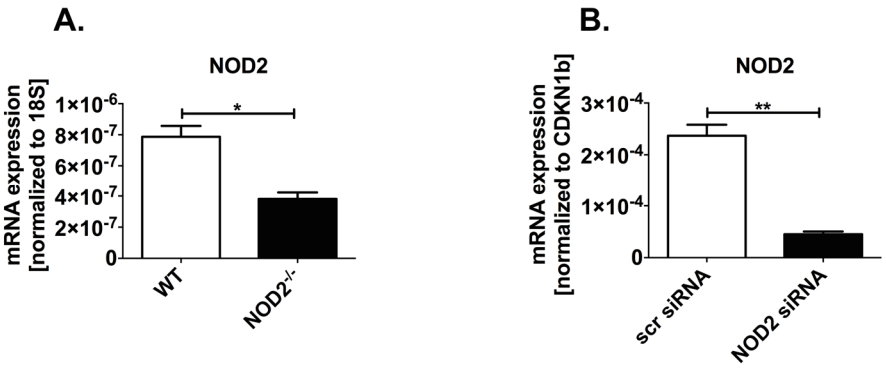

Figure 4.3.1. Left ventricular and HL-1 cell NOD2 knockdown. A. Left ventricular (LV) mRNA expression of NOD2 in WT compared to NOD2$^{-/-}$ mice. **B.** mRNA expression of NOD2 in scr siRNA compared to NOD2 siRNA HL-1 cells 24 hours post transfection. All data are reported as the mean ± SEM with n=6/group, with *$p<0.005$ and **$p<0.0005$. The unpaired t-test was used. WT=wild-type; NOD2=nucleotide binding oligomerization domain; siRNA=small interference RNA; scr=scrambled.

4.3.2. Impact of NOD2$^{-/-}$ on left ventricular TLR4 and downstream signaling in Coxsackievirus B3-infected mice

Collectively, CVB3 infection of WT mice led to a 1.6-fold ($p<0.005$), 1.3-fold ($p<0.05$), 3.1-fold ($p<0.0005$), 1.4-fold ($p<0.05$), and 159-fold ($p<0.0005$) increase of RIPK2, TLR4, MyD88, TRIF, and IFN-β mRNA expression, respectively, versus WT mice **(Figure 4.3.2**. **A-E)**. NOD2$^{-/-}$ CVB3 mice exhibited 1.2-fold ($p<0.05$) lower RIPK2 mRNA expression, which is a downstream kinase of the NOD2 receptor, responsible among others for NF-κB activation[117], in comparison to WT CVB3 mice. Moreover, NOD2$^{-/-}$ CVB3 mice exhibited 1.4-fold ($p<0.05$) and 2.1-fold ($p<0.0005$) lower TLR4 and MyD88 mRNA expression, respectively, in comparison to WT CVB3 mice, whereas TRIF mRNA expression was unaltered **(Figure 4.3.2**. **B-C and D)**. LV IFN-β mRNA expression was 8.0-fold ($p<0.0005$) lower in NOD2$^{-/-}$ CVB3 compared to WT CVB3 mice **(Figure 4.3.2**. **E)**. NOD2$^{-/-}$ CVB3 mice showed no increase in RIPK2, TLR4, MyD88, TRIF, and IFN-β mRNA expression compared to their controls **(Figure 4.3.2**. **A-E)**.

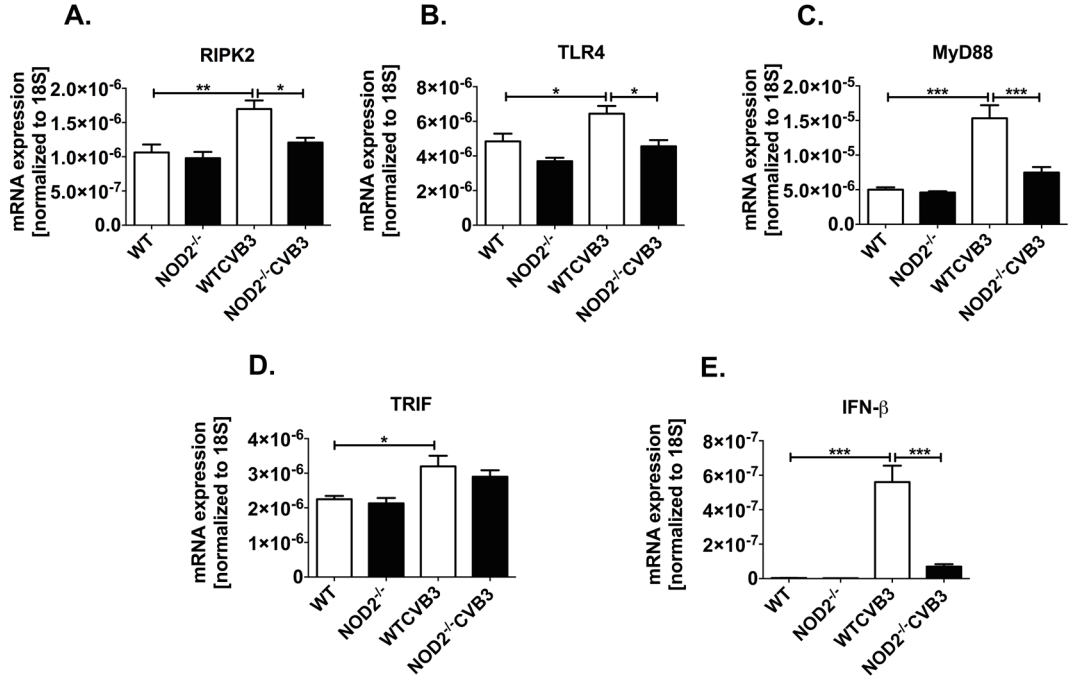

Figure 4.3.2. Impact of NOD2$^{-/-}$ on left ventricular RIPK2, TLR4, MyD88, TRIF, and IFN-β mRNA levels in Coxsackievirus B3-infected mice. Left ventricular (LV) mRNA expression of **A.** RIPK2, **B.** TLR4, **C.** MyD88, **D.** TRIF, and **E.** IFN-β in NOD2$^{-/-}$ CVB3 and WT CVB3 mice versus their respective control groups. All data are reported as the mean ± SEM with n=6-9/group, with *$p<0.05$, **$p<0.005$, and ***$p<0.0005$. WT=wild-type; CVB3=Coxsackievirus B3; NOD2=nucleotide binding oligomerization domain.

4.3.3. Impact of NOD2$^{-/-}$ on TLR4 and downstream signaling in Coxsackievirus B3-infected HL-1 cells

In vitro, knockdown of NOD2 did not affect TLR4 protein expression compared to the scr siRNA control group **(Figure 4.3.3. B)**. CVB3 infection of scr siRNA HL-1 cells resulted in 1.2-fold ($p<0.05$), 2.0-fold ($p<0.05$), 1.4-fold ($p<0.0005$), and 247-fold ($p<0.0005$) higher RIPK2 mRNA levels, TLR4 protein levels, MyD88, and IFN-β mRNA expression compared to the non-infected control group, respectively **(Figure 4.3.3. A-C and E)**, whereas TRIF mRNA levels decreased 1.5-fold ($p<0.0005$) in scr siRNA CVB3 HL-1 cells versus scr siRNA cells **(Figure 4.3.3. D)**. In contrast, in NOD2 siRNA CVB3 cells, RIPK2, TLR4 protein levels, MyD88, TRIF, and downstream IFN-β mRNA expression were 1.6-fold ($p<0.0005$), 3.4-fold ($p<0.005$), 1.8-fold ($p<0.0005$), 1.5-fold ($p<0.005$), and 4.1-fold ($p<0.0005$) lower compared to scr siRNA CVB3 24 hours post infection **(Figure 4.3.3. A-E)**. Additionally, NOD2 siRNA CVB3 cells showed a 81.0-fold ($p<0.05$) enhancement of IFN-β mRNA expression **(Figure 4.3.3. E)**, but a 1.8-fold ($p<0.0005$) decrease in TRIF mRNA levels versus NOD2 siRNA cells, respectively **(Figure 4.3.3. D)**. RIPK2 mRNA expression, TLR4 protein, and MyD88 mRNA levels showed no significant change in NOD2 siRNA CVB3 cells compared to the NOD2 siRNA control **(Figure 4.3.3. A-C)**.

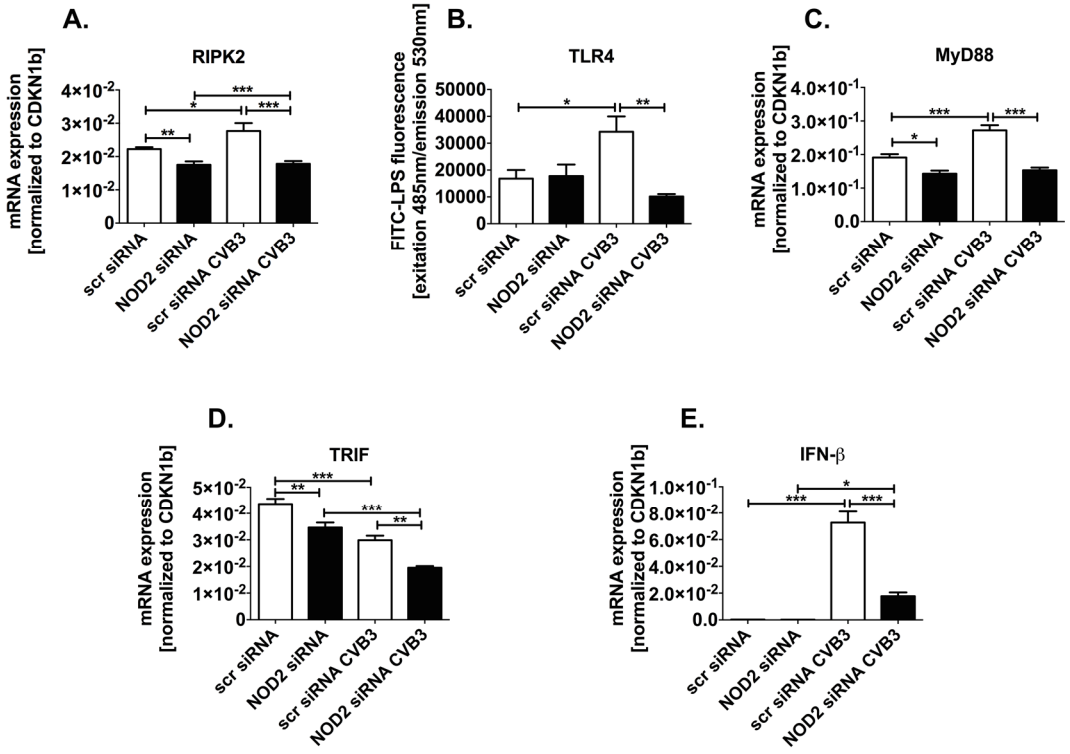

Figure 4.3.3. Impact of NOD2$^{-/-}$ on RIPK2, TLR4, MyD88, TRIF, and IFN-β mRNA levels in Coxsackievirus B3-infected HL-1 cells. A. RIPK2, **B.** TLR4 protein expression, **C.** MyD88, **D.** TRIF, and **E.** IFN-β mRNA expression 24 hours post infection in scr siRNA CVB3 and NOD2 siRNA Coxsackievirus B3 (CVB3)-infected HL-1 cells versus respective controls. All data are reported as the mean ± SEM with n=5-6/group, with *p<0.05, **p<0.005, and ***p<0.0005. CVB3=Coxsackievirus B3; siRNA=small interference RNA; scr=scrambled; NOD2=nucleotide binding oligomerization domain 2.

4.3.4. Impact of NOD2$^{-/-}$ on left ventricular NLRP3, ASC, and IL-1β formation in Coxsackievirus B3-infected mice

Due to the fact that NOD2 and TLR4 are involved in the priming of NLRP3 and IL-1β[72], we further investigated the impact of NOD2 on the expression of NLRP3, ASC, and IL-1β. Overall, WT CVB3 mice showed 3.6-fold (p<0.0005), 2.4-fold (p<0.0005), and 2.0-fold (p<0.05) higher NLRP3 and ASC LV mRNA expression, and IL-1β serum levels versus WT mice, respectively **(Figure 4.3.4. A-C)**. Whereas, NOD2$^{-/-}$ CVB3 mice revealed a 2.3-fold (p<0.0005), 2.0-fold (p<0.0005), and 1.4-fold (p=0.0512) lower NLRP3 and ASC LV mRNA expression, and IL-1β serum levels compared to WT CVB3 mice, respectively **(Figure 4.3.4. A-C)**.

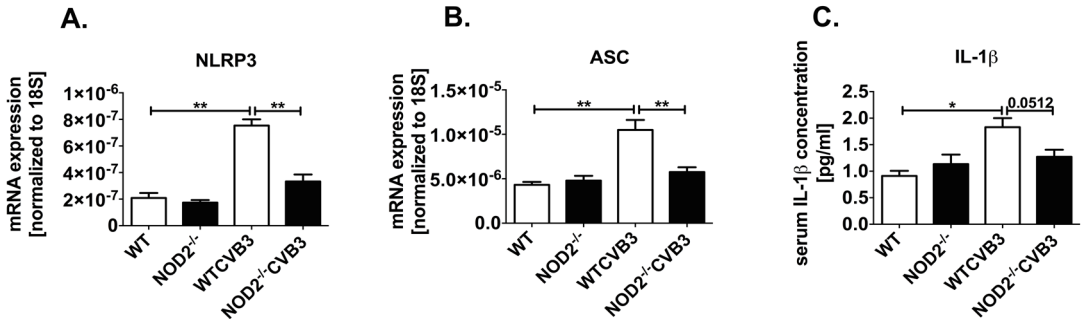

Figure 4.3.4. Impact of NOD2$^{-/-}$ on left ventricular NLRP3 inflammasome activation in Coxsackievirus B3-infected mice. Bar graphs represent the mean ± SEM of left ventricular (LV) **A.** NLRP3 and **B.** ASC mRNA expression in NOD2$^{-/-}$ CVB3 and WT CVB3 mice compared to their respective control groups with n=6-9/group. **C.** Bar graphs represent the mean ± SEM of IL-1β serum levels in NOD2$^{-/-}$ CVB3 and WT CVB3 groups compared to their respective control mice with n=4 for WT, n=4 for NOD2$^{-/-}$, n=5 for WT CVB3, and n=9 for NOD2$^{-/-}$ CVB3. For the whole graph panel with *p<0.05 and **p<0.0005. WT=wild-type; CVB3=Coxsackievirus B3, NOD2=nucleotide binding oligomerization domain 2.

4.3.5. Impact of NOD2$^{-/-}$ on NLRP3, ASC, caspase-1 activity, and IL-1β formation in Coxsackievirus B3-infected HL-1 cells

NOD2 mRNA expression was not significantly induced in scr siRNA CVB3 cells versus scr siRNA 4 hours post infection, whereas NLRP3 mRNA, ASC protein levels, caspase-1 activity, and IL-1β protein levels were 1.7-fold (p<0.05), 1.5-fold (p<0.0005), 1.7-fold (p<0.0005), and 1.5-fold (p<0.0005) increased versus controls, respectively **(Figure 4.3.5. A-D and F)**. In agreement with the *in vivo* data, CVB3-infected NOD2 siRNA cells displayed 1.9-fold (p<0.05) and 1.4-fold (p<0.005) lower mRNA expression of NLRP3 and lower protein levels of ASC compared to infected scr siRNA cells, respectively **(Figure 4.3.5. B-C)**. Interestingly, NOD2 siRNA CVB3 cells exhibited a 1.3-fold (p<0.05) lower caspase-1 activity and 1.3-fold (p<0.0005) lower IL-1β protein levels versus scr siRNA CVB3 cells **(Figure 4.3.5. D and F)**, whereas, pro-IL-1β protein levels did not change in any of the four groups **(Figure 4.3.5. E)**.

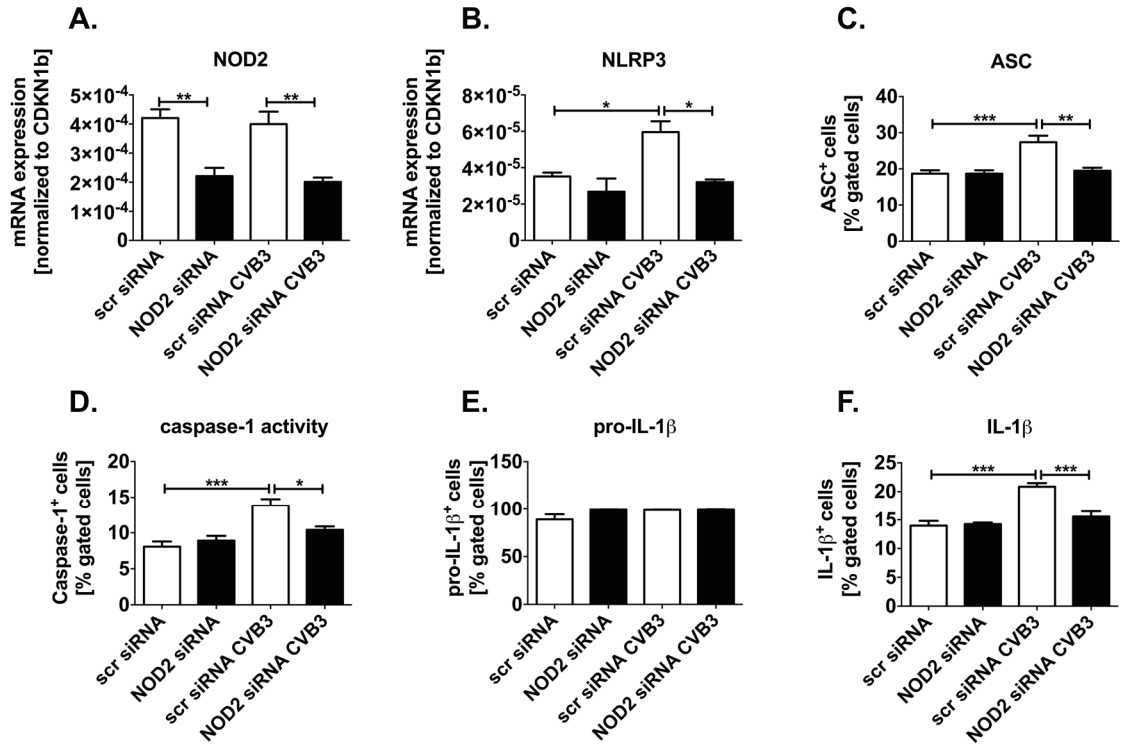

Figure 4.3.5. Impact of NOD2$^{-/-}$ on NLRP3 inflammasome activation in Coxsackievirus B3-infected HL-1 cells. A. NOD2 mRNA expression in scr siRNA CVB3 and NOD2 siRNA Coxsackievirus B3 (CVB3)-infected HL-1 cells compared to their respective controls 4 hours post infection. NLRP3 inflammasome activation, displayed as **B.** NLRP3 mRNA and **C.** ASC protein levels, **D.** caspase 1 activity, **E.** pro-IL-1β, and **F.** IL-1β protein levels in scr siRNA CVB3 and NOD2 siRNA CVB3-infected HL-1 cells versus respective controls 4 hours post infection. All data are reported as the mean ± SEM with n=4-6 for scr siRNA, n=5-6 for NOD2 siRNA, scr siRNA CVB3, and NOD2 siRNA CVB3-infected HL-1 cells, with *p<0.05, **p<0.005, and ***p<0.0005. CVB3=Coxsackievirus B3; siRNA=small interference RNA; scr=scrambled; NOD2=nucleotide binding oligomerization domain 2.

4.3.6. Impact of NOD2$^{-/-}$ on IL-6, TNF-α, and IFN-γ in Coxsackievirus B3-infected HL-1 cells

In general, scr siRNA CVB3 HL-1 cells showed an increase of 9.5-fold (p<0.0005) for TNF-α and 9.4-fold (p<0.0005) for IL-6 mRNA expression versus non-infected scr siRNA 24 hours post infection **(Figure 4.3.6**. **A-B)**. In agreement with the previously described *in vivo* NOD2$^{-/-}$ data, NOD2 knockdown in HL-1 cells was associated with a decreased inflammatory response after 24 hours of CVB3 infection, as indicated by 3.1-fold (p<0.0005) and 2.2-fold (p<0.0005) lower mRNA expression of TNF-α and IL-6, respectively, in CVB3-infected NOD2 siRNA compared to scr siRNA CVB3 HL-1 cells **(Figure 4.3.6**. **A-B)**. IFN-γ mRNA expression was indetectable in HL-1 cells 24 hours post infection **(Figure 4.3.6**. **C)**.

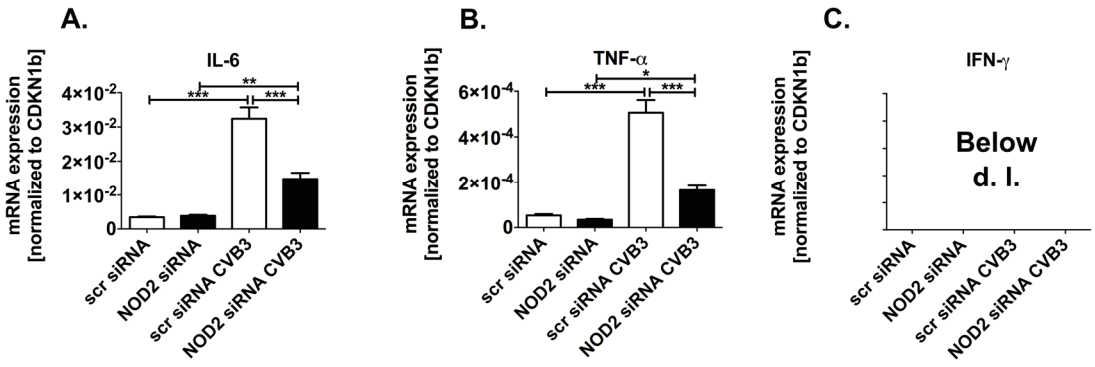

Figure 4.3.6. Impact of NOD2$^{-/-}$ on IL-6, TNF-α, and IFN-γ in Coxsackievirus B3-infected HL-1 cells. mRNA expression of **A.** IL-6, **B.** TNF-α, and **C.** IFN-γ in scr siRNA CVB3 and NOD2 siRNA CVB3 HL-1 cells compared to respective controls. All data are reported as the mean ± SEM with n=6/group, with *p<0.05, **p<0.005, and ***p<0.0005. CVB3=Coxsackievirus B3; NOD2=nucleotide binding oligomerization domain; siRNA=small interference RNA; scr=scrambled.

4.3.7. Impact of NOD2$^{-/-}$ on splenic Coxsackievirus B3 copy number in Coxsackievirus B3-infected mice and on Coxsackievirus B3 copy number and apoptosis in Coxsackievirus B3-infected HL-1 cells

In accordance with the LV *in vivo* NOD2$^{-/-}$ animal study, splenic CVB3 copy number was 4.2-fold (p<0.0005) less abundant in NOD2$^{-/-}$ CVB3 mice compared to WT CVB3 mice (NOD2$^{-/-}$ CVB3: 5.2x10^5 ± 1.1x10^5 (n=9) versus WT CVB3: 2.2x10^6 ± 2.8x10^5 (n=9); p<0.0005). *In* vitro, NOD2 siRNA CVB3 HL-1 cells showed a 1.4-fold (p<0.0005) lower CVB3 copy number in comparison to the scr siRNA CVB3 cells 14 hours post infection **(Figure 4.3.7**. **A)**. *In vitro*, caspase 3/7 activity was 1.2-fold (p<0.05) lower in the NOD2 siRNA CVB3-infected versus scr siRNA CVB3 cells 24 hours post infection **(Figure 4.3.7**. **B)**. CVB3 infection of scr siRNA and NOD2 siRNA HL-1 cells resulted in a 4.5-fold (p<0.0005) and 3.1-fold (p<0.0005) higher caspase 3/7 activity compared to non-infected control groups, respectively **(Figure 4.3.7**. **B)**.

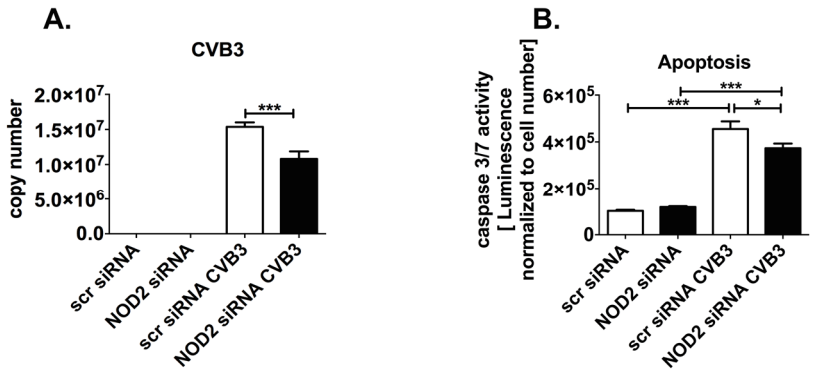

Figure 4.3.7. Impact of NOD2$^{-/-}$ on Coxsackievirus B3 copy number and caspase 3/7 activity in Coxsackievirus B3-infected HL-1 cells. Bar graphs represent the mean ± SEM of **A.** Coxsackievirus B3 (CVB3) copy number and **B.** caspase 3/7 activity in scr siRNA CVB3 and NOD2 siRNA CVB3-infected HL-1 cells compared to their respective controls 14 or 24 hours post-infection, respectively, for CVB3 copy number with n=5-6/group and for caspase 3/7 activity with n=9-12/group, with *p<0.05, **p<0.005, and ***p<0.0005. CVB3=Coxsackievirus B3; siRNA=small interference RNA; scr=scrambled; NOD2=nucleotide binding oligomerization domain 2.

4.4. Characterization of the effect of S100A8 and S100A9 in experimental Coxsackievirus B3 myocarditis models

4.4.1. S100A9$^{-/-}$ in experimental Coxsackievirus B3 myocarditis models

The S100A9 knockout efficacy was 100%, as shown by an indetectable left ventricular S100A9 mRNA expression in S100A9$^{-/-}$ mice and as well in S100A9$^{-/-}$ CVB3 hearts **(Figure 4.4.1.1. A)**. Manitz *et al.*[113] demonstrated that these animals are also deficient of S100A8 on protein level and thus represent a functional double$^{-/-}$ mouse model due to the lack of the binding partner S100A9. Our data concur with these observations as 1) we detected S100A8 mRNA **(Figure 4.4.1.1. B)**, but 2) no S100A8 proteins **(Figure 4.4.1.1. C)**.

In vitro, the S100A8 knockdown efficacy values at the chosen siRNA concentration **(see paragraph 3.2.5.)** were 51% (p<0.05), 35% (p<0.005), and 71.2% (p<0.0005) in HL-1 cells, RAW cells, and cardiac murine fibroblasts, respectively **(Figure 4.4.1.2. A-C)**.

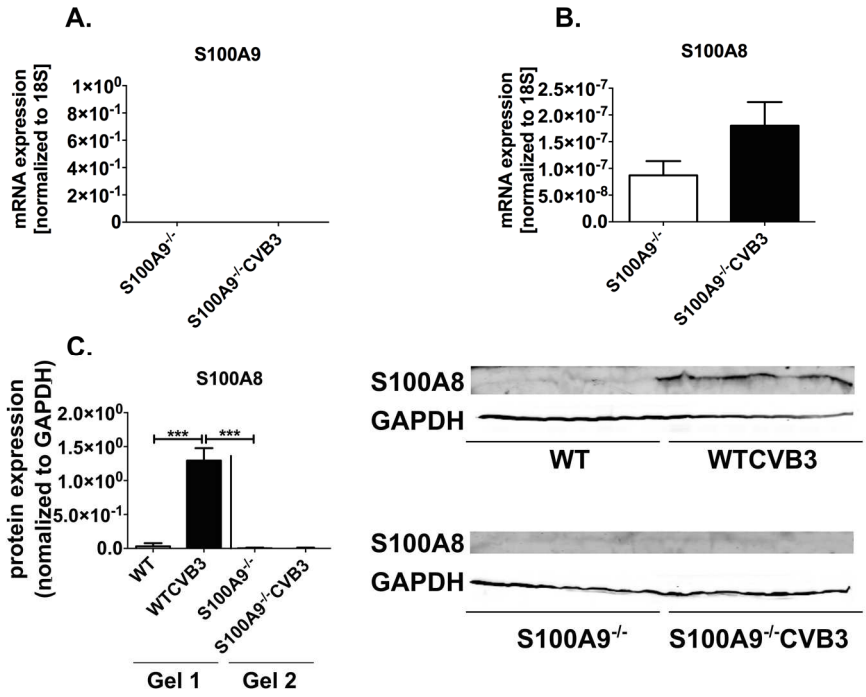

Figure 4.4.1.1. Left ventricular S100A9, S100A8 mRNA levels, and S100A8 protein expression in Coxsackievirus B3-infected mice. Left ventricular (LV) mRNA expression of **A.** S100A9 and **B.** S100A8 in S100A9$^{-/-}$ and S100A9$^{-/-}$ CVB3 mice. Bar graphs represent the mean of ± SEM with n=8-10/group. **C.** LV protein expression of S100A8 in WT CVB3 and S100A9$^{-/-}$ CVB3 mice compared to non-infected mice. Bar graphs show the mean ± SEM of S100A8 expression in WT versus WT CVB3 mice (left) and S100A9$^{-/-}$ versus S100A9$^{-/-}$ CVB3 mice (right) from 2 different gels. The line indicates that the proteins of WT versus WT CVB3 and S100A9$^{-/-}$ versus S100A9$^{-/-}$ CVB3 were loaded on two seperate gels, with n=7/group, with ***p<0.0005. WT=wild-type; CVB3=Coxsackievirus B3. The right panel demonstrates representative pictures of the western blot nitrocellulose membranes.

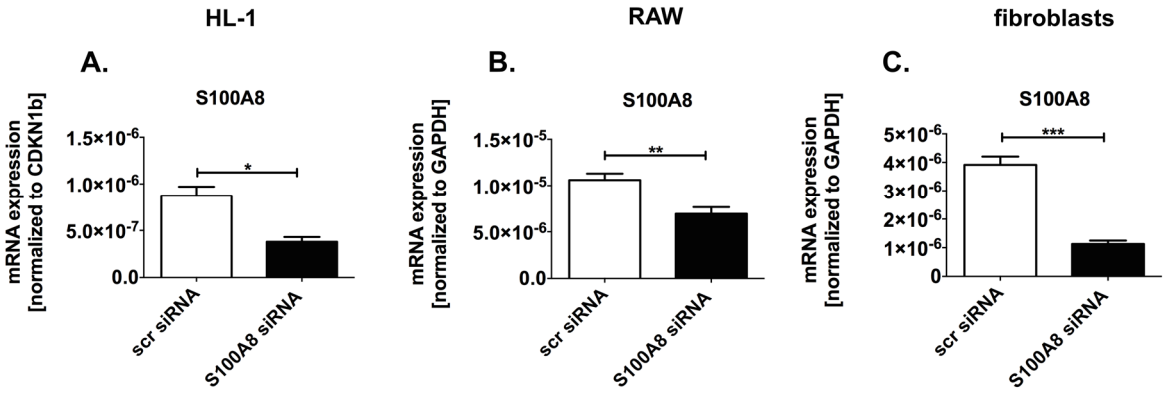

Figure 4.4.1.2. S100A8 knockdown efficacy in HL-1 cells, RAW macrophages, and cardiac fibroblasts. mRNA expression of S100A8 in **A.** HL-1 cells, **B.** in RAW macrophages, and **C.** cardiac fibroblasts in scr siRNA compared to S100A8 siRNA HL-1 cells 24 hours post-transfection. All data are reported as the mean ± SEM with n=6/group, with *p<0.05, **p<0.005 and ***p<0.0005. The unpaired t-test was used. siRNA= small interference RNA; scr= scrambled.

4.4.2. Impact of S100A9$^{-/-}$ on left ventricular expression of macrophage inflammatory protein-2 chemokine in Coxsackievirus B3-infected mice

The interplay between chemokines, such as macrophage inflammatory protein-2 (MIP-2), and the subsequent cardiac infiltration of inflammatory cells, plays a key role in the pathophysiology of CVB3-induced myocarditis[118]. As shown in **Figure 4.4.2. A**, i.p. CVB3 infection of WT and S100A9$^{-/-}$ mice resulted in a 6.7-fold ($p<0.0005$) and 5.1 ($p<0.05$) enhancement of MIP-2 LV mRNA levels compared to the corresponding controls, respectively. S100A9$^{-/-}$ CVB3 showed a 2.0-fold ($p<0.05$) decrease of MIP-2 mRNA levels versus WT CVB3 mice **(Figure 4.4.2. A)**.

To further understand the impact of S100A8 and S100A9 on the chemokine MIP-2, we carried out *in vitro* stimulation and transfection experiments. Since macrophages are the main source of MIP-2[118, 119], we examined the expression of MIP-2 in RAW macrophages after stimulation with S100A8 or S100A9 homodimers. In a subsequent experiment, we knocked-down S100A8 in RAW macrophages. CVB3-infected macrophages showed a 4.0-fold ($p=0.069$) enhancement of MIP-2 mRNA levels compared to the non-infected controls (**Figure 4.4.2. B)**. Interestingly, S100A8 and S100A9 stimulation of non-infected RAW cells enhanced MIP-2 mRNA levels, as shown by 27.0-fold ($p<0.0005$) and 16.2-fold ($p<0.0005$) higher mRNA levels in comparison to the control group, respectively (**Figure 4.4.2. B)**. Furthermore, S100A8 supplementation to CVB3-infected RAW cells increased MIP-2, as shown by 8.4-fold ($p<0.0005$) higher mRNA levels compared to non-stimulated CVB3-infected macrophages (**Figure 4.4.2. B)**. All together, S100A8 enhances MIP-2 mRNA expression in non-infected as well as infected cells, whereby the enhancement in CVB3 S100A8 RAW cells is 1.2-fold ($p<0.005$) higher then in S100A8 stimulated non-infected RAW cells (**Figure 4.4.2. B)**. Despite a 4.6-fold ($p<0.0005$) increase of MIP-2 in CVB3 S100A9 cells versus CVB3 cells, CVB3 S100A9 RAW cells showed no further elevation of MIP-2 mRNA levels compared to S100A9 supplemented non-infected RAW cells **(Figure 4.4.2. B)**. Furthermore, scr siRNA CVB3 and S100A8 siRNA CVB3 cells displayed a 3.4-fold ($p<0.0005$) and 2.0-fold ($p<0.0005$) elevation in MIP-2 transcript levels versus the corresponding controls, respectively **(Figure 4.4.2. C)**. The *in vivo* reported decrease in MIP-2 mRNA expression in S100A9$^{-/-}$ CVB3 mice versus WT CVB3 mice, has been confirmed in S100A8 siRNA CVB3 RAW cells, which was displayed by a 1.2-fold ($p<0.05$) decrease of MIP-2 mRNA levels in comparison to scr siRNA CVB3 cells **(Figure 4.4.2. C)**.

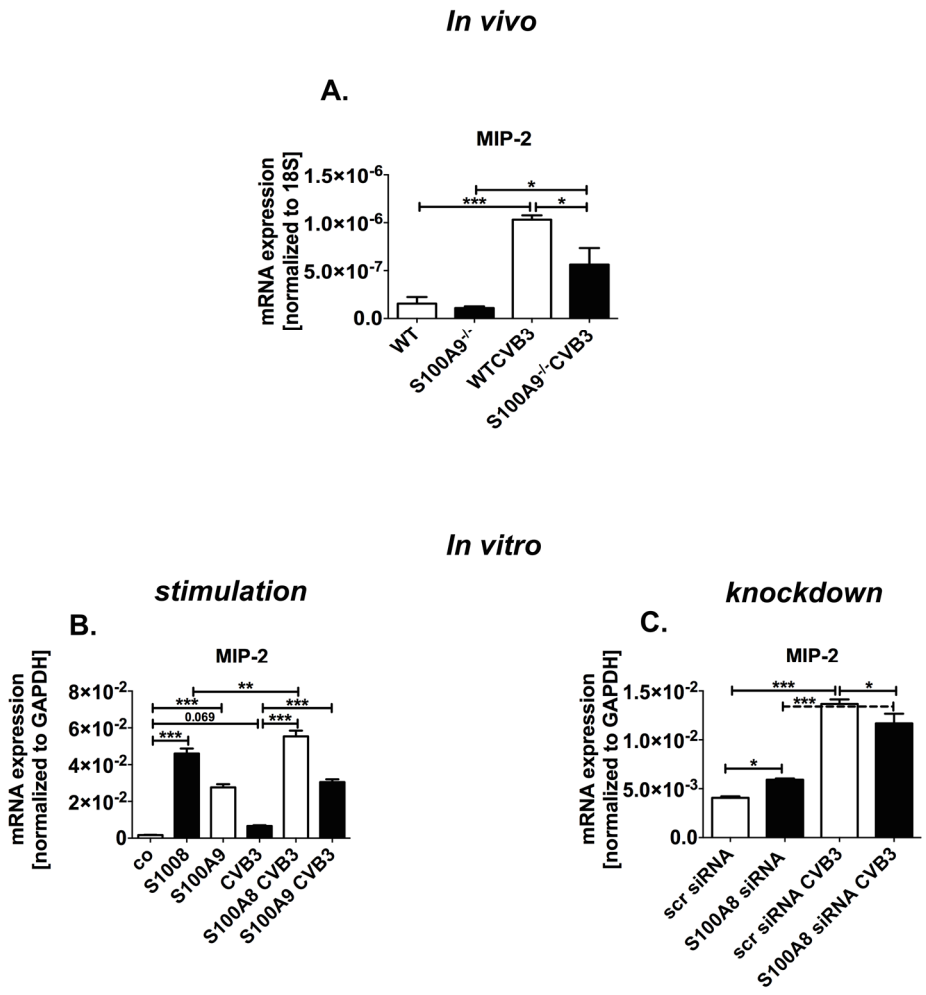

Figure 4.4.2. Impact of S100A8 and/or S100A9 on macrophage inflammatory protein-2 chemokine mRNA expression in Coxsackievirus B3-infected mice and RAW macrophages. A. Left ventricular (LV) mRNA expression of macrophage inflammatory protein-2 (MIP-2) in WT CVB3 and S100A9$^{-/-}$ CVB3 mice compared to non-infected control mice. **B.** mRNA expression of MIP-2 in Coxsackievirus B3 (CVB3)-infected, CVB3 S100A8- and CVB3 S100A9-stimulated RAW macrophages versus their respective controls, 24 hours post infection and stimulation. **C.** MIP-2 mRNA expression in scr siRNA CVB3 and S100A8$^{-/-}$ CVB3 RAW macrophages compared to respective controls, 24 hours post infection. All data are reported as the mean ± SEM with n=6 in WT, n=7-8 in S100A9$^{-/-}$, n=5-6 in WT CVB3, and n=7-9 in S100A9$^{-/-}$ CVB3 mice. For stimulation and transfection experiments with n=5-6/group. For all graphs, *p<0.05, **p<0.005, and ***p<0.0005. WT=wild-type; CVB3=Coxsackievirus B3; siRNA=small interference RNA; scr=scrambled.

4.4.3. Impact of S100A9$^{-/-}$ on left ventricular inflammatory cells infiltration in Coxsackievirus B3-infected mice

Given the fact that MIP-2 is a major macrophage and neutrophil chemoattractant[118, 119], we examined the cardiac presence of inflammatory mononuclear cells. CVB3-infected WT mice displayed a 4.1-fold ($p<0.05$) and 3.4-fold ($p<0.05$) enhanced LV mRNA expression of Ly6g, the neutrophil marker, and of the monocyte marker Ly6c compared to non-infected WT mice, respectively (**Figure 4.4.3. A-B)**. In addition, a 3.2-fold ($p<0.0005$) increase was found in CD68 positive macrophages compared to non-infected WT mice (**Figure 4.4.3. C)**. LVs of S100A9$^{-/-}$ CVB3 animals showed a 2.1-fold ($p<0.05$), 2.2-fold ($p<0.05$), and a 1.3-fold ($p<0.05$) decrease of Ly6g and Ly6c mRNA levels, and CD68 positive cells compared to infected WT mice, respectively (**Figure 4.4.3. A-C)**.

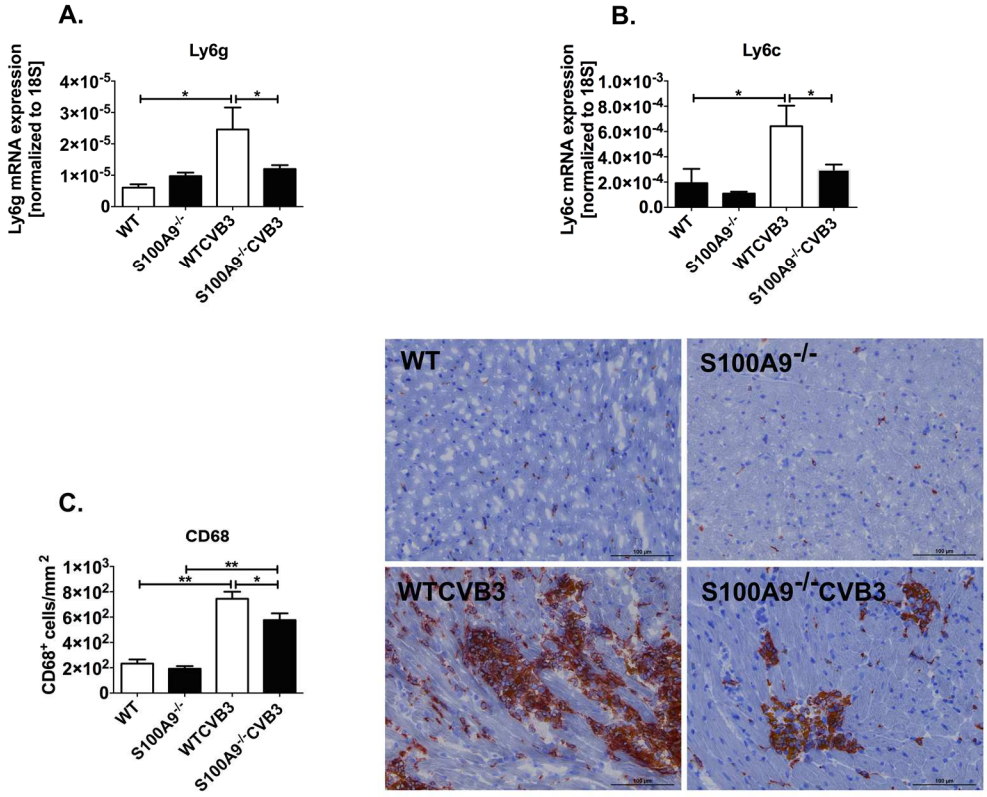

Figure 4.4.3. Impact of S100A9$^{-/-}$ on left ventricular Ly6g and Ly6c mRNA expression, and presence of CD68^{+} cells in Coxsackievirus B3-infected mice. Left ventricular (LV) mRNA expression of **A.** Ly6g and **B.** Ly6c in WT CVB3 and S100A9$^{-/-}$ CVB3 mice compared to non-infected control mice. Bar graphs represent the mean ± SEM with n=5-6 in WT and WT CVB3, n=7-9 in S100A9$^{-/-}$, and S100A9$^{-/-}$ CVB3 mice. **C.** LV infiltration of CD68 positive cells in WT, S100A9$^{-/-}$, WT CVB3, and S100A9$^{-/-}$ CVB3 mice. Bar graphs (left) represent the mean ± SEM of CD68 positive cells per mm^2 heart area with n=7-8 in WT and S100A9$^{-/-}$, and n=9-10 in WT CVB3 and S100A9$^{-/-}$ CVB3 mice. Photographs (right) show representative CD68-stained LV sections. For all graphs, *$p<0.05$ and **$p<0.0005$. WT=wild-type; CVB3=Coxsackievirus B3.

4.4.4. Impact of S100A9$^{-/-}$ on left ventricular oxidative stress in Coxsackievirus B3-infected mice

The enhanced infiltration of immune cells, especially Ly6g^{+} neutrophils, was associated with a higher oxidative stress in WT CVB3 mice compared to WT mice as shown by a 2.0-fold ($p<0.005$) enhancement of MPO **(Figure 4.4.4. A)**. In contrast, S100A9$^{-/-}$ CVB3 mice showed a 3.0-fold ($p<0.0005$) lower MPO activity versus WT CVB3 mice **(Figure 4.4.4. A)**. The NADPH oxidase 1 (Nox1) mRNA expression was 7.1-fold ($p<0.05$) increased in infected WTs versus control animals and was 3.3-fold ($p<0.05$) lower in S100A9$^{-/-}$ CVB3 animals compared to WT CVB3 mice **(Figure 4.4.4. B)**. Infected S100A9$^{-/-}$ mice showed no change in MPO activity, nor in Nox1 mRNA levels compared to control mice **(Figure 4.4.4. A-B)**.

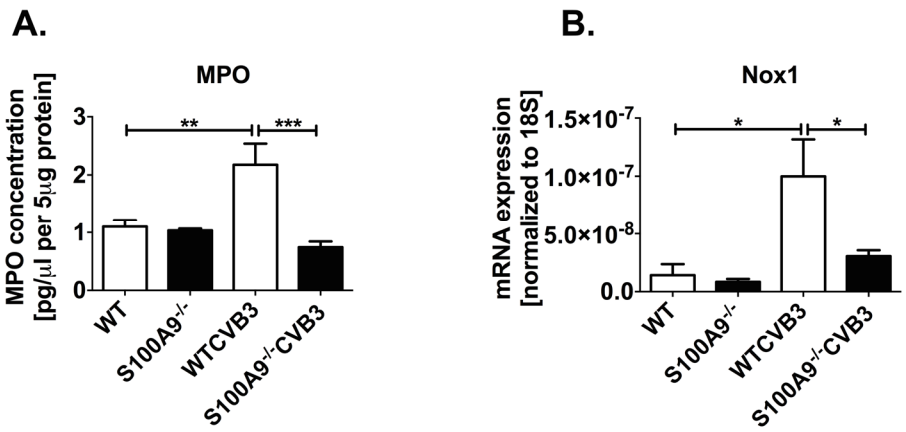

Figure 4.4.4. Impact of S100A9$^{-/-}$ on left ventricular myeloperoxidase activity and Nox1 mRNA expression in Coxsackievirus B3-infected mice. Left ventricular (LV) **A.** myeloperoxidase (MPO) activity and **B.** mRNA expression of Nox1 in WT CVB3 and S100A9$^{-/-}$ CVB3 mice compared to non-infected control mice. All data are reported as the mean ± SEM with n=6-10/group, except for Nox1 with n=4 in WT mice, with *$p<0.05$, **$p<0.005$, and ***$p<0.0005$. WT=wild-type; CVB3=Coxsackievirus B3.

4.4.5. Impact of S100A8 and S100A9 stimulation on oxidative stress in Coxsackievirus B3-infected HL-1 cells

Overall, CVB3 infection of HL-1 cells resulted in a 2.0-fold ($p<0.0005$) enhancement of ROS, as determined by flow cytometry **(Figure 4.4.5.)**. Furthermore, CVB3 S100A8- and CVB3 S100A9-stimulated HL-1 cells showed each a 1.3-fold ($p<0.05$) increase of ROS levels compared to non-stimulated CVB3-infected cells **(Figure 4.4.5.)**.

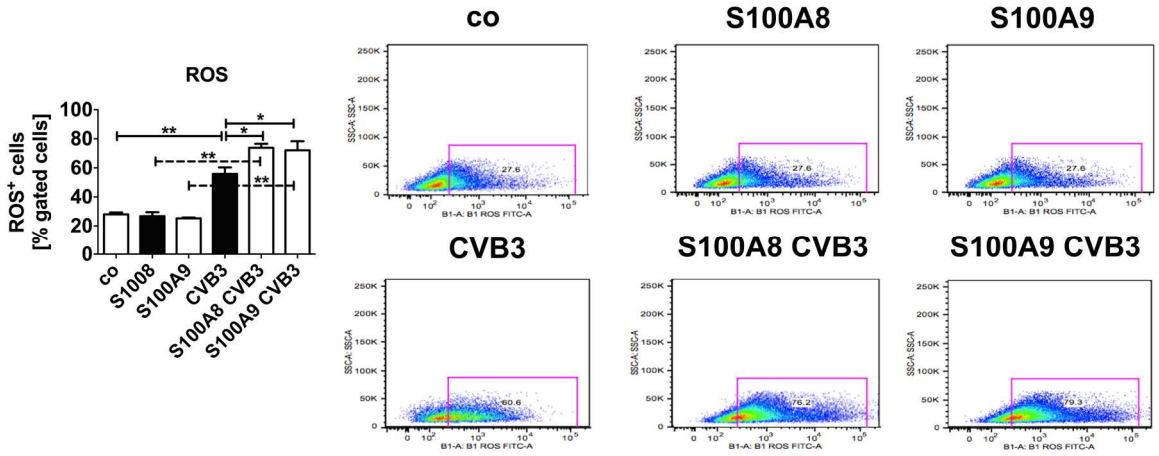

Figure 4.4.5. Impact of S100A8 and S100A9 stimulation on reactive oxygen species levels in Coxsackievirus B3-infected HL-1 cells. Bar graphs (left) demonstrate reactive oxygen species (ROS) levels expressed as % of ROS^+ gated cells in Coxsackievirus B3 (CVB3)-infected, CVB3 S100A8- and CVB3 S100A9-stimulated HL-1 cells versus their respective controls, 4 hours post-infection and stimulation. Data are reported as the mean ± SEM with n=5-6/group, with *p<0.05 and **p<0.0005. CVB3=Coxsackievirus B3. Representative dot blot pictures (right) show ROS^+ HL-1 cells.

4.4.6. Impact of alarmins on diastolic Ca^{2+} signal

Given the relevance of S100A8 and S100A9 in cardiovascular diseases[66, 120], the fact that these alarmins are Ca^{2+} binding proteins[28, 30] and the importance of Ca^{2+} in cardiomyocyte functionality[121], the effect of S100A8, S100A9, and S100A8/S100A9 stimulation on the Ca^{2+} diastolic signal in adult rat ventricular cardiomyocytes was evaluated. Briefly, the Ca^{2+} diastolic signal is decreased under normal conditions by re-uptake into the endoplasmatic reticulum and thus ensures efficient ventricular filling[122]. These experiments were done with the cooperation of Dr. David Rhode and Prof. Patrick Most (Center for Molecular and Translational Cardiology, Department of Internal Medicine III, University of Heidelberg, Heidelberg, Germany). Our preliminary data showed that S100A9 and S100A8/S100A9 each

led to a 1.1-fold ($p<0.05$) enhancement of the Ca^{2+} diastolic signal compared to PBS controls, whereas supplementation with S100A8 showed no effect compared to the PBS group **(Figure 4.4.6.)**.

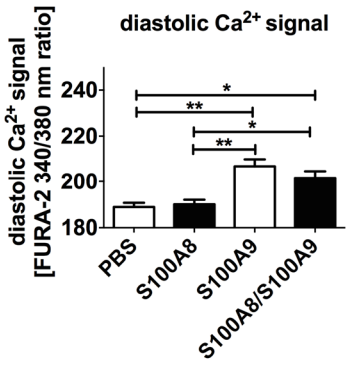

Figure 4.4.6. Diastolic Ca^{2+} signal of adult rat ventricular cardiomyocytes. The diastolic Ca^{2+} signal was assessed by changes in FURA-2 340/380 nm ratios during electric pacing at 1 Hz. Adult rat ventricular cardiomyocytes were incubated with PBS (control) or S100 proteins (1 µM) for 24 hours prior to loading with FURA-2. All data are reported as the mean ± SEM with n=20/group, with *p<0.05 and **p<0.0005.

4.4.7. Impact of S100A9$^{-/-}$ on left ventricular fibrosis in Coxsackievirus B3-infected mice

Collagen I and *Collagen III* mRNA expression was 5.0-fold ($p<0.005$) and 3.4-fold ($p<0.05$) increased in WT CVB3 compared to WT mice **(Figure 4.4.7. A-B)**. Also S100A9$^{-/-}$ CVB3 animals displayed enhanced *Collagen I* and *Collagen III* mRNA expression compared to control mice, as shown by 5.0-fold ($p<0.0005$) and 5.1-fold ($p<0.0005$) increased expression, respectively **(Figure 4.4.7. A-B)**. As shown in **Figure 4.4.7. A and B**, S100A9$^{-/-}$ CVB3 mice did not show any differences in collagen levels versus WT CVB3 mice, neither for *Collagen I* nor for *Collagen III* mRNA expression. Additionally, immunohistological examinations of LV collagen turnover revealed no change for any of the experimental groups, as shown by the collagen I / III protein ratio **(Figure 4.4.7. E)**. Analysis of the pro-fibrotic factor TGF-β, which is responsible for the transformation of fibroblasts into myofibroblasts[123], showed a 4.1-fold ($p<0.0005$) increase in WT CVB3 mice, and in S100A9$^{-/-}$ CVB3 mice a 1.2-fold ($p<0.05$) enhanced mRNA expression versus their corresponding controls **(Figure 4.4.7. C)**. No altered TGF-β mRNA levels were seen in S100A9$^{-/-}$ CVB3 mice compared to WT CVB3 mice **(Figure 4.4.7. C)**. Further evaluation of the myofibroblast marker α-SMA[123], showed no difference between any corresponding groups, as displayed by unaltered mRNA levels in **Figure 4.4.7. D**.

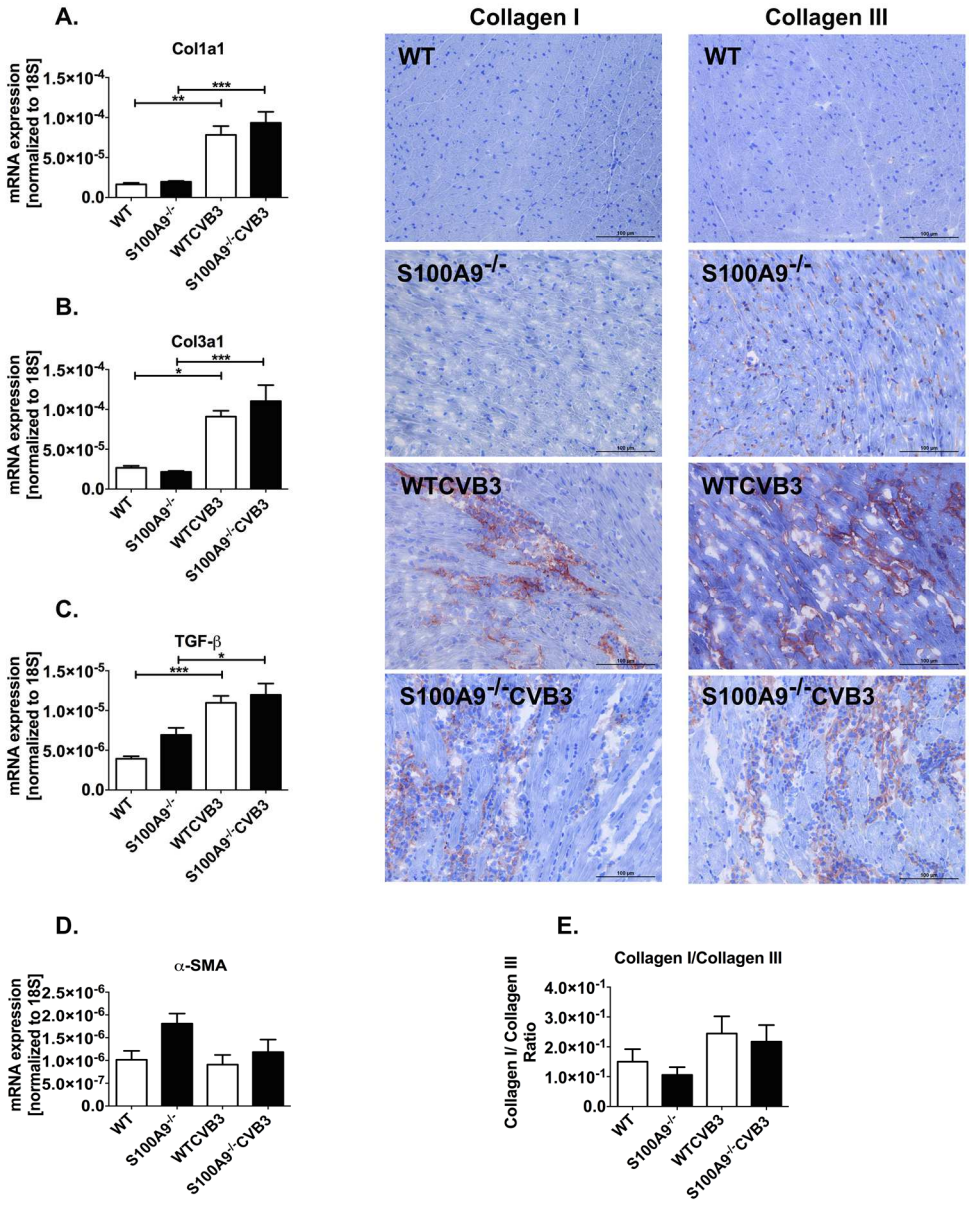

Figure 4.4.7. Impact of S100A9$^{-/-}$ on left ventricular Col1a1, Col3a1, TGF-β, and α-SMA mRNA levels and Collagen I / Collagen III protein ratio in Coxsackievirus B3-infected mice. Left ventricular (LV) mRNA expression of **A.** Col1a1, **B.** Col3a1, **C.** TGF-β, and **D.** α-SMA in WT CVB3 and S100A9$^{-/-}$ CVB3 mice compared to non-infected control mice. Bar graphs represent the mean ± SEM with n=8 in WT and S100A9$^{-/-}$, n=6 in WT CVB3, n=9 for S100A9$^{-/-}$ CVB3 for Col1a1 and Col3a1, and for TGF-β and α-SMA with n=5-6 in WT and WT CVB3 and n=7-9 in S100A9$^{-/-}$ and S100A9$^{-/-}$ CVB3 animals. **E.** Upper panel demonstrates representative collagen I and collagen III LV sections of WT CVB3 and S100A9$^{-/-}$ CVB3 mice compared to respective non-infected mice at 200x magnification. Bar graphs (bottom right) represent the mean ± SEM of the collagen I / collagen III ratio (where the primarily analysis of each represents the protein content per area fraction mean), with n=7-9/group, except with n=4 in S100A9$^{-/-}$ mice. For all graphs, *p<0.05, **p<0.005 and ***p<0.0005. WT=wild-type; CVB3=Coxsackievirus B3.

4.4.8. Impact of S100A9$^{-/-}$ on left ventricular Coxsackievirus B3 copy number and IFN-β expression in Coxsackievirus B3-infected mice

As expected, infected WT and S100A9$^{-/-}$ mice showed a higher CVB3 copy number in comparison to their respective controls **(Figure 4.4.8. A)**. In general, infection of WT and S100A9$^{-/-}$ mice resulted in a 173.0-fold ($p<0.05$) and 204.3-fold ($p<0.0005$) enhancement of IFN-β mRNA levels in comparison to their non-infected controls, respectively **(Figure 4.4.8. B)**. The loss of S100A9 resulted in a 2.3-fold ($p<0.05$) reduction of CVB3 copy number when comparing S100A9$^{-/-}$ CVB3 mice with WT CVB3 **(Figure 4.4.8. A)**. Concomitantly, IFN-β mRNA expression increased 2.0-fold ($p<0.05$) in S100A9$^{-/-}$ CVB3 versus the infected WT group **(Figure 4.4.8. B)**. Given the importance of the Coxsackievirus- and adenovirus receptor (CAR) for the infectivity of cells by CVB3[124], we next evaluated whether the lower CVB3 copy number in S100A9$^{-/-}$ CVB3 versus WT CVB3 mice could be due to differences in CAR expression. S100A9$^{-/-}$ CVB3 mice exhibited 1.5-fold ($p<0.005$) lower CAR mRNA levels compared to WT CVB3 animals (WT: $7.5x10^{-7} \pm 5.9x10^{-8}$ (n=8); S100A9$^{-/-}$: $8.4x10^{-7} \pm 3.4x10^{-8}$ (n=8); WT CVB3: $1.4x10^{-6} \pm 1.1x10^{-7}$ (n=7) versus S100A9$^{-/-}$ CVB3: $9.2x10^{-7} \pm 8.3x10^{-8}$ (n=10).

To further explain the effect of S100A8 and S100A9 on CVB3 copy number, we stimulated HL-1 cells with these two proteins. Complementary to the *in vivo* results, CVB3 S100A8- and CVB3 S100A9-stimulated HL-1 cells both displayed a 2.0-fold ($p<0.0005$) increase of CVB3 copy number compared to the non-stimulated CVB3-infected controls **(Figure 4.4.8. C)**. The mRNA levels of the anti-viral cytokine[125] IFN-β decreased by 4.4-fold ($p<0.0005$) and 7.3-fold ($p<0.0005$) in CVB3 S100A8- and CVB3 S100A9-stimulated HL-1 cells compared to CVB3-infected non-stimulated HL-1 cells, respectively **(Figure 4.4.8. D)**.

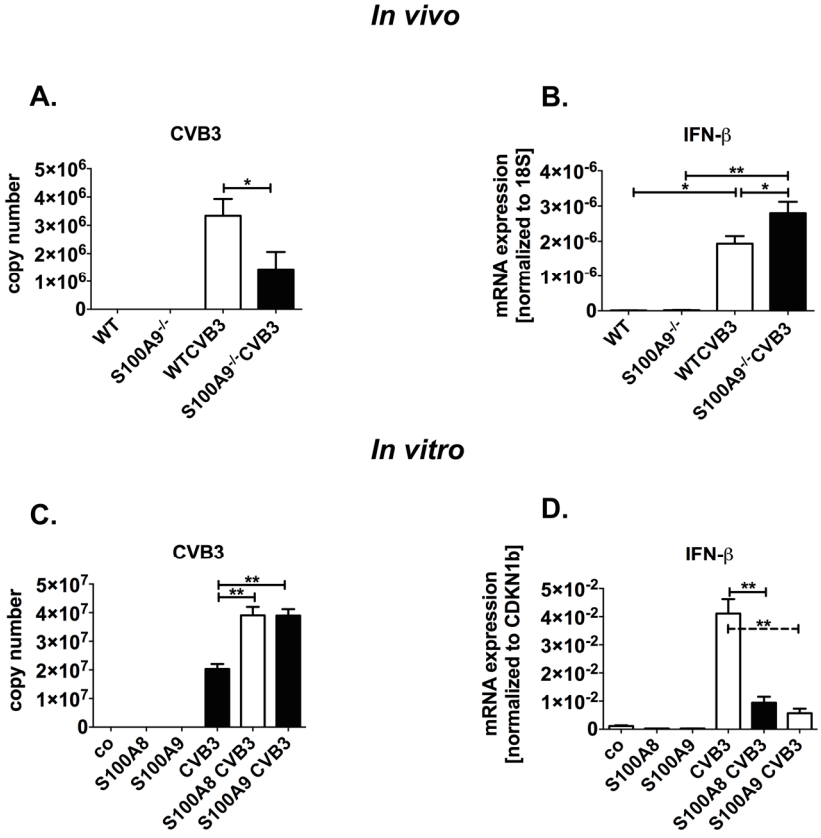

Figure 4.4.8. Impact of S100A8 and/or S100A9 on Coxsackievirus B3 copy number, and IFN-β mRNA expression in Coxsackievirus B3-infected mice and HL-1 cells. Left ventricular (LV) **A.** Coxsackievirus B3 (CVB3) copy number and **B.** mRNA expression of IFN-β in WT CVB3 and S100A9$^{-/-}$ CVB3 mice compared to non-infected control mice. Bar graphs represent the mean ± SEM with n=6-9/group. **C.** CVB3 copy number and **D.** IFN-β mRNA levels in CVB3-infected, CVB3 S100A8- and CVB3 S100A9-stimulated HL-1 cells versus their respective controls, 24 hours post infection and stimulation. Bar graphs represent the mean ± SEM with n=4-6/group. For all graphs, *p<0.05 and **p<0.0005. WT=wild-type; CVB3=Coxsackievirus B3.

4.4.9. Impact of S100A9$^{-/-}$ on left ventricular caspase-1 activity and IL-1β expression in Coxsackievirus B3-infected mice

Reports describing a potential activation of inflammasomes via S100A8 and S100A9[93, 95] have encouraged us to investigate this correlation in LVs of S100A9$^{-/-}$ mice. In general, WT CVB3 mice displayed a 1.4-fold (p<0.05) increase in caspase-1 p10 activity, which is besides p20, the active form of pro-caspase-1[126], compared to control mice **(Figure 4.4.9. A)**. Furthermore, S100A9$^{-/-}$ mice showed a 1.6-fold (p<0.0005) higher caspase-1 p10 protein expression versus WT mice **(Figure 4.4.9. A)**. Indeed, CVB3-infected S100A9$^{-/-}$ mice displayed 1.3-fold (p<0.05) lower protein levels of caspase-1 p10 compared to WT CVB3

mice **(Figure 4.4.9. A)**. The decreased caspase-1 p10 activity in S100A9$^{-/-}$ CVB3 mice was accompanied by a 1.7-fold ($p<0.0005$) lower IL-1β protein expression compared to CVB3 mice **(Figure 4.4.9. B)**. CVB3 WT mice showed no enhanced IL-1β protein levels versus the control group **(Figure 4.4.9. B)**.

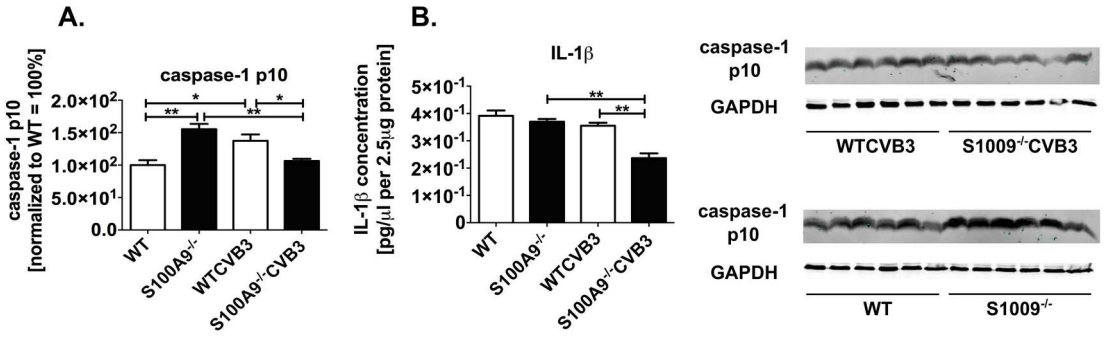

Figure 4.4.9. Impact of S100A9$^{-/-}$ on left ventricular caspase-1 p10 and IL-1β protein levels in Coxsackievirus B3-infected mice. A. Left ventricular (LV) caspase-1 p10 protein levels in WT CVB3 and S100A9$^{-/-}$ CVB3 mice compared to non-infected control mice. The right panel shows representative pictures of the western blot nitrocellulose membranes. Bar graphs (left) show the mean of ± SEM with n=5-6 in WT, S100A9$^{-/-}$, and n=4 in WT CVB3 and S100A9$^{-/-}$ CVB3 mice. **B.** LV IL-1β protein levels in WT CVB3 and S100A9$^{-/-}$ CVB3 mice compared to non-infected mice. Bar graphs represent the mean of ± SEM with n=7-8 in WT, S100A9$^{-/-}$, and WT CVB3, n=10 in S100A9$^{-/-}$ CVB3 mice. For the whole panel with *$p<0.05$ and **$p<0.0005$. WT=wild-type; CVB3=Coxsackievirus B3.

4.4.10. Impact of stimulation and S100A8$^{-/-}$ on NLRP3 expression in Coxsackievirus B3-infected cardiac fibroblasts

Since fibroblasts are activated by macrophage-released S100A8/S100A9[127] and are important for initial inflammasome activation[128], we examined the effect of S100A8 and S100A9 stimulation on the inflammasome activation in cardiac fibroblasts.

In general, CVB3, CVB3 S100A8-, and CVB3 S100A9-stimulated fibroblasts showed 6.0-fold ($p<0.05$), 12.5-fold ($p<0.0005$), and 6.6-fold ($p<0.005$) enhanced NLRP3 mRNA levels compared to the corresponding controls, respectively **(Figure 4.4.10. A)**. Complementary to the *in vivo* data, S100A8 supplementation to CVB3-infected cells resulted in a 1.7-fold ($p<0.05$) enhancement of NLRP3 mRNA expression versus non-stimulated CVB3-infected fibroblasts **(Figure 4.4.10. A)**. S100A9 stimulation of CVB3-infected cells showed no difference versus non-stimulated CVB3-infected fibroblasts. Furthermore, scr siRNA CVB3 fibroblasts showed a 1.6-fold ($p<0.005$) higher NLRP3 mRNA expression versus scr siRNA control cells **(Figure 4.4.10. B)**. In line with the *in vivo* data, S100A8$^{-/-}$ CVB3 fibroblasts

showed a decrease in the inflammasome, as shown by 1.4-fold ($p<0.05$) decreased mRNA levels of NLRP3 compared to the scr siRNA CVB3 group **(Figure 4.4.10. B)**.

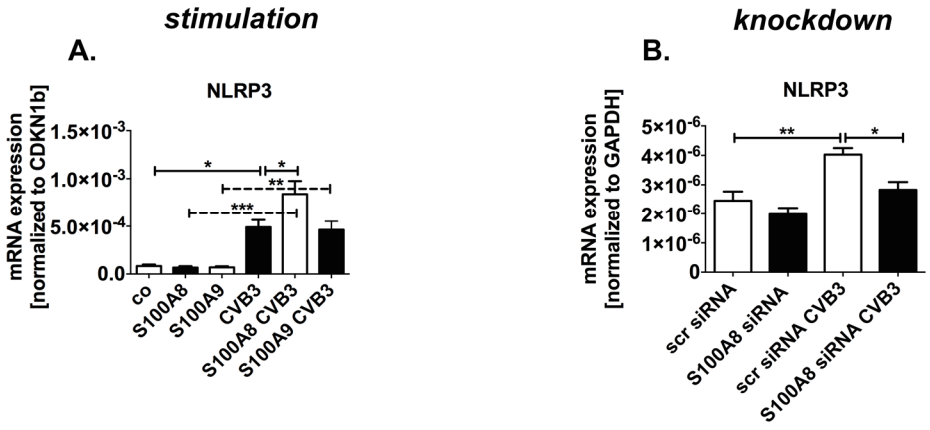

Figure 4.4.10. Impact of stimulation and S100A8$^{-/-}$ on NLRP3 mRNA levels in Coxsackievirus B3-infected cardiac fibroblasts. A. NLRP3 mRNA levels in Coxsackievirus B3 (CVB3)-infected and CVB3 S100A8- or CVB3 S100A9-stimulated fibroblasts versus their respective controls, 24 hours post-infection and stimulation. **B.** NLRP3 mRNA levels in scr siRNA CVB3-infected and S100A8 siRNA CVB3 fibroblasts versus their respective controls, 14 hours post-infection. All data are reported as the mean ± SEM for stimulation experiments with n=5-6/group and for transfection experiments with n=6/group. For all graphs, *$p<0.05$, **$p<0.005$, and ***$p<0.0005$. CVB3=Coxsackievirus B3; siRNA=small interference RNA; scr=scrambled.

4.4.11. Impact of S100A9$^{-/-}$ on left ventricular TLR4/RAGE signaling in Coxsackievirus B3-infected mice

Since S100A8 and S100A9 alarmins are known to signal via TLR4 and/or RAGE[22], we next evaluated the impact of S100A9$^{-/-}$ on TLR4 and RAGE signaling. As shown in **Figure 4.4.11. A**, TLR4 mRNA levels increased 1.8-fold ($p<0.005$) in S100A9$^{-/-}$ CVB3 animals compared to their respective control group. Measurement of TLR4 mRNA levels in WT CVB3 mice showed no difference compared to the WT group **(Figure 4.4.11. A)**. TLR4 mRNA expression was not changed between S100A9$^{-/-}$ CVB3 and WT CVB3 groups **(Figure 4.4.11. A)**. Infection of WT mice resulted in a 5.0-fold ($p<0.0005$) and 5.2-fold ($p<0.005$) enhancement of LV RAGE and its adaptor Dia-1 (Diaphanous-1)[25] mRNA levels compared to WT mice **(Figure 4.4.11. B and E)**, whereas S100A9$^{-/-}$ CVB3 mice showed no increased mRNA levels of RAGE and Dia-1 compared to S100A9$^{-/-}$ mice **(Figure 4.4.11. B and E)**. Furthermore, RAGE and Dia-1 mRNA expression decreased 2.2-fold ($p<0.005$) and 3.0-fold ($p<0.05$) in S100A9$^{-/-}$ CVB3 versus WT CVB3 mice, respectively **(Figure 4.4.11. B and E)**.

Moreover, we evaluated the expression of the downstream targets MyD88 and TRIF, by which RAGE signaling only proceeds via MyD88 and TLR4 signaling via potentially both adaptors[22]. In general, CVB3 infection of WT mice led to a 6.0-fold ($p<0.0005$) and 1.6-fold ($p<0.05$) enhancement of MyD88 and TRIF mRNA expression compared to WT mice, respectively **(Figure 4.4.11. C-D)**. Whereas, S100A9$^{-/-}$ CVB3 animals displayed a 3.7-fold ($p<0.0005$) MyD88 mRNA expression enhancement and a slight, but not significant, elevation of TRIF compared to S100A9$^{-/-}$ animals **(Figure 4.4.11. C-D)**. Neither MyD88 nor TRIF mRNA levels showed any differences between S100A9$^{-/-}$ CVB3 and WT CVB3 animals **(Figure 4.4.11. C-D)**. Moreover, S100A9$^{-/-}$ animals showed a 1.6-fold ($p<0.05$) enhancement of TRIF mRNA **(Figure 4.4.11. D)**, but displayed no change in MyD88 mRNA levels compared to WT mice **(Figure 4.4.11. C)**.

In vivo

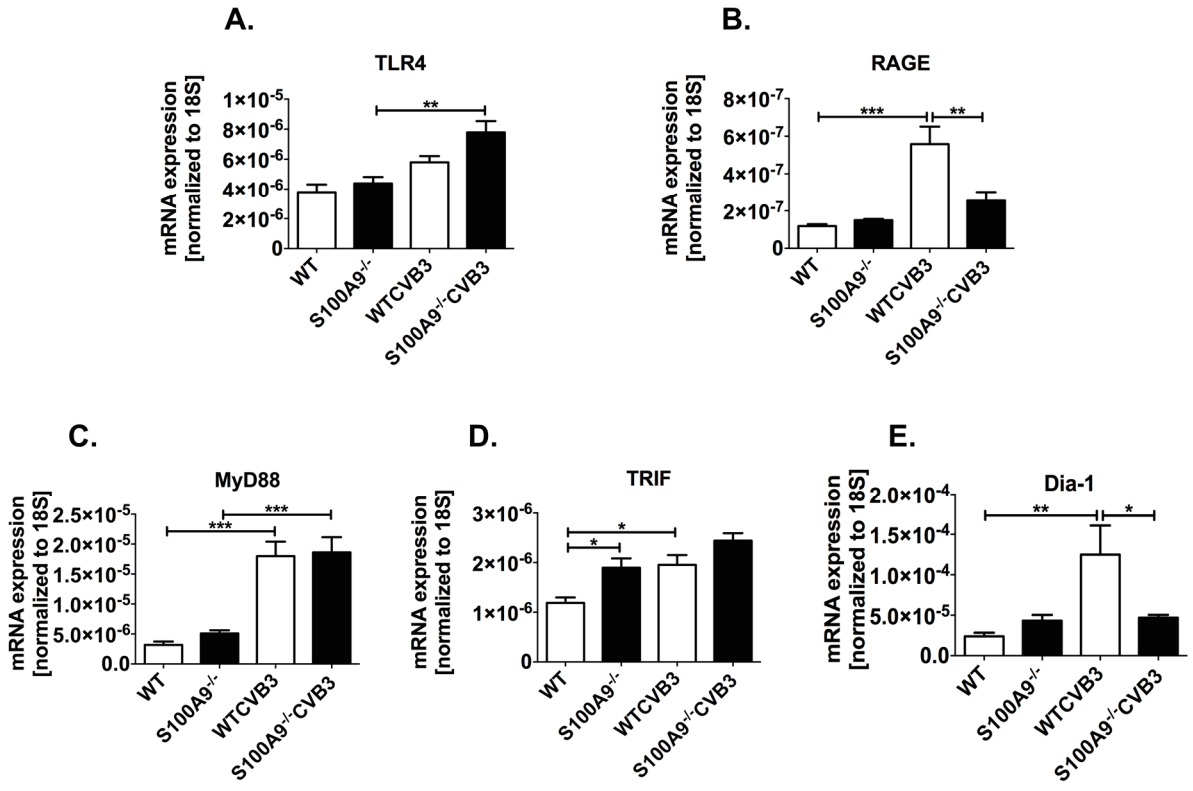

Figure 4.4.11. Impact of S100A9$^{-/-}$ on left ventricular TLR4 and RAGE signaling in Coxsackievirus B3-infected mice. Left ventricular (LV) **A.** TLR4 and **B.** RAGE mRNA expression in WT CVB3 and S100A9$^{-/-}$ CVB3 mice compared to non-infected control mice. Bar graphs represent the mean ± SEM with n=6-10/group. LV mRNA levels of **C.** MyD88, **D.** TRIF, and **E.** Dia-1 in WT, S100A9$^{-/-}$, WT CVB3, and S100A9$^{-/-}$ CVB3 mice. Bar graphs represent the mean ± SEM with n=6-10/group, except for MyD88 with n=5 in WT and S100A9$^{-/-}$ mice. For all graphs, *$p<0.05$, **$p<0.005$, and ***$p<0.0005$. WT=wild-type; CVB3=Coxsackievirus B3.

4.4.12. Impact of S100A8$^{-/-}$ on TLR4/RAGE signaling in Coxsackievirus B3-infected HL-1 cells

Depletion of S100A8 showed no significant effect on TLR4 protein levels, when comparing S100A8 siRNA CVB3 with scr siRNA CVB3 cells, which is in agreement with our *in vivo* observations **(Figure 4.4.12. A)**. Furthermore, scr siRNA CVB3 cells showed no enhanced TLR4 protein levels versus scr siRNA HL-1 cells, which also aligns with the *in vivo* results **(Figure 4.4.12. A)**. Infection of scr siRNA HL-1 cells, led to a 1.4-fold ($p<0.005$) elevation of RAGE protein levels in comparison to scr siRNA cells **(Figure 4.4.12. B)**. According to the *in vivo* data, RAGE expression was decreased in S100A8 siRNA CVB3 HL-1 cells versus scr siRNA CVB3 cells 6 hours post infection, as shown by 1.4-fold ($p<0.05$) lower protein levels **(Figure 4.4.12. B)**.

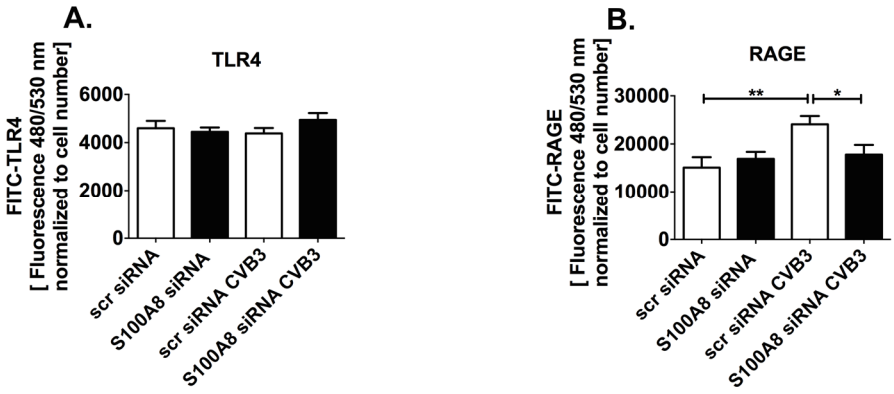

Figure 4.4.12. Impact of S100A8$^{-/-}$ on TLR4 and RAGE protein levels in Coxsackievirus B3-infected HL-1 cells. A. TLR4 and **B.** RAGE protein levels in scr siRNA Coxsackievirus B3 (CVB3)-infected and S100A8 siRNA CVB3 HL-1 cells versus their respective controls, 8 and 6 hours post infection, respectively. All data are reported as the mean ± SEM with n=6-9/group, with *$p<0.05$ and **$p<0.005$. CVB3=Coxsackievirus B3; siRNA=small interference RNA; scr=scrambled.

4.4.13. Impact of S100A9$^{-/-}$ on left ventricular hemodynamic function in Coxsackievirus B3-infected mice

Global heart function was improved in S100A9$^{-/-}$ CVB3 mice compared to WT CVB3 mice, as shown by a 69% ($p<0.0005$), 251% ($p<0.05$), and 343% ($p<0.05$) enhancement of EF, CO, and SW function, respectively **(Table 4.4.13.)**. Moreover, S100A9$^{-/-}$ CVB3 mice exhibited an improved systolic and diastolic function compared to WT CVB3 mice as indicated by 34%

($p<0.05$), 96% ($p<0.05$), and 150% ($p<0.05$) improved LVP_{max}, dP/dt_{max}, and dP/dt_{min}, respectively **(Table 4.4.13.)**.

Table 4.4.13. Hemodynamic function of wild type, S100A9$^{-/-}$ wild type and CVB3-infected mice.

	WT	S100A9$^{-/-}$	WT CVB3	S100A9$^{-/-}$ CVB3
Global cardiac function				
EF (%)	73±3.4	79±1.7	39±5.4***	66±2.5$^{\#\#\#\,\$}$
CO (µl/min)	16778±2213	15354±2341	3933 ±784**	13827±2330$^{\#}$
LVESV (µl)	15±3.0	15 ±3.0	25±7.3	20±4.0
LVEDV (µl)	47±5.4	38±5.1	32 ±5.2	49±8.4
SV (µl)	34±4.0	30±4.0	11±1.4**	31±5.0$^{\#}$
SW (mmHg/ml)	2177±307	1936 ±371	353±22**	1565±264$^{\#}$
Systolic function				
LVP_{max} (mmHg)	82±4.0	72±3.0	41±3.0***	55±3.5$^{\#\,\$}$
dP/dt_{max} (mmHg/s)	6183±660	5412±556	2616±330**	5118±615$^{\#}$
Diastolic function				
LVEDP (mmHg)	2.0±0.3	2.0±0.1	6.1±0.2***	2.6±0.4$^{\#\#\#}$
dP/dt_{min} (mmHg/s)	-3955±385	-3535±337	-1236±108***	-3091±440$^{\#}$
Tau (ms)	11 ±0.4	12±0.4	18±2.0***	11±0.3$^{\#\#\#}$

All data are reported as the mean ± SEM. (EF=ejection fraction, CO=cardiac output, LVESV=end-systolic left ventricular (LV) volume, LVEDV=end-diastolic LV volume, SV=stroke volume, SW=stroke work, LVP_{max}=maximum LV pressure, dP/dt_{max}=maximal LV pressure rise rate, LVEDP=end-diastolic LV pressure, dP/dt_{min}=maximum LV pressure drop rate, Tau=time of the LV pressure decrease, *$p<0.05$, **$p<0.005$, ***$p<0.0005$ versus WT mice, #$p<0.05$, ##$p<0.005$, and ###$p<0.0005$ versus WT CVB3 mice, \$$p<0.05$ versus S100A9$^{-/-}$).

4.4.14. Impact of S100A8 supplementation on left ventricular Coxsackievirus B3 copy number, inflammation, and left ventricular function in S100A9$^{-/-}$ Coxsackievirus B3-infected mice

To further confirm the deteriorating effect of S100A8 and S100A9, we supplemented S100A8, which is the active part of the heterodimer S100A8/S100A9[33], to S100A9$^{-/-}$ CVB3 mice. S100A8 supplementation resulted in a higher CVB3 copy number (S100A9$^{-/-}$ CVB3: $1.2x10^6 \pm 0.54x10^6$ (n=4) versus S100A9$^{-/-}$ CVB3+S100A8: $5.6x10^6 \pm 1.4x10^6$ (n=6); $p<0.05$), an enhanced LV mRNA expression of IL-6 (S100A9$^{-/-}$ CVB3: $1.0\ x10^{-7} \pm 3.2x10^{-8}$ (n=5) versus S100A9$^{-/-}$ CVB3+S100A8: $3.8x10^{-7} \pm 4.7x10^{-8}$ (n=6); $p<0.005$), TNF-α (S100A9$^{-/-}$ CVB3: $5.0x10^{-7} \pm 4.1x10^{-8}$ (n=4) versus S100A9$^{-/-}$ CVB3+S100A8: $1.7x10^{-6} \pm 2.7x10^{-7}$ (n=6); $p<0.05$), and IL-1β (S100A9$^{-/-}$ CVB3: $3.0x10^{-7} \pm 6.9x10^{-8}$ (n=4) versus S100A9$^{-/-}$ CVB3+S100A8:

$5.9x10^{-7}$ ± $5.1x10^{-8}$ (n=6); p<0.05) Global heart function was impaired in S100A9$^{-/-}$ CVB3+S100A8 mice compared to S100A9$^{-/-}$ CVB3 mice, as shown by a 51% (p<0.0005), 56% (p<0.005), and 74% (p<0.0005) decrease of EF, CO, and SW function versus S100A9$^{-/-}$ CVB3 mice, respectively **(Table 4.4.14.)**. Moreover, S100A9$^{-/-}$ CVB3+S100A8 mice exhibited a decreased systolic and diastolic function compared to S100A9$^{-/-}$ CVB3 mice as indicated by a 49% (p<0.0005), 60% (p<0.0005), and 66% (p<0.0005) impaired LVP_{max}, dP/dt_{max}, and dP/dt_{min}, versus S100A9$^{-/-}$ CVB3 mice, respectively **(Table 4.4.14.)**.

Table 4.4.14. Left ventricular hemodynamic function of CVB3-infected S100A9$^{-/-}$ animals with and without co-treatment of S100A8

	S100A9$^{-/-}$ CVB3	**S100A9$^{-/-}$ CVB3+S100A8**
Global cardiac function		
HR (bpm)	557.7 ± 37.6	490.9 ± 27.3
EF (%)	72 ± 1.7	35 ± 2.1***
CO (µl/min)	15,385 ± 1449	6,823 ± 1180**
LVESV (µl)	11 ± 1.1	28 ± 4.6*
LVEDV (µl)	38 ± 3.4	41 ± 6.6
SV (µl)	28 ± 3.0	14 ± 2.5*
SW (mmHg/ml)	1,892 ± 165.2	496.6 ± 142.0***
Systolic function		
LVP_{max} (mmHg)	79 ± 1.7	40 ± 3.0***
dP/dt_{max} (mmHg/s)	7,647 ± 654.6	3,027 ± 264.8***
Diastolic function		
LVEDP (mmHg)	1.2 ± 0.4	4.3 ± 0.4***
dP/dt_{min} (mmHg/s)	-5,179 ± 236	-1,755 ± 248.5***
Tau (ms)	8.7 ± 0.6	13 ± 1.1*
PHT (ms)	4.4 ± 0.3	7.9 ± 0.8**

All data are reported as the mean ± SEM. (HR=heart rate, EF=ejection fraction, CO=cardiac output, LVESV=end-systolic left ventricular (LV) volume, LVEDV=end-diastolic LV volume, SV=stroke volume, SW=stroke work, LVP_{max}=maximum LV pressure, dP/dt_{max}=maximal LV pressure rise rate, LVEDP=end-diastolic LV pressure, dP/dt_{min}=maximum LV pressure drop rate, Tau=time of the LV pressure decrease, PHT=pressure half time, *p<0.05, **p<0.005, ***p<0.0005 vs S100A9$^{-/-}$ CVB3 mice. The unpaired t-test was used.

5. DISCUSSION

In the present study, we further confirmed the relevance of NOD2 in CVB3-induced myocarditis and demonstrated its link to the NLRP3 inflammasome. Briefly, within the medical doctoral thesis of *Xia Yu*, our group recently demonstrated that NOD2$^{-/-}$ mice are protected from the deleterious CVB3-induced effects as demonstrated by reduced amounts of cardiac inflammation, cardiac fibrosis, apoptosis, and CVB3 copy number, and an ameliorated LV function in NOD2$^{-/-}$ CVB3 mice versus WT CVB3 mice. Based on these *in vivo* findings, we further confirmed the protective role of a NOD2 knockdown *in vitro*, by showing an impaired CVB3-mediated inflammatory effect **(Figure 4.3.6. A-B)**, lower CVB3 copy number and less apoptosis *in vitro* **(Figure 4.3.7. A-B)**. Further investigation on downstream signaling pathways revealed that a NOD2$^{-/-}$ in both *in vivo* and *in vitro* experiments was associated with a decreased NLRP3 expression and/or activity **(Figure 4.3.4. A-C and Figure 4.3.5. B-F)** and was accompanied by suppressed TLR4 signaling **(Figure 4.3.2. B-E and Figure 4.3.3. B-E)**. In a second study, we demonstrated the relevance of the DAMPs S100A8 and S100A9 and their link to the inflammasome system and RAGE/Dia-1 signaling pathway in CVB3-induced myocarditis. This follows from the observations that CVB3-infected S100A9$^{-/-}$ mice showed an improved LV function (**Table 4.4.13.)**, and lower MIP-2 expression **(Figure 4.4.2. A)**, associated with less cardiac infiltrates of neutrophils and monocytes **(Figure 4.4.3. A-C)**, as well as reduced oxidative stress **(Figure 4.4.4. A-B)**, lower CAR expression **(paragraph 4.4.8.)** lower CVB3 copy number **(Figure 4.4.8. A)**, decreased caspase-1 activity **(Figure 4.4.9. A)**, and a diminished RAGE and Dia-1 expression **(Figure 4.4.11. B and E)** compared to WT CVB3 mice. Intraperitoneal application of S100A8 in S100A9$^{-/-}$ CVB3 mice enhanced the CVB3 copy number and cardiac inflammation versus S100A9$^{-/-}$ CVB3 mice and resulted in an impaired cardiac function **(paragraph 4.4.14.)**. In accordance with our *in vivo* findings, we confirmed the deteriorating effects of S100A8 and S100A9 also *in vitro*, where stimulation with S100A8 or S100A9 of CVB3-infected cells, such as RAW macrophages, HL-1 cells and cardiac fibroblasts, resulted in an enhanced MIP-2 expression **(Figure 4.4.2. B)**, higher oxidative stress **(Figure 4.4.5.)**, higher CVB3 copy number **(Figure 4.4.8. C)**, and enhanced NLRP3 inflammasome expression **(Figure 4.4.10. A)**. Whereby S100A8$^{-/-}$ in RAW cells resulted in lower MIP-2 expression **(Figure 4.4.2. C)** and S100A8$^{-/-}$ in cardiac fibroblasts led to lower NLRP3 inflammasome expression **(Figure 4.4.10. B)**. Finally, the relevance of NOD2, S100A8, and S100A9 follows from our observations in EMBs of CVB3-positive patients who express more NOD2, S100A8, and S100A9 versus CVB3-negative patients **(Figure 4.1.1. A-**

C), and from the findings that NOD2, S100A8, and S100A9 expression drops in EMBs of CVB3-positive patients, who eliminated the virus over time **(Figure 4.1.2. A, D, E)**.

5.1. NOD2, NLRP3, IL-1β, S100A8, and S100A9 expression is associated with pathophysiological effects in myocarditis patients and in Coxsackievirus B3-infected mice

5.1.1. Association of NOD2, NLRP3, IL-1β, S100A8, and S100A9 expression with the myocarditis state in myocarditis patients and Coxsackievirus B3-infected mice

The first evidence for the detrimental role of NOD2, S100A8, and S100A9 in viral-myocarditis was given by enhanced mRNA levels in EMBs of CVB3-positive myocarditis patients versus controls **(Figure 4.1.1. A-C)**. In line with these clinical data, we saw enhanced levels of NOD2, S100A8, and S100A9 in LVs of CVB3-infected mice compared to control mice **(Figure 4.2.1. A-C)**. Recently, the key role of NOD2 in the recognition of ssRNA viruses was discovered[52]. Since CVB3 is a ssRNA virus, our data emphasises the role of NOD2 in detecting ssRNA viruses. In respect to the alarmins, enhanced cardiac S100A8 and S100A9 levels have been detected in mouse models of doxorubicin-induced cardiac dysfunction[129] and post-ischemic HF[130]. As far as we know, we were able to show for the first time that these alarmins are elevated in EMBs of CVB3-positive myocarditis patients. The group of Katashima *et. al.*[131] showed that patients with acute myocardial infarction displayed enhanced cardiac S100A8 and S100A9 levels. Moreover, clinical evidence highlights that high plasma levels of S100A8/S100A9 are a risk factor for future myocardial infarcts and cardiovascular death in healthy individuals[65]. The potential use of plasma levels of S100A8/S100A9 as a biomarker for myocarditis and/or to follow the course of myocarditis will be further investigated in detail in the future (see outlook).

Some patients are able to eliminate the virus accompanied with a decline in inflammation and undergo recovery[13]. We were able to demonstrate, that enhanced levels of NOD2, NLRP3, IL-1β, S100A8, or S100A9 expression in EMBs are elevated under pathological conditions **(Figure 4.1.2. A-E)**. Additionally, for the first time to our knowledge, we were able to show that a decrease of NOD2, NLRP3, IL-1β, S100A8, and S100A9 is associated with an improved clinical course, as displayed in CVB3-positive patients, who eliminated the CVB3 virus over time **(Figure 4.1.2. A-E)**. Moreover, the group of Wang *et al.*[88] elucidated the

importance of the NLRP3 inflammasome in the pathophysiology of experimental CVB3-induced myocarditis. Additionally, Toldo *et al.*[86] revealed a positive correlation between a detoriating NYHA class, indicative for a worse cardiac condition[132], and enhanced NLRP3 inflammasome activity in biopsies of myocarditis patients.

5.2. Effect of NOD2$^{-/-}$ in experimental Coxsackievirus B3 myocarditis models

5.2.1. NOD2$^{-/-}$ decreases NLRP3 inflammasome formation in experimental Coxsackievirus B3 myocarditis models

In the present investigation, we demonstrated that the NOD2 receptor plays a crucial role in mediating NLRP3 inflammasome activation in experimental CVB3-induced myocarditis and *in vitro* experiments **(Figure 4.3.4. A-C and Figure 4.3.5. B-F)**. Considering the diversity of molecules capable of triggering NLRP3 inflammasome assembly, the demand for specific checkpoints, such as NLRP3 priming at a transcriptional level, is necessary to avoid a deceptive immune response[72, 80]. The initial priming step, which is up-stream of NLRP3 activation, includes among others the NOD2 and TLR4 receptor, but by two discrete initial pathways which in general lead to NF-κB activation and enhancement of pro-IL-1β and NLRP3 transcription. In contrast, the other NLRP3 imflammasome components, such as ASC and pro-caspase-1 are present in requisite concentrations[72, 80]. In general, stimulation of NOD2 recruits the RIPK2 adaptor, which subsequently activates NF-κB[45]. Indeed, in our *in vivo* and *in vitro* experiments, CVB3 infection resulted in transcript enhancement of RIPK2 **(Figure 4.3.2. and Figure 4.3.3., A)** and of the downstream NLRP3 target **(Figure 4.3.4. A and Figure 4.3.5. B)**. This induction was abolished by NOD2 knockdown, which confirms the role of NOD2 in the transcriptional priming of NLRP3. The NLRP3 transcriptional priming signaling, immediately downstream of TLR4, includes MyD88 recruitment, resulting in NF-κB activation as well[72, 80].

Furthermore, our data support a positive synergy between TLR4 and NOD2. In detail, TLR4 mRNA or protein expression and downstream signaling including MyD88 are lower in the NOD2$^{-/-}$ CVB3 or NOD2 siRNA CVB3 groups versus the corresponding CVB3-infected groups, respectively, whereas NOD2 ablation had no effect on TLR4 levels in control mice or under basal conditions **(Figure 4.3.2. and Figure 4.3.3., B-C)**. Interestingly, TRIF mRNA expression was only decreased in NOD2 siRNA CVB3 versus scr siRNA CVB3 HL-1 cells **(Figure 4.3.3. D)**, but not in the LV of NOD2$^{-/-}$ CVB3 versus WT CVB3 mice **(Figure 4.3.2.**

D). The connection between NOD2 and TLR4 is further supported by Farzi *et al.*[133], who recently reported that NOD2 stimulation exacerbates the LPS-induced TLR4 immune response. On the other hand, Zong *et al.*[134] demonstrated increased TLR4 mRNA and protein expression in NOD2 knockout mice in a pressure overload mouse model, indicating that further investigation is needed to shed more light on the interaction between NOD2 and TLR4. Besides the transcriptional-dependent priming described, also a transcriptional-independent priming mechanism of the NLRP3 inflammasome exists. This has been described for the TLR4/MyD88 signaling, which leads to an immediate NLRP3 inflammasome activation within 10 minutes, whereas the transcriptional-dependent priming takes 2 hours for NLRP3 up-regulation[81].

Two other groups showed that via the TLRs/MyD88/IRAK1 signaling pathway, a direct and priming-independent activation of NLRP3 inflammasome is possible, through direct interaction of IRAK1 with ASC[82, 83]. A transcriptional priming-mechanism via NOD2 receptor seems possible since we demonstrated an elevation of mRNA levels of NLRP3 *in vitro*, which was disrupted after NOD2 knockdown **(Figure 4.3.5. B)**. Whether NOD2 is also involved in a transcriptional-independent or even direct activation mechanism in the context of CVB3 has to be clarified by further experiments with earlier time points on mRNA and protein levels. The idea that NOD2 could act as a post-transcriptional primer or even as a direct activator of the NLRP3 inflammasome is supported by Wagner *et al.*[90], who showed direct interaction between NOD2 and NLRP3. Collectively, the link between NOD2 and the NLRP3 inflammasome seems to play a pivotal role in the inflammatory disorder of CVB3-induced myocarditis.

5.2.2. NOD2$^{-/-}$ decreases inflammation, Coxsackievirus B3 copy number, and apoptosis in experimental Coxsackievirus B3 myocarditis models

Cardiac damage occurs via a direct CVB3-induced cardiomyocyte cytopathic effect[135, 136] and results in an increased inflammatory response involving an induction of chemokines and pro-inflammatory cytokines such as MCP-1, TNF-α, and IL-6[114, 137-139]. Shortly, within the doctoral thesis of *Xia Yu*, our group demonstrated recently that LV expression of MCP-1 was significantly lower in NOD2$^{-/-}$ CVB3 mice compared to WT CVB3. This was accompanied by decreased cardiac infiltration of macrophages (CD68^{+}) and T cells (CD3^{+} and CD4^{+}) into the LVs of NOD2$^{-/-}$ CVB3 compared to WT CVB3 mice. Additionally, the increased LV MCP-1 mRNA expression and cardiac infiltration of immune cells was associated with an enhanced

mRNA expression of pro-inflammatory cytokines such as TNF-α and IL-6 in WT CVB3 mice compared to control mice as shown by Gui *et al.*[7]. In contrast, NOD2$^{-/-}$ CVB3 mice expressed lower LV mRNA levels of TNF-α and IL-6 compared to WT CVB3 mice. In the context of these *in vivo* findings, we were further able to show that the inflammatory response in NOD2 siRNA CVB3-infected HL-1 cells was diminished compared to scr siRNA CVB3 cells **(Figure 4.3.6. A-B)**. This impaired inflammatory response in HL-1 cells compared to controls might be explained by a decrease in the NF-κB signaling pathway as shown by the finding that NOD2 knockdown in cells diminishes NF-κB phosphorylation, and subsequent levels of TNF-α and IL-6 upon stimulation with the porcine reproductive respiratory syndrome virus[53]. Besides pro-inflammatory cytokines, anti-viral LV IFN-β and IFN-γ are induced in CVB3 mice[125, 140, 141]. Referring to the findings of *Xia Yu*, our group demonstrated that IFN-β and IFN-γ mRNA expression was less pronounced in NOD2$^{-/-}$ CVB3 animals compared to WT CVB3 mice. In agreement with these *in vivo* data, we further demonstrated that infected NOD2 siRNA HL-1 cells expressed less IFN-β mRNA than the infected scr siRNA cells **(Figure 4.3.3. E)**. These results in turn correspond with the findings of Sabbah *et al.*[52], who demonstrated that NOD2 mediates IFN-β production in cells stimulated *in vitro* with ssRNA. Interestingly, another study demonstrated that IFN-β is not only critical for control of viral propagation, but also potentiates the NOD1/NOD2 signaling pathway and thus harmful cytokines[142]. Despite the decreased anti-viral IFN-β expression, CVB3 copy number was reduced in NOD2 siRNA CVB3 compared to scr siRNA CVB3 HL-1 cells **(Figure 4.3.7. A)**. CVB3 replication relies on the autophagosome and subsequently induces its release via apoptosis[114, 136]. Since NOD2 induces autophagy and potentially interacts with the apoptotic pathway[44, 143], ablation of NOD2 may account for the impairment of these phenomena and subsequent reduction in viral copy number in NOD2$^{-/-}$ CVB3 compared to WT CVB3 mice and respective NOD2 siRNA CVB3 versus scr siRNA CVB3 HL-1 cells. Our *in vitro* examinations confirmed lower apoptosis in NOD2 siRNA CVB3 compared to scr siRNA CVB3 HL-1 cells **(Figure 4.3.7. B)**. Furthermore, CVB3 infects not only cardiomyocytes, but also cells of the immune system, including CD4^{+} T cells, which contribute to viral persistence[144]. Given the importance of the cardiosplenic axis in CVB3-induced myocarditis[137, 145, 146], the impaired cardiac infiltration of CD4^{+} T cells in NOD2$^{-/-}$ CVB3 mice compared to WT CVB3, as reported by *Yu Xia*, as well as the lower viral copy number in the spleen of NOD2$^{-/-}$ CVB3 versus WT CVB3 mice, both might have further contributed to the lower LV CVB3 copy number in NOD2$^{-/-}$ CVB3 versus WT CVB3 mice. Collectively, the diminished inflammatory response in NOD2 siRNA CVB3 HL-1 cells compared to scr siRNA CVB3 cells was consistent with the previous *in vivo* findings in NOD2$^{-/-}$ CVB3 mice.

5.3. Effect of S100A8 and S100A9 in experimental Coxsackievirus B3 myocarditis models

5.3.1. S100A9$^{-/-}$ decreases inflammatory cell infiltration and oxidative stress in experimental Coxsackievirus B3 myocarditis models

As noted above, cardiac damage is caused by a direct CVB3-induced cardiomyocyte cytopathic effect[135, 136] and results in an increased inflammatory response involving an induction of chemokines such as MIP-2, which is produced by monocytes and neutrophils[119, 147] and plays a crucial role in the inflammatory course of CVB3-induced myocarditis by attracting inflammatory cells to the heart[118]. Our results showed an enhanced MIP-2 mRNA expression in LVs of CVB3-infected mice, whereas S100A9$^{-/-}$ CVB3 mice showed abrogated MIP-2 mRNA expression compared to infected WT mice **(Figure 4.4.2. A)**, which was confirmed by our *in vitro* S100A8 knockdown experiment, where S100A8 siRNA CVB3 RAW cells showed lower MIP-2 levels versus scr siRNA CVB3 cells **(Figure 4.4.2. C)**. On the other hand, S100A8 and S100A9 stimulation of CVB3-infected RAW cells enhanced MIP-2 levels versus non-stimulated CVB3-infected RAW cells **(4.4.2. B)**. Our data are supported by Vogl *et al.*[33], who demonstrated decreased MIP-2 expression after LPS stimulation of bone marrow-derived cells originated from S100A9$^{-/-}$ mice compared to those of WT mice. Furthermore, in the course of decreased MIP-2 levels, S100A9$^{-/-}$ CVB3 mice exhibited lower mRNA levels of Ly6g^{+} and Ly6c^{+} and less infiltration of CD68^{+} monocytes compared to WT CVB3 mice **(Figure 4.4.3**. **A-C)**. S100A8 and S100A9 also have their own chemo-attractant properties and are crucial for the recruitment of neutrophils and monocytes[148-150]. Therefore, the loss of S100A9 and S100A8 may account for the diminished neutrophil and monocyte invasion described above, either directly or indirectly via downregulated MIP-2 expression. The mechanism, which influences phagocyte migration, is regulated by tubulin polymerization via S100A8 and S100A9[148]. Overall, these findings concur with previous studies, which showed a diminished leukocyte presence as a common feature in S100A9$^{-/-}$ mice, which were protected from symptoms including endotoxin-induced shock, acute pancreatitis, and atherosclerosis[33, 149, 151]. The reduced infiltration of neutrophils and monocytes in S100A9$^{-/-}$ CVB3 mice compared to WT CVB3 mice was accompanied by reduced LV MPO activity **(Figure 4.4.4**. **A)**. MPO is mainly stored in primary granules of neutrophils and macrophages[152]. These findings are corroborated by Schenkenberg *et al.*[151], who showed a reduced MPO activity in a S100A9$^{-/-}$ pancreatitis mouse model and by Averill

et al.[153], who confirmed this in a S100A9$^{-/-}$ atherosclerosis model. MPO contributes to oxidative stress[152] by chlorinating molecules, following the generation of hypochlorous acid from hydrogen peroxide and chloride ions[154]. Investigations showed enhanced plasma MPO chlorination activity in elderly chronic HF patients and suggest an involvement in HF progression[152]. A further cause of oxidative stress is the NADPH oxidase complex, which is a major source of ROS[155]. Activation of the NADPH oxidases complex has been shown in HF patients, which may play a critical pathophysiological role in cardiac dysfunction[155]. Additionally, experimental studies showed a pathogenic role of oxidative stress in failing hearts[156, 157]. S100A8 and S100A9 are important activators of NADPH oxidase and consequently of ROS production, by which S100A8/S100A9 transfers the cofactor arachidonic acid to NADPH oxidases[158]. Our investigations showed a decreased LV mRNA expression of Nox1, which comprises one of the seven NADPH oxidase members[159], in S100A9$^{-/-}$ CVB3 versus WT CVB3 mice **(Figure 4.4.4**. **B)**. An additional association of S100A8 and S100A9 with ROS production was obvious in our *in vitro* experiment, where S100A8 or S100A9 stimulation of CVB3-infected cells resulted in elevated ROS protein production compared to non-stimulated CVB3 cells **(Figure 4.4.5.)**. Collectively, S100A9$^{-/-}$ CVB3 mice showed a prominent reduction of oxidative stress versus WT CVB3 animals, which indicates an important role of S100A8 and S100A9 in oxidative stress by CVB3-induced myocarditis.

5.3.2. S100A9$^{-/-}$ decreases Coxsackievirus B3 copy number and inflammasome expression in experimental Coxsackievirus B3 myocarditis models

S100A8 and S100A9 are elevated in patients with viral infection[69], such as human papillomavirus[67], acute respiratory syndrome[68] and HIV-1[160]. With respect to HIV-1, Ryckman *et al.*[70] showed that both S100A8 and S100A9 alarmins induce HIV-1 transcription activity and virus replication in CD4^{+} T-lymphocytes. Also, ROS production is associated with the replication of CVB3 in cells[161]. Our observation that CVB3 copy number levels are reduced in S100A9$^{-/-}$ CVB3 versus WT CVB3 animals **(Figure 4.4.8. A**), which also exhibit decreased MPO levels and Nox1 expression **(Figure 4.4.4.)**, indicating less oxidative stress, are consistent with these published results. Concomitantly, the anti-viral cytokine[125] IFN-β was enhanced in S100A9$^{-/-}$ CVB3 versus WT CVB3 mice **(Figure 4.4.8**. **B)**. Furthermore, the decreased CVB3 copy number in infected animals might be explained by the lower cardiac expression of CAR **(paragraph 4.4.8.)**, relevant for CVB3 uptake,[124] compared to WT CVB3

mice. *In vitro*, S100A8 or S100A9 stimulation of CVB3-infected HL-1 cells resulted in elevated CVB3 copy number and was accompanied by reduced IFN-β levels versus non-stimulated CVB3-infected cells, which complements the *in vivo* results **(Figure 4.4.8. C and D)**. In summary, the reduced CVB3 copy number levels *in vivo* are associated with; 1) reduced CD68 macrophage infiltration, which contributes to viral persistence since macrophages as well as cardiomyocytes are infected by CVB3 virus[144]; 2) reduced oxidative stress, which is mainly induced by inflammatory cells such as macrophages[162, 163]; 3) enhanced IFN-β levels; and 4) lower CAR levels. In addition, i.p. application of S100A8 to S100A9$^{-/-}$ CVB3 mice increased the CVB3 copy number versus S100A9$^{-/-}$ CVB3 mice, further confirming the deterimental character of this alarmin **(paragraph 4.4.14.)**.

Interestingly, S100A9$^{-/-}$ CVB3-infected mice exhibited decreased activity of the pyroptosis marker and NLRP3 inflammasome component caspase-1[72, 73] versus CVB3-infected mice **(Figure 4.4.9. A)**. This was then translated into lower mature IL-1β levels compared to WT CVB3 mice **(Figure 4.4.9. B)**. Intriguingly, a similar observation has been made in a study where caspase-1-induced pyroptosis of human HIV-1-infected CD4^{+} T-lymphocytes was the main trigger for cell death[164]. Finally, Gastaldello *et al.*[165] described the capability of caspase-1 to promote viral replication, as shown for the Epstein-Barr virus. Due to these observations, the decreased caspase-1 activity in our S100A9$^{-/-}$ CVB3 model compared to WT CVB3 mice could probably also account for the diminished CVB3 copy number. In two further experiments, we could confirm the role of S100A8 in the regulation of the NLRP3 inflammasome, where S100A8 supplementation to CVB3-infected fibroblasts led to an elevation of NLRP3 expression compared to non-stimulated CVB3-infected cells **(Figure 4.4.10. A)**, whereas S100A9 stimulation of CVB3-infected fibroblasts led to no enhancement of NLRP3 compared to non-stimulated CVB3-infected cells **(Figure 4.4.10. A)**. Knockdown of S100A8 in CVB3-infected fibroblasts resulted in diminished NLRP3 expression compared to scr siRNA CVB3 cells **(Figure 4.4.10. B)**. S100A8 seems to be involved in NLRP3 inflammasome activation probably via ROS enhancement, which has been described previously by Simard *et al.*[93]. The enhanced IFN-β levels in S100A9$^{-/-}$ CVB3 animals versus WT CVB3 mice could also be a source of the diminished IL-1β levels, since an inhibiting effect of IFN-β on the inflammasome and thus IL-1β has also been shown[166]. The reduced caspase-1 activity and IL-1β expression in S100A9$^{-/-}$ CVB3 mice versus WT CVB3 animals further supports the impact of S100A8 and S100A9 on pyroptosis under CVB3 conditions.

5.3.3. S100A9$^{-/-}$ attenuates RAGE signaling in experimental Coxsackievirus B3 myocarditis models

As noted previously, S100A8 and S100A9 belong to the DAMP family[39, 167] and are abundantly expressed by neutrophils and monocytes[19]. S100A8 and S100A9 are associated with autoimmune and inflammatory disorders, such as arthritis[39], systemic lupus erythematosus[40] and Crohn's disease[41]. Furthermore, S100A8/S100A9 serve as an excellent biomarker in rheumatoid arthritis, juvenile idiopathic arthritis, and inflammatory bowel disease[42]. S100A8, S100A9, and S100A8/S100A9 are ligands of TLR4[33] and RAGE[168], whereby both receptors share the adaptor MyD88 to initiate downstream signaling[22]. Vogl *et al.*[33] demonstrated for the first time that S100A8/S100A9 signal via TLR4 and promote lethal endotoxin-induced shock. Further studies indicated the involvement of S100A8/S100A9 and TLR4 in diseases such as lung injury[169], arthritis[170] and acute coronary syndrome[63]. In cancer, S100A8/S100A9 signals via RAGE[168]. In addition, S100A8 and S100A9 promote endotoxin-induced cardiomyocyte dysfunction via RAGE[171] and post-ischemic HF is aggravated via S100A8/S100A9 initiated activation of the RAGE signaling cascade[130]. Furthermore, neutrophil-released S100A8/S100A9 activates cardiac fibroblasts via RAGE and leads to an angiotensin II-induced cardiac inflammation and injury[172]. Bangert *et al.*[173] established further evidence for the involvement of RAGE in inflammatory heart disease. The group of Yu[174] demonstrated a role for the RAGE/NF-κB axis in CVB3-induced myocarditis. Recently, Hofer *et al.*[175] showed that S100A8/S100A9 mediates inflammation via RAGE in patients with septic shock. In agreement with all the RAGE-related studies mentioned, our investigations showed that S100A9$^{-/-}$ CVB3 mice exhibited reduced RAGE mRNA levels **(Figure 4.4.11. B)**, whereas TLR4-TRIF **(Figure 4.4.11. A and D)** and MyD88 **(Figure 4.4.11. C)** expression was unaltered compared to CVB3 mice. *In vitro*, we confirmed these results for S100A8, where S100A8 siRNA CVB3 HL-1 cells also showed unchanged TLR4 expression and decreased RAGE levels versus CVB3-infected scr siRNA cells **(Figure 4.4.12. A-B)**. Multiple signaling pathways can be initiated via RAGE, which are also initiated by TLR4, including Ras-mediated ERK, Akt, JNK, p38 MAPK, and small GTPase Cdc42/Rac1, which activate various transcription factors such as NF-kB and Egr-1[22, 24]. Besides the transduction pathway via MyD88, RAGE initiates signaling pathways via a newly discovered binding partner called Dia-1, which is required for the activation of Rac-1 and Cdc42 and thus controls cellular migration[25] and ROS production, via activation of NADPH oxidase[26]. Interestingly, we confirmed the involvement of the adaptor Dia-1, since S100A9$^{-/-}$

CVB3 mice showed lower Dia-1 expression compared to WT CVB3 animals. Based on our findings where S100A9$^{-/-}$ CVB3 mice compared to CVB3 littermates exhibited reduced RAGE and Dia-1 levels **(Figure 4.4.11. B and E)**, decreased inflammatory cell migration **(Figure 4.4.3. A-C)** and reduced oxidative stress **(Figure 4.4.4. A-B)**, while TLR4/TRIF **(Figure 4.4.11. A and D)** and MyD88 **(Figure 4.4.11. C)** expression stayed unaltered, we suggest that RAGE and Dia-1 downregulation could account for the diminished cell migration and reduced NADPH oxidase activity. In summary, these data indicate a possible signaling pathway of S100A8 and S100A9 via RAGE and Dia-1 in CVB3-induced myocarditis. This connection needs to be investigated in detail. As mentioned in the introduction, the specific receptors and pathways for all three alarmin combinations, S100A8/S100A8, S100A9/S100A9, and S100A8/S100A9, depends on the cell type[36] and probably also on the disease.

5.3.4. S100A9$^{-/-}$ improves cardiac function in Coxsackievirus B3-infected mice

S100A9$^{-/-}$ CVB3 mice showed a less pronounced cardiac dysfunction, which was demonstrated by an improved systolic and diastolic function versus CVB3 mice **(Table 4.4.13.)**, which could be abolished by exogenous S100A8 application, indicating the significant and specific involvement of the deleterious effects of this alarmin in myocarditis **(Table 4.4.14.)**. Myocardtis is associated with left ventricular dysfunction and is connected to collagen dysregulation[176]. Cardiac fibrosis was not less pronounced in S100A9$^{-/-}$ CVB3 versus WT CVB3 mice and is therefore probably not the underlying cause of the improved cardiac function observed in CVB3-infected knockout mice versus infected WT animals. In detail, evaluation of the pro-fibrotic marker TGF-β[123], which is responsible for the trans-differentiation of fibroblasts to myofibroblasts, the source of Col I and Col III, did not show any changes between the two infected groups (**Figure 4.4.7. C)**. LV mRNA expression of the myofibroblast marker α-SMA[123] was not elevated in any of the four experimental groups (**Figure 4.4.7. D)**.

We speculate that the decreased CVB3 copy number in S100A9$^{-/-}$ CVB3 versus WT CVB3 mice contributes to the improved cardiac function, since CVB3 is known to cause direct cardiomyocyte injury leading to an induction of chemokines such as MIP-2[119], which plays a crucial role in the inflammatory course of CVB3-induced myocarditis by attracting inflammatory cells to the heart[118]. The enhanced LV presence of inflammatory immune cells, results in enhanced oxidative stress[162] and has been shown to be involved in cardiac

disorders[155, 152]. Since S100A9$^{-/-}$ CVB3 mice displayed reduced inflammatory cell migration and oxidative stress, we assume that these factors are also responsible for the improved cardiac function versus WT CVB3 mice. Furthermore, our preliminary data with respect to Ca^{2+} signaling are a first hint that S100A8 and S100A9 might play a role in the diastolic Ca^{2+} signal, since *in vitro* supplementation of S100A9 and S100A8/S100A9 increased the diastolic Ca^{2+} signal in rat cardiomyocytes. The Ca^{2+} diastolic signal is decreased under normal conditions by re-uptake into the endoplasmatic reticulum, thus allowing efficient ventricular filling[122]. Our *in vitro* data agree with the observations of Boyd *et al.*[171], who clearly showed that cardiac overexpression of S100A8 and S100A9 led to a decrease of Ca^{2+} influx into the endoplasmatic reticulum, which was RAGE-dependent, whereas a loss of S100A9 attenuated the LPS-induced cardiac dysfunction. The adverse effect of these alarmins was further confirmed by Raphael *et al.*[177], where S100A8 treatment negatively influenced the electrophysiology of iPS-induced cardiomyocytes. However, our results are still preliminary and further investigation is warranted.

Taken together, the decreased CVB3 copy number, the lower numbers of inflammatory cells and reduced oxidative stress in S100A9$^{-/-}$ CVB3 versus WT CVB3 mice may account for the improved cardiac function in S100A9$^{-/-}$ CVB3 mice versus WT CVB3 animals described in paragraph 4.4.13., whereas S100A9$^{-/-}$ seems to have no influence on collagen metabolism, suggesting that mechanisms independent of S100A8 and S100A9 are more prominent for collagen regulation under these conditions. Furthermore, exogenous S100A8 application reversed the protective character of S100A9$^{-/-}$ CVB3 mice, indicating the significant effects of this alarmin in myocarditis **(Table 4.4.14.)**.

6. SUMMARY

In the pathogenesis of CVB3-induced myocarditis, cardiac inflammation plays a crucial role[114, 178]. Cardiac inflammation is a consequence of viral-related cardiomyocyte injury, which activates the innate immune system[12, 13]. NOD2 belongs to the innate immune system[45] and one of the factors responsible for the recognition of ssRNA[52], and thus CVB3 viruses. Moreover, the NLRP3 inflammasome is enhanced in experimental CVB3-mediated myocarditis[88] and plays a role in acute myocarditis[86]. In the present study, we demonstrated that NOD2 is up-regulated in CVB3-positive patients compared to AMC and DCM and control patients **(Figure 4.1.1. A)**, which also indicates NOD2 specificity in CVB3-induced cardiac disease. *In vitro*, we further confirmed the relevance of NOD2 in experimental CVB3-mediated myocarditis and determined its link to the NLRP3 inflammasome, as shown data from the patients, as well as *in vivo* and *in vitro* **(Figure 4.1.2. A-C, 4.3.4. A-C, Figure 4.3.5. A-F)**. In a second study, we demonstrated that the DAMPs S100A8 and S100A9 are elevated in EMBs of CVB3-positive patients compared to control patients, whereas the cardiac alarmin expression levels were not increased in DCM patients versus controls **(Figure 4.1.1. B-C)**. The S100A9$^{-/-}$ animal study demonstrated the detrimental role of S100A8 and S100A9 in CVB3-induced myocarditis, as shown by reduced cardiac chemokine production **(Figure 4.4.2. A)**, fewer cardiac immune cell infiltrates **(Figure 4.4.3.)**, suppression of cardiac oxidative stress **(Figure 4.4.4. A-B)**, less RAGE signaling **(Figure 4.4.11. B)**, lower CAR levels **(paragraph 4.4.8.)**, reduced CVB3 copy number **(Figure 4.4.8. A)**, and an improved LV function **(Table 4.4.13.)** in S100A9$^{-/-}$ CVB3-infected mice versus WT CVB3 animals. Intraperitoneal application of S100A8 in S100A9$^{-/-}$ CVB3 mice increased the CVB3 copy number and cardiac inflammation versus S100A9$^{-/-}$ CVB3 mice and resulted in impaired cardiac function **(paragraph 4.4.14.)**. Using *in vitro* experiments, we confirmed the negative effect of both alarmins, where S100A8 or S100A9 stimulation of CVB3-infected RAW macrophages induced the chemokine MIP-2 versus non-stimulated CVB3-infected cells, whereas S100A8 knockdown reduced the MIP-2 levels **(Figure 4.4.2. B and C)**. Moreover, supplementation of these alarmins in CVB3-infected HL-1 cells enhanced oxidative stress **(Figure 4.4.5.)**, CVB3 copy number, and reduced IFN-β expression **(Figure 4.4.8. C and D)** compared to non-stimulated infected cells. Furthermore, our *in vivo* and *in vitro* results demonstrated a link between alarmins and the NLRP3 inflammasome system **(Figure 4.1.2. B-E, Figure 4.4.9. A-B and Figure 4.4.10. A-B)**. The decreased RAGE and Dia-1 expression in CVB3-infected S100A9$^{-/-}$ mice compared to respective CVB3 controls

(Figure 4.4.11. B and E), which in the case of RAGE was also confirmed *in vitro* **(Figure 4.4.12. B)**, may be an indicator for S100A8- and S100A9-signaling via RAGE and Dia-1 in CVB3-induced myocarditis. By extrapolation, these data predict a model **(Figure 6)** for CVB3-induced myocarditis where NOD2 is responsible for CVB3 sensing and thus initiates a NLRP3 inflammasome-dependent inflammatory response, which could be the main source of the inflammatory disorder. In parallel, the CVB3 infection results in an elevation of DAMPs, particularly S100A8 and S100A9, which induce a signaling cascade via RAGE and Dia-1, resulting in an increased inflammatory cell migration and oxidative stress, particularly ROS. The latter is considered to lead to myocardial injury in AMC patients[104] and to exacerbate inflammation[179]. High ROS production in myocarditis[179] in turn boosts the inflammatory disorder. In this vicious cycle, ROS activates the NLRP3 inflammasome and in turn boosts the inflammatory disorder.

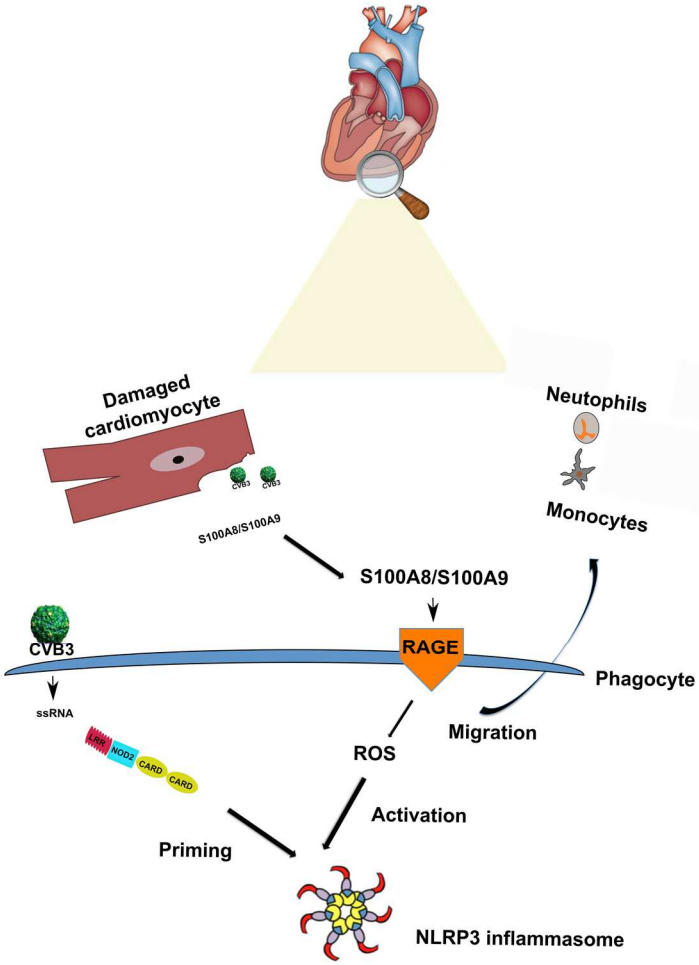

Figure 6: Hypothetical scheme of NOD2 signaling and a S100A8/S100A9-induced RAGE/Dia-1 pathway in Coxsackievirus B3-induced myocarditis (heart picture adapted from Frangogiannis *et al.* Nature Reviews Cardiology 2014 11: 255-265; NLRP3 inflammasome picture adapted from Elliot *et al.* Immunological Reviews 2015 265: 35-52).

Current pharmacological treatment of myocarditis-associated cardiomyopathy targets mainly the neuroendocrine system but does not directly influence the virus-induced inflammation and oxidative stress[11]. Based on our findings, which comprise; 1) a further confirmation of the deleterious role of NOD2 in experimental CVB3-induced myocarditis, as shown in myocarditis patients and *in vitro* experiments; 2) demonstration of the link between NOD2 and the NLRP3 inflammasome *in vivo* and *in vitro*, which seems to play a pivotal role in the inflammatory disorder of CVB3-induced myocarditis, and the decrease of NOD2 and NLRP3 in CVB3-positive patients, who eliminated the virus over time; and 3) the demonstration of a pathological role of S100A8 and S100A9 in CVB3-myocarditis patients, experimental CVB3-induced myocarditis and *in vitro* experiments, we conclude that NOD2, the NLRP3 inflammasome, S100A8, and S100A9 may represent pharmacological targets in (CVB3)-induced myocarditis.

7. Outlook

As previously mentioned, S100A8/S100A9 serves as an excellent biomarker in rheumatoid arthritis, juvenile idiopathic arthritis, and inflammatory bowel disease[42]. Moreover, several clinical studies described high S100A8/S100A9 plasma levels in patients with cardiovascular diseases, and S100A8/S100A9 was found to be a risk factor for future myocardial infarctions, cardiovascular death in healthy individuals[120], and for recurrent cardiovascular events[66]. S100A8 and S100A9 have already been suggested to serve as potential prognostic markers for cardiovascular disorders[180, 181].

Our clinical results demonstrate clearly that the S100A8/S100A9 system is enhanced in CVB3 myocarditis patients. Moreover, CVB3-positive patients, who eventually eliminated the virus, displayed decreased EMB mRNA expression of S100A8 and S100A9 over time. Future patient examinations will also include EMBs of CVB3-negative myocarditis patients. Moreover, serum S100A8/S100A9 levels will be measured from the patients included here, as well as from CVB3-negative myocarditis patients. These examinations will serve to determine whether S100A8 and S100A9 could be CVB3 specific, and if they could be valuable as potential serum or EMB prognostic biomarkers for (CVB3) myocarditis.

Anti-S100A9 and -S100A8 specific compounds, which belong to the quinoline-3-carboxamide group, have already been discovered and are approved for human use[180]. Experimentally, administration of one of these compounds, the quinoline-3-carboxamide derivate ABR-215757, showed biological relevance in a LPS-challenged mouse model[40] as well as in lupus-prone mice[182]. This compound was further tested in a clinical trial in patients with systemic lupus erythematosus[182]. Further *in vivo* and *in vitro* experiments with the molecular anti-S100A8 and -S100A9 compounds mentioned will evaluate whether S100A8/S100A9 could be a potential therapeutic target.

Finally, network analysis shows an interaction between the alarmins S100A8, S100A9, and NOD2 **(Figure 7.)**. Regulation of those interactions will now be further investigated.

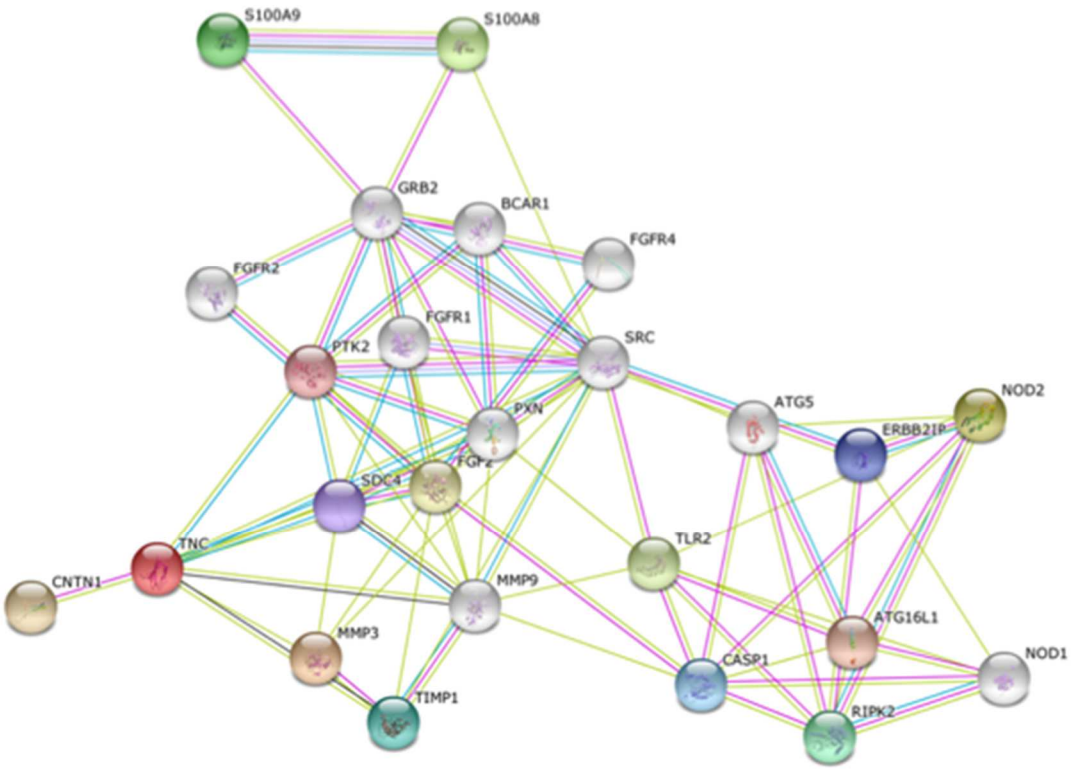

Figure 7. Network analysis shows an interaction between S100A8, S100A9, and NOD2. Analysis performed by the cardioproteomics lab using the string-db platform, BCRT, Oliver Klein.

8. REFERENCES

1. Lv S, Rong J, Ren S, Wu M, Li M, Zhu Y and Zhang J. Epidemiology and diagnosis of viral myocarditis. *Hellenic journal of cardiology : HJC = Hellenike kardiologike epitheorese*. 2013;54:382-91.
2. Bowles NE, Ni J, Kearney DL, Pauschinger M, Schultheiss HP, McCarthy R, Hare J, Bricker JT, Bowles KR and Towbin JA. Detection of viruses in myocardial tissues by polymerase chain reaction. evidence of adenovirus as a common cause of myocarditis in children and adults. *Journal of the American College of Cardiology*. 2003;42:466-72.
3. Kuhl U, Pauschinger M, Noutsias M, Seeberg B, Bock T, Lassner D, Poller W, Kandolf R and Schultheiss HP. High prevalence of viral genomes and multiple viral infections in the myocardium of adults with "idiopathic" left ventricular dysfunction. *Circulation*. 2005;111:887-93.
4. Matsumori A. Hepatitis C virus infection and cardiomyopathies. *Circulation research*. 2005;96:144-7.
5. Patane S, Marte F, Sturiale M, Dattilo G and Albanese A. Myocarditis and cardiomyopathy HIV associated. *International journal of cardiology*. 2011;146:e56-7.
6. Greaves K, Oxford JS, Price CP, Clarke GH and Crake T. The prevalence of myocarditis and skeletal muscle injury during acute viral infection in adults: measurement of cardiac troponins I and T in 152 patients with acute influenza infection. *Archives of internal medicine*. 2003;163:165-8.
7. Gui J, Yue Y, Chen R, Xu W and Xiong S. A20 (TNFAIP3) alleviates CVB3-induced myocarditis via inhibiting NF-kappaB signaling. *PloS one*. 2012;7:e46515.
8. Grun S, Schumm J, Greulich S, Wagner A, Schneider S, Bruder O, Kispert EM, Hill S, Ong P, Klingel K, Kandolf R, Sechtem U and Mahrholdt H. Long-term follow-up of biopsy-proven viral myocarditis: predictors of mortality and incomplete recovery. *Journal of the American College of Cardiology*. 2012;59:1604-15.
9. Freimuth P, Philipson L and Carson SD. The coxsackievirus and adenovirus receptor. *Current topics in microbiology and immunology*. 2008;323:67-87.
10. Shi Y, Chen C, Lisewski U, Wrackmeyer U, Radke M, Westermann D, Sauter M, Tschope C, Poller W, Klingel K and Gotthardt M. Cardiac deletion of the Coxsackievirus-adenovirus receptor abolishes Coxsackievirus B3 infection and prevents myocarditis in vivo. *Journal of the American College of Cardiology*. 2009;53:1219-26.
11. Schultheiss HP, Kuhl U and Cooper LT. The management of myocarditis. *European heart journal*. 2011;32:2616-25.
12. Shauer A, Gotsman I, Keren A, Zwas DR, Hellman Y, Durst R and Admon D. Acute viral myocarditis: current concepts in diagnosis and treatment. *The Israel Medical Association journal : IMAJ*. 2013;15:180-5.
13. Kindermann I, Barth C, Mahfoud F, Ukena C, Lenski M, Yilmaz A, Klingel K, Kandolf R, Sechtem U, Cooper LT and Bohm M. Update on myocarditis. *Journal of the American College of Cardiology*. 2012;59:779-92.
14. Liu PP and Mason JW. Advances in the understanding of myocarditis. *Circulation*. 2001;104:1076-82.
15. Thaiss CA, Levy M, Itav S and Elinav E. Integration of Innate Immune Signaling. *Trends in immunology*. 2016;37:84-101.
16. Lupfer C and Kanneganti TD. The expanding role of NLRs in antiviral immunity. *Immunological reviews*. 2013;255:13-24.
17. Savva A and Roger T. Targeting toll-like receptors: promising therapeutic strategies for the management of sepsis-associated pathology and infectious diseases. *Frontiers in immunology*. 2013;4:387.
18. Xie P. TRAF molecules in cell signaling and in human diseases. *Journal of molecular signaling*. 2013;8:7.

19. Ehrchen JM, Sunderkotter C, Foell D, Vogl T and Roth J. The endogenous Toll-like receptor 4 agonist S100A8/S100A9 (calprotectin) as innate amplifier of infection, autoimmunity, and cancer. *Journal of leukocyte biology*. 2009;86:557-66.
20. Chavakis T, Bierhaus A, Al-Fakhri N, Schneider D, Witte S, Linn T, Nagashima M, Morser J, Arnold B, Preissner KT and Nawroth PP. The pattern recognition receptor (RAGE) is a counterreceptor for leukocyte integrins: a novel pathway for inflammatory cell recruitment. *The Journal of experimental medicine*. 2003;198:1507-15.
21. Lin L, Park S and Lakatta EG. RAGE signaling in inflammation and arterial aging. *Frontiers in bioscience*. 2009;14:1403-13.
22. Sakaguchi M, Murata H, Yamamoto K, Ono T, Sakaguchi Y, Motoyama A, Hibino T, Kataoka K and Huh NH. TIRAP, an adaptor protein for TLR2/4, transduces a signal from RAGE phosphorylated upon ligand binding. *PloS one*. 2011;6:e23132.
23. Xie J, Mendez JD, Mendez-Valenzuela V and Aguilar-Hernandez MM. Cellular signalling of the receptor for advanced glycation end products (RAGE). *Cellular signalling*. 2013;25:2185-97.
24. Litwinoff E, Hurtado Del Pozo C, Ramasamy R and Schmidt AM. Emerging Targets for Therapeutic Development in Diabetes and Its Complications: The RAGE Signaling Pathway. *Clinical pharmacology and therapeutics*. 2015;98:135-44.
25. Hudson BI, Kalea AZ, Del Mar Arriero M, Harja E, Boulanger E, D'Agati V and Schmidt AM. Interaction of the RAGE cytoplasmic domain with diaphanous-1 is required for ligand-stimulated cellular migration through activation of Rac1 and Cdc42. *The Journal of biological chemistry*. 2008;283:34457-68.
26. Daffu G, del Pozo CH, O'Shea KM, Ananthakrishnan R, Ramasamy R and Schmidt AM. Radical roles for RAGE in the pathogenesis of oxidative stress in cardiovascular diseases and beyond. *International journal of molecular sciences*. 2013;14:19891-910.
27. Bianchi ME. DAMPs, PAMPs and alarmins: all we need to know about danger. *Journal of leukocyte biology*. 2007;81:1-5.
28. Vogl T, Gharibyan AL and Morozova-Roche LA. Pro-inflammatory S100A8 and S100A9 proteins: self-assembly into multifunctional native and amyloid complexes. *International journal of molecular sciences*. 2012;13:2893-917.
29. Moore BW. A soluble protein characteristic of the nervous system. *Biochemical and biophysical research communications*. 1965;19:739-44.
30. Heizmann CW, Fritz G and Schafer BW. S100 proteins: structure, functions and pathology. *Frontiers in bioscience : a journal and virtual library*. 2002;7:d1356-68.
31. Vogl T, Roth J, Sorg C, Hillenkamp F and Strupat K. Calcium-induced noncovalently linked tetramers of MRP8 and MRP14 detected by ultraviolet matrix-assisted laser desorption/ionization mass spectrometry. *Journal of the American Society for Mass Spectrometry*. 1999;10:1124-30.
32. Van Crombruggen K, Vogl T, Perez-Novo C, Holtappels G and Bachert C. Differential release and deposition of S100A8/A9 proteins in inflamed upper airway tissue. *The European respiratory journal*. 2016;47:264-74.
33. Vogl T, Tenbrock K, Ludwig S, Leukert N, Ehrhardt C, van Zoelen MA, Nacken W, Foell D, van der Poll T, Sorg C and Roth J. Mrp8 and Mrp14 are endogenous activators of Toll-like receptor 4, promoting lethal, endotoxin-induced shock. *Nature medicine*. 2007;13:1042-9.
34. Loser K, Vogl T, Voskort M, Lueken A, Kupas V, Nacken W, Klenner L, Kuhn A, Foell D, Sorokin L, Luger TA, Roth J and Beissert S. The Toll-like receptor 4 ligands Mrp8 and Mrp14 are crucial in the development of autoreactive CD8+ T cells. *Nature medicine*. 2010;16:713-7.
35. Riva M, Kallberg E, Bjork P, Hancz D, Vogl T, Roth J, Ivars F and Leanderson T. Induction of nuclear factor-kappaB responses by the S100A9 protein is Toll-like receptor-4-dependent. *Immunology*. 2012;137:172-82.

36. Gao H, Zhang X, Zheng Y, Peng L, Hou J and Meng H. S100A9-induced release of interleukin (IL)-6 and IL-8 through toll-like receptor 4 (TLR4) in human periodontal ligament cells. *Molecular immunology*. 2015;67:223-32.
37. Xu X, Chen H, Zhu X, Ma Y, Liu Q, Xue Y, Chu H, Wu W, Wang J and Zou H. S100A9 promotes human lung fibroblast cells activation through receptor for advanced glycation end-product-mediated extracellular-regulated kinase 1/2, mitogen-activated protein-kinase and nuclear factor-kappaB-dependent pathways. *Clinical and experimental immunology*. 2013;173:523-35.
38. Wang L, Luo H, Chen X, Jiang Y and Huang Q. Functional characterization of S100A8 and S100A9 in altering monolayer permeability of human umbilical endothelial cells. *PloS one*. 2014;9:e90472.
39. Foell D, Wittkowski H and Roth J. Mechanisms of disease: a 'DAMP' view of inflammatory arthritis. *Nature clinical practice Rheumatology*. 2007;3:382-90.
40. Bjork P, Bjork A, Vogl T, Stenstrom M, Liberg D, Olsson A, Roth J, Ivars F and Leanderson T. Identification of human S100A9 as a novel target for treatment of autoimmune disease via binding to quinoline-3-carboxamides. *PLoS biology*. 2009;7:e97.
41. Lugering N, Stoll R, Kucharzik T, Schmid KW, Rohlmann G, Burmeister G, Sorg C and Domschke W. Immunohistochemical distribution and serum levels of the Ca(2+)-binding proteins MRP8, MRP14 and their heterodimeric form MRP8/14 in Crohn's disease. *Digestion*. 1995;56:406-14.
42. Foell D, Frosch M, Sorg C and Roth J. Phagocyte-specific calcium-binding S100 proteins as clinical laboratory markers of inflammation. *Clinica chimica acta; international journal of clinical chemistry*. 2004;344:37-51.
43. Chaput C, Sander LE, Suttorp N and Opitz B. NOD-Like Receptors in Lung Diseases. *Frontiers in immunology*. 2013;4:393.
44. Moreira LO and Zamboni DS. NOD1 and NOD2 Signaling in Infection and Inflammation. *Frontiers in immunology*. 2012;3:328.
45. Antosz H and Osiak M. NOD1 and NOD2 receptors: integral members of the innate and adaptive immunity system. *Acta biochimica Polonica*. 2013;60:351-60.
46. Hsu YM, Zhang Y, You Y, Wang D, Li H, Duramad O, Qin XF, Dong C and Lin X. The adaptor protein CARD9 is required for innate immune responses to intracellular pathogens. *Nature immunology*. 2007;8:198-205.
47. Carneiro LA and Travassos LH. The Interplay between NLRs and Autophagy in Immunity and Inflammation. *Frontiers in immunology*. 2013;4:361.
48. Yazdanyar S and Nordestgaard BG. NOD2/CARD15 genotype, cardiovascular disease and cancer in 43,600 individuals from the general population. *Journal of internal medicine*. 2010;268:162-70.
49. El Mokhtari NE, Ott SJ, Nebel A, Schafer A, Rosenstiel P, Forster M, Nothnagel M, Simon R and Schreiber S. Role of NOD2/CARD15 in coronary heart disease. *BMC genetics*. 2007;8:76.
50. Kwon MY, Liu X, Lee SJ, Kang YH, Choi AM, Lee KU, Perrella MA and Chung SW. Nucleotide-binding oligomerization domain protein 2 deficiency enhances neointimal formation in response to vascular injury. *Arteriosclerosis, thrombosis, and vascular biology*. 2011;31:2441-7.
51. Li X, Li F, Chu Y, Wang X, Zhang H, Hu Y, Zhang Y, Wang Z, Wei X, Jian W, Zhang X and Yi F. NOD2 deficiency protects against cardiac remodeling after myocardial infarction in mice. *Cellular physiology and biochemistry : international journal of experimental cellular physiology, biochemistry, and pharmacology*. 2013;32:1857-66.
52. Sabbah A, Chang TH, Harnack R, Frohlich V, Tominaga K, Dube PH, Xiang Y and Bose S. Activation of innate immune antiviral responses by Nod2. *Nature immunology*. 2009;10:1073-80.

53. Jing H, Fang L, Wang D, Ding Z, Luo R, Chen H and Xiao S. Porcine reproductive and respiratory syndrome virus infection activates NOD2-RIP2 signal pathway in MARC-145 cells. *Virology*. 2014;458-459:162-71.
54. Wagner KB, Felix SB and Riad A. Innate immune receptors in heart failure: Side effect or potential therapeutic target? *World journal of cardiology*. 2014;6:791-801.
55. Riad A, Jager S, Sobirey M, Escher F, Yaulema-Riss A, Westermann D, Karatas A, Heimesaat MM, Bereswill S, Dragun D, Pauschinger M, Schultheiss HP and Tschope C. Toll-like receptor-4 modulates survival by induction of left ventricular remodeling after myocardial infarction in mice. *Journal of immunology*. 2008;180:6954-61.
56. Riad A, Bien S, Gratz M, Escher F, Westermann D, Heimesaat MM, Bereswill S, Krieg T, Felix SB, Schultheiss HP, Kroemer HK and Tschope C. Toll-like receptor-4 deficiency attenuates doxorubicin-induced cardiomyopathy in mice. *European journal of heart failure*. 2008;10:233-43.
57. Ehrentraut H, Weber C, Ehrentraut S, Schwederski M, Boehm O, Knuefermann P, Meyer R and Baumgarten G. The toll-like receptor 4-antagonist eritoran reduces murine cardiac hypertrophy. *European journal of heart failure*. 2011;13:602-10.
58. Hua F, Ha T, Ma J, Li Y, Kelley J, Gao X, Browder IW, Kao RL, Williams DL and Li C. Protection against myocardial ischemia/reperfusion injury in TLR4-deficient mice is mediated through a phosphoinositide 3-kinase-dependent mechanism. *Journal of immunology*. 2007;178:7317-24.
59. Fairweather D, Yusung S, Frisancho S, Barrett M, Gatewood S, Steele R and Rose NR. IL-12 receptor beta 1 and Toll-like receptor 4 increase IL-1 beta- and IL-18-associated myocarditis and coxsackievirus replication. *Journal of immunology*. 2003;170:4731-7.
60. Fuse K, Chan G, Liu Y, Gudgeon P, Husain M, Chen M, Yeh WC, Akira S and Liu PP. Myeloid differentiation factor-88 plays a crucial role in the pathogenesis of Coxsackievirus B3-induced myocarditis and influences type I interferon production. *Circulation*. 2005;112:2276-85.
61. Riad A, Westermann D, Zietsch C, Savvatis K, Becher PM, Bereswill S, Heimesaat MM, Lettau O, Lassner D, Dorner A, Poller W, Busch M, Felix SB, Schultheiss HP and Tschope C. TRIF is a critical survival factor in viral cardiomyopathy. *Journal of immunology*. 2011;186:2561-70.
62. Altwegg LA, Neidhart M, Hersberger M, Muller S, Eberli FR, Corti R, Roffi M, Sutsch G, Gay S, von Eckardstein A, Wischnewsky MB, Luscher TF and Maier W. Myeloid-related protein 8/14 complex is released by monocytes and granulocytes at the site of coronary occlusion: a novel, early, and sensitive marker of acute coronary syndromes. *European heart journal*. 2007;28:941-8.
63. Yonekawa K, Neidhart M, Altwegg LA, Wyss CA, Corti R, Vogl T, Grigorian M, Gay S, Luscher TF and Maier W. Myeloid related proteins activate Toll-like receptor 4 in human acute coronary syndromes. *Atherosclerosis*. 2011;218:486-92.
64. McCormick MM, Rahimi F, Bobryshev YV, Gaus K, Zreiqat H, Cai H, Lord RS and Geczy CL. S100A8 and S100A9 in human arterial wall. Implications for atherogenesis. *The Journal of biological chemistry*. 2005;280:41521-9.
65. Cotoi OS, Duner P, Ko N, Hedblad B, Nilsson J, Bjorkbacka H and Schiopu A. Plasma S100A8/A9 correlates with blood neutrophil counts, traditional risk factors, and cardiovascular disease in middle-aged healthy individuals. *Arteriosclerosis, thrombosis, and vascular biology*. 2014;34:202-10.
66. Morrow DA, Wang Y, Croce K, Sakuma M, Sabatine MS, Gao H, Pradhan AD, Healy AM, Buros J, McCabe CH, Libby P, Cannon CP, Braunwald E and Simon DI. Myeloid-related protein 8/14 and the risk of cardiovascular death or myocardial infarction after an acute coronary syndrome in the Pravastatin or Atorvastatin Evaluation and Infection Therapy: Thrombolysis in Myocardial Infarction (PROVE IT-TIMI 22) trial. *American heart journal*. 2008;155:49-55.

67. Tugizov S, Berline J, Herrera R, Penaranda ME, Nakagawa M and Palefsky J. Inhibition of human papillomavirus type 16 E7 phosphorylation by the S100 MRP-8/14 protein complex. *Journal of virology*. 2005;79:1099-112.
68. Reghunathan R, Jayapal M, Hsu LY, Chng HH, Tai D, Leung BP and Melendez AJ. Expression profile of immune response genes in patients with Severe Acute Respiratory Syndrome. *BMC immunology*. 2005;6:2.
69. Endoh Y, Chung YM, Clark IA, Geczy CL and Hsu K. IL-10-dependent S100A8 gene induction in monocytes/macrophages by double-stranded RNA. *Journal of immunology*. 2009;182:2258-68.
70. Ryckman C, Robichaud GA, Roy J, Cantin R, Tremblay MJ and Tessier PA. HIV-1 transcription and virus production are both accentuated by the proinflammatory myeloid-related proteins in human CD4+ T lymphocytes. *Journal of immunology*. 2002;169:3307-13.
71. Man SM and Kanneganti TD. Regulation of inflammasome activation. *Immunological reviews*. 2015;265:6-21.
72. Sutterwala FS, Haasken S and Cassel SL. Mechanism of NLRP3 inflammasome activation. *Annals of the New York Academy of Sciences*. 2014;1319:82-95.
73. Bergsbaken T, Fink SL and Cookson BT. Pyroptosis: host cell death and inflammation. *Nature reviews Microbiology*. 2009;7:99-109.
74. Yang CS, Shin DM and Jo EK. The Role of NLR-related Protein 3 Inflammasome in Host Defense and Inflammatory Diseases. *International neurourology journal*. 2012;16:2-12.
75. So A, De Smedt T, Revaz S and Tschopp J. A pilot study of IL-1 inhibition by anakinra in acute gout. *Arthritis research & therapy*. 2007;9:R28.
76. Zhou R, Tardivel A, Thorens B, Choi I and Tschopp J. Thioredoxin-interacting protein links oxidative stress to inflammasome activation. *Nature immunology*. 2010;11:136-40.
77. Duewell P, Kono H, Rayner KJ, Sirois CM, Vladimer G, Bauernfeind FG, Abela GS, Franchi L, Nunez G, Schnurr M, Espevik T, Lien E, Fitzgerald KA, Rock KL, Moore KJ, Wright SD, Hornung V and Latz E. NLRP3 inflammasomes are required for atherogenesis and activated by cholesterol crystals. *Nature*. 2010;464:1357-61.
78. Zhou R, Yazdi AS, Menu P and Tschopp J. A role for mitochondria in NLRP3 inflammasome activation. *Nature*. 2011;469:221-5.
79. Mayor A, Martinon F, De Smedt T, Petrilli V and Tschopp J. A crucial function of SGT1 and HSP90 in inflammasome activity links mammalian and plant innate immune responses. *Nature immunology*. 2007;8:497-503.
80. Elliott EI and Sutterwala FS. Initiation and perpetuation of NLRP3 inflammasome activation and assembly. *Immunological reviews*. 2015;265:35-52.
81. Juliana C, Fernandes-Alnemri T, Kang S, Farias A, Qin F and Alnemri ES. Non-transcriptional priming and deubiquitination regulate NLRP3 inflammasome activation. *The Journal of biological chemistry*. 2012;287:36617-22.
82. Fernandes-Alnemri T, Kang S, Anderson C, Sagara J, Fitzgerald KA and Alnemri ES. Cutting edge: TLR signaling licenses IRAK1 for rapid activation of the NLRP3 inflammasome. *Journal of immunology*. 2013;191:3995-9.
83. Lin KM, Hu W, Troutman TD, Jennings M, Brewer T, Li X, Nanda S, Cohen P, Thomas JA and Pasare C. IRAK-1 bypasses priming and directly links TLRs to rapid NLRP3 inflammasome activation. *Proceedings of the National Academy of Sciences of the United States of America*. 2014;111:775-80.
84. Chen IY and Ichinohe T. Response of host inflammasomes to viral infection. *Trends in microbiology*. 2015;23:55-63.
85. Marchetti C, Toldo S, Chojnacki J, Mezzaroma E, Liu K, Salloum FN, Nordio A, Carbone S, Mauro AG, Das A, Zalavadia AA, Halquist MS, Federici M, Van Tassell BW, Zhang S and Abbate A. Pharmacologic Inhibition of the NLRP3 Inflammasome Preserves Cardiac Function After Ischemic and Nonischemic Injury in the Mouse. *Journal of cardiovascular pharmacology*. 2015;66:1-8.

86. Toldo S, Kannan H, Bussani R, Anzini M, Sonnino C, Sinagra G, Merlo M, Mezzaroma E, De-Giorgio F, Silvestri F, Van Tassell BW, Baldi A and Abbate A. Formation of the inflammasome in acute myocarditis. *International journal of cardiology*. 2014;171:e119-21.
87. Toldo S, Mezzaroma E, McGeough MD, Pena CA, Marchetti C, Sonnino C, Van Tassell BW, Salloum FN, Voelkel NF, Hoffman HM and Abbate A. Independent roles of the priming and the triggering of the NLRP3 inflammasome in the heart. *Cardiovascular research*. 2015;105:203-12.
88. Wang Y, Gao B and Xiong S. Involvement of NLRP3 inflammasome in CVB3-induced viral myocarditis. *American journal of physiology Heart and circulatory physiology*. 2014;307:H1438-47.
89. Barlan AU, Griffin TM, McGuire KA and Wiethoff CM. Adenovirus membrane penetration activates the NLRP3 inflammasome. *Journal of virology*. 2011;85:146-55.
90. Wagner RN, Proell M, Kufer TA and Schwarzenbacher R. Evaluation of Nod-like receptor (NLR) effector domain interactions. *PloS one*. 2009;4:e4931.
91. Pan Q, Mathison J, Fearns C, Kravchenko VV, Da Silva Correia J, Hoffman HM, Kobayashi KS, Bertin J, Grant EP, Coyle AJ, Sutterwala FS, Ogura Y, Flavell RA and Ulevitch RJ. MDP-induced interleukin-1beta processing requires Nod2 and CIAS1/NALP3. *Journal of leukocyte biology*. 2007;82:177-83.
92. Hsu LC, Ali SR, McGillivray S, Tseng PH, Mariathasan S, Humke EW, Eckmann L, Powell JJ, Nizet V, Dixit VM and Karin M. A NOD2-NALP1 complex mediates caspase-1-dependent IL-1beta secretion in response to Bacillus anthracis infection and muramyl dipeptide. *Proceedings of the National Academy of Sciences of the United States of America*. 2008;105:7803-8.
93. Simard JC, Cesaro A, Chapeton-Montes J, Tardif M, Antoine F, Girard D and Tessier PA. S100A8 and S100A9 induce cytokine expression and regulate the NLRP3 inflammasome via ROS-dependent activation of NF-kappaB(1.). *PloS one*. 2013;8:e72138.
94. Nagareddy PR, Kraakman M, Masters SL, Stirzaker RA, Gorman DJ, Grant RW, Dragoljevic D, Hong ES, Abdel-Latif A, Smyth SS, Choi SH, Korner J, Bornfeldt KE, Fisher EA, Dixit VD, Tall AR, Goldberg IJ and Murphy AJ. Adipose tissue macrophages promote myelopoiesis and monocytosis in obesity. *Cell metabolism*. 2014;19:821-35.
95. Koy M, Hambruch N, Hussen J, Pfarrer C, Seyfert HM and Schuberth HJ. Recombinant bovine S100A8 and A9 enhance IL-1beta secretion of interferon-gamma primed monocytes. *Veterinary immunology and immunopathology*. 2013;155:162-70.
96. Moll M and Kuemmerle-Deschner JB. Inflammasome and cytokine blocking strategies in autoinflammatory disorders. *Clinical immunology*. 2013;147:242-75.
97. Van Linthout S, Tschope C and Schultheiss HP. Lack in treatment options for virus-induced inflammatory cardiomyopathy: can iPS-derived cardiomyocytes close the gap? *Circulation research*. 2014;115:540-1.
98. Fechner H, Pinkert S, Geisler A, Poller W and Kurreck J. Pharmacological and biological antiviral therapeutics for cardiac coxsackievirus infections. *Molecules*. 2011;16:8475-503.
99. Leung YY, Yao Hui LL and Kraus VB. Colchicine-Update on mechanisms of action and therapeutic uses. *Seminars in arthritis and rheumatism*. 2015;45:341-50.
100. Gultekin N and Kucukates E. Microtubule inhibition therapy by colchicine in severe myocarditis especially caused by Epstein-Barr and cytomegalovirus co-infection during a two-year period: a novel therapeutic approach. *JPMA The Journal of the Pakistan Medical Association*. 2014;64:1420-3.
101. Randle JC, Harding MW, Ku G, Schonharting M and Kurrle R. ICE/Caspase-1 inhibitors as novel anti-inflammatory drugs. *Expert opinion on investigational drugs*. 2001;10:1207-9.

102. Abbate A, Van Tassell BW, Biondi-Zoccai G, Kontos MC, Grizzard JD, Spillman DW, Oddi C, Roberts CS, Melchior RD, Mueller GH, Abouzaki NA, Rengel LR, Varma A, Gambill ML, Falcao RA, Voelkel NF, Dinarello CA and Vetrovec GW. Effects of interleukin-1 blockade with anakinra on adverse cardiac remodeling and heart failure after acute myocardial infarction [from the Virginia Commonwealth University-Anakinra Remodeling Trial (2) (VCU-ART2) pilot study]. *The American journal of cardiology*. 2013;111:1394-400.
103. Yajima T. Viral myocarditis: potential defense mechanisms within the cardiomyocyte against virus infection. *Future microbiology*. 2011;6:551-66.
104. Li YC, Ge LS, Yang PL, Tang JF, Lin JF, Chen P and Guan XQ. Carvedilol treatment ameliorates acute coxsackievirus B3-induced myocarditis associated with oxidative stress reduction. *European journal of pharmacology*. 2010;640:112-6.
105. Foell D and Roth J. Proinflammatory S100 proteins in arthritis and autoimmune disease. *Arthritis and rheumatism*. 2004;50:3762-71.
106. Angelow A, Weitmann K, Schmidt M, Schwedler S, Vogt H, Havemann C, Staudt A, Felix SB, Stangl K, Klingel K, Kandolf R, Kuhl U, Lassner D, v Schlippenbach J, Schultheiss HP and Hoffmann W. The German Transregional Collaborative Research Centre 'Inflammatory Cardiomyopathy--Molecular Pathogenesis and Therapy'. Methods and baseline results from a 3-centre clinical study. *Cardiology*. 2009;113:222-30.
107. Caforio AL, Pankuweit S, Arbustini E, Basso C, Gimeno-Blanes J, Felix SB, Fu M, Helio T, Heymans S, Jahns R, Klingel K, Linhart A, Maisch B, McKenna W, Mogensen J, Pinto YM, Ristic A, Schultheiss HP, Seggewiss H, Tavazzi L, Thiene G, Yilmaz A, Charron P, Elliott PM, European Society of Cardiology Working Group on M and Pericardial D. Current state of knowledge on aetiology, diagnosis, management, and therapy of myocarditis: a position statement of the European Society of Cardiology Working Group on Myocardial and Pericardial Diseases. *European heart journal*. 2013;34:2636-48, 2648a-2648d.
108. Dominguez F, Kuhl U, Pieske B, Garcia-Pavia P and Tschope C. Update on Myocarditis and Inflammatory Cardiomyopathy: Reemergence of Endomyocardial Biopsy. *Revista espanola de cardiologia*. 2016;69:178-87.
109. Aretz HT. Myocarditis: the Dallas criteria. *Human pathology*. 1987;18:619-24.
110. Kuhl U, Noutsias M, Seeberg B and Schultheiss HP. Immunohistological evidence for a chronic intramyocardial inflammatory process in dilated cardiomyopathy. *Heart*. 1996;75:295-300.
111. Noutsias M, Pauschinger M, Poller WC, Schultheiss HP and Kuhl U. Immunomodulatory treatment strategies in inflammatory cardiomyopathy: current status and future perspectives. *Expert review of cardiovascular therapy*. 2004;2:37-51.
112. Heimesaat MM, Dunay IR, Alutis M, Fischer A, Mohle L, Gobel UB, Kuhl AA and Bereswill S. Nucleotide-oligomerization-domain-2 affects commensal gut microbiota composition and intracerebral immunopathology in acute Toxoplasma gondii induced murine ileitis. *PloS one*. 2014;9:e105120.
113. Manitz MP, Horst B, Seeliger S, Strey A, Skryabin BV, Gunzer M, Frings W, Schonlau F, Roth J, Sorg C and Nacken W. Loss of S100A9 (MRP14) results in reduced interleukin-8-induced CD11b surface expression, a polarized microfilament system, and diminished responsiveness to chemoattractants in vitro. *Molecular and cellular biology*. 2003;23:1034-43.
114. Van Linthout S, Savvatis K, Miteva K, Peng J, Ringe J, Warstat K, Schmidt-Lucke C, Sittinger M, Schultheiss HP and Tschope C. Mesenchymal stem cells improve murine acute coxsackievirus B3-induced myocarditis. *European heart journal*. 2011;32:2168-78.
115. Kuhl U, Lassner D, Dorner A, Rohde M, Escher F, Seeberg B, Hertel E, Tschope C, Skurk C, Gross UM, Schultheiss HP and Poller W. A distinct subgroup of cardiomyopathy patients characterized by transcriptionally active cardiotropic erythrovirus and altered cardiac gene expression. *Basic research in cardiology*. 2013;108:372.

116. Rohde D, Schon C, Boerries M, Didrihsone I, Ritterhoff J, Kubatzky KF, Volkers M, Herzog N, Mahler M, Tsoporis JN, Parker TG, Linke B, Giannitsis E, Gao E, Peppel K, Katus HA and Most P. S100A1 is released from ischemic cardiomyocytes and signals myocardial damage via Toll-like receptor 4. *EMBO molecular medicine*. 2014;6:778-94.
117. Philpott DJ, Sorbara MT, Robertson SJ, Croitoru K and Girardin SE. NOD proteins: regulators of inflammation in health and disease. *Nature reviews Immunology*. 2014;14:9-23.
118. Kishimoto C, Kawamata H, Sakai S, Shinohara H and Ochiai H. Role of MIP-2 in coxsackievirus B3 myocarditis. *Journal of molecular and cellular cardiology*. 2000;32:631-8.
119. De Filippo K, Dudeck A, Hasenberg M, Nye E, van Rooijen N, Hartmann K, Gunzer M, Roers A and Hogg N. Mast cell and macrophage chemokines CXCL1/CXCL2 control the early stage of neutrophil recruitment during tissue inflammation. *Blood*. 2013;121:4930-7.
120. Healy AM, Pickard MD, Pradhan AD, Wang Y, Chen Z, Croce K, Sakuma M, Shi C, Zago AC, Garasic J, Damokosh AI, Dowie TL, Poisson L, Lillie J, Libby P, Ridker PM and Simon DI. Platelet expression profiling and clinical validation of myeloid-related protein-14 as a novel determinant of cardiovascular events. *Circulation*. 2006;113:2278-84.
121. Volkers M, Rohde D, Goodman C and Most P. S100A1: a regulator of striated muscle sarcoplasmic reticulum Ca2+ handling, sarcomeric, and mitochondrial function. *Journal of biomedicine & biotechnology*. 2010;2010:178614.
122. Linke WA and Hamdani N. Gigantic business: titin properties and function through thick and thin. *Circulation research*. 2014;114:1052-68.
123. Westermann D, Lindner D, Kasner M, Zietsch C, Savvatis K, Escher F, von Schlippenbach J, Skurk C, Steendijk P, Riad A, Poller W, Schultheiss HP and Tschope C. Cardiac inflammation contributes to changes in the extracellular matrix in patients with heart failure and normal ejection fraction. *Circulation Heart failure*. 2011;4:44-52.
124. Miteva K, Haag M, Peng J, Savvatis K, Becher PM, Seifert M, Warstat K, Westermann D, Ringe J, Sittinger M, Schultheiss HP, Tschope C and Van Linthout S. Human cardiac-derived adherent proliferating cells reduce murine acute Coxsackievirus B3-induced myocarditis. *PloS one*. 2011;6:e28513.
125. Horwitz MS, La Cava A, Fine C, Rodriguez E, Ilic A and Sarvetnick N. Pancreatic expression of interferon-gamma protects mice from lethal coxsackievirus B3 infection and subsequent myocarditis. *Nature medicine*. 2000;6:693-7.
126. Thornberry NA, Bull HG, Calaycay JR, Chapman KT, Howard AD, Kostura MJ, Miller DK, Molineaux SM, Weidner JR, Aunins J and et al. A novel heterodimeric cysteine protease is required for interleukin-1 beta processing in monocytes. *Nature*. 1992;356:768-74.
127. Zhang W, Lavine KJ, Epelman S, Evans SA, Weinheimer CJ, Barger PM and Mann DL. Necrotic myocardial cells release damage-associated molecular patterns that provoke fibroblast activation in vitro and trigger myocardial inflammation and fibrosis in vivo. *Journal of the American Heart Association*. 2015;4:e001993.
128. Kawaguchi M, Takahashi M, Hata T, Kashima Y, Usui F, Morimoto H, Izawa A, Takahashi Y, Masumoto J, Koyama J, Hongo M, Noda T, Nakayama J, Sagara J, Taniguchi S and Ikeda U. Inflammasome activation of cardiac fibroblasts is essential for myocardial ischemia/reperfusion injury. *Circulation*. 2011;123:594-604.
129. Pei XM, Tam BT, Sin TK, Wang FF, Yung BY, Chan LW, Wong CS, Ying M, Lai CW and Siu PM. S100A8 and S100A9 Are Associated with Doxorubicin-Induced Cardiotoxicity in the Heart of Diabetic Mice. *Frontiers in physiology*. 2016;7:334.
130. Volz HC, Laohachewin D, Seidel C, Lasitschka F, Keilbach K, Wienbrandt AR, Andrassy J, Bierhaus A, Kaya Z, Katus HA and Andrassy M. S100A8/A9 aggravates post-ischemic heart failure through activation of RAGE-dependent NF-kappaB signaling. *Basic research in cardiology*. 2012;107:250.
131. Katashima T, Naruko T, Terasaki F, Fujita M, Otsuka K, Murakami S, Sato A, Hiroe M, Ikura Y, Ueda M, Ikemoto M and Kitaura Y. Enhanced expression of the S100A8/A9

complex in acute myocardial infarction patients. *Circulation journal : official journal of the Japanese Circulation Society*. 2010;74:741-8.
132. Ponikowski P, Voors AA, Anker SD, Bueno H, Cleland JG, Coats AJ, Falk V, Gonzalez-Juanatey JR, Harjola VP, Jankowska EA, Jessup M, Linde C, Nihoyannopoulos P, Parissis JT, Pieske B, Riley JP, Rosano GM, Ruilope LM, Ruschitzka F, Rutten FH, van der Meer P, Authors/Task Force M and Document R. 2016 ESC Guidelines for the diagnosis and treatment of acute and chronic heart failure: The Task Force for the diagnosis and treatment of acute and chronic heart failure of the European Society of Cardiology (ESC). Developed with the special contribution of the Heart Failure Association (HFA) of the ESC. *European journal of heart failure*. 2016.
133. Farzi A, Reichmann F, Meinitzer A, Mayerhofer R, Jain P, Hassan AM, Frohlich EE, Wagner K, Painsipp E, Rinner B and Holzer P. Synergistic effects of NOD1 or NOD2 and TLR4 activation on mouse sickness behavior in relation to immune and brain activity markers. *Brain, behavior, and immunity*. 2014.
134. Zong J, Salim M, Zhou H, Bian ZY, Dai J, Yuan Y, Deng W, Zhang JY, Zhang R, Wu QQ and Tang QZ. NOD2 deletion promotes cardiac hypertrophy and fibrosis induced by pressure overload. *Laboratory investigation; a journal of technical methods and pathology*. 2013;93:1128-36.
135. Badorff C, Lee GH, Lamphear BJ, Martone ME, Campbell KP, Rhoads RE and Knowlton KU. Enteroviral protease 2A cleaves dystrophin: evidence of cytoskeletal disruption in an acquired cardiomyopathy. *Nature medicine*. 1999;5:320-6.
136. Xin L, Xiao Z, Ma X, He F, Yao H and Liu Z. Coxsackievirus B3 induces crosstalk between autophagy and apoptosis to benefit its release after replicating in autophagosomes through a mechanism involving caspase cleavage of autophagy-related proteins. *Infection, genetics and evolution : journal of molecular epidemiology and evolutionary genetics in infectious diseases*. 2014;26:95-102.
137. Savvatis K, van Linthout S, Miteva K, Pappritz K, Westermann D, Schefold JC, Fusch G, Weithauser A, Rauch U, Becher PM, Klingel K, Ringe J, Kurtz A, Schultheiss HP and Tschope C. Mesenchymal stromal cells but not cardiac fibroblasts exert beneficial systemic immunomodulatory effects in experimental myocarditis. *PloS one*. 2012;7:e41047.
138. Savvatis K, Muller I, Frohlich M, Pappritz K, Zietsch C, Hamdani N, Grote K, Schieffer B, Klingel K, Van Linthout S, Linke WA, Schultheiss HP and Tschope C. Interleukin-6 receptor inhibition modulates the immune reaction and restores titin phosphorylation in experimental myocarditis. *Basic research in cardiology*. 2014;109:449.
139. Shen Y, Xu W, Chu YW, Wang Y, Liu QS and Xiong SD. Coxsackievirus group B type 3 infection upregulates expression of monocyte chemoattractant protein 1 in cardiac myocytes, which leads to enhanced migration of mononuclear cells in viral myocarditis. *Journal of virology*. 2004;78:12548-56.
140. Rutschow S, Leschka S, Westermann D, Puhl K, Weitz A, Ladyszenskij L, Jaeger S, Zeichhardt H, Noutsias M, Schultheiss HP, Tschope C and Pauschinger M. Left ventricular enlargement in coxsackievirus-B3 induced chronic myocarditis--ongoing inflammation and an imbalance of the matrix degrading system. *European journal of pharmacology*. 2010;630:145-51.
141. Riad A, Westermann D, Escher F, Becher PM, Savvatis K, Lettau O, Heimesaat MM, Bereswill S, Volk HD, Schultheiss HP and Tschope C. Myeloid differentiation factor-88 contributes to TLR9-mediated modulation of acute coxsackievirus B3-induced myocarditis in vivo. *American journal of physiology Heart and circulatory physiology*. 2010;298:H2024-31.
142. Kim YG, Park JH, Reimer T, Baker DP, Kawai T, Kumar H, Akira S, Wobus C and Nunez G. Viral infection augments Nod1/2 signaling to potentiate lethality associated with secondary bacterial infections. *Cell host & microbe*. 2011;9:496-507.

143. Liu Y, Yang H, Liu LX, Yan W, Guo HJ, Li WJ, Tian C, Li HH and Wang HX. NOD2 contributes to myocardial ischemia/reperfusion injury by regulating cardiomyocyte apoptosis and inflammation. *Life sciences*. 2016;149:10-7.
144. Kandolf R, Sauter M, Aepinus C, Schnorr JJ, Selinka HC and Klingel K. Mechanisms and consequences of enterovirus persistence in cardiac myocytes and cells of the immune system. *Virus research*. 1999;62:149-58.
145. Van Linthout S, Stamm C, Schultheiss HP and Tschope C. Mesenchymal stem cells and inflammatory cardiomyopathy: cardiac homing and beyond. *Cardiology research and practice*. 2011;2011:757154.
146. Miteva K, Van Linthout S, Volk HD and Tschope C. Immunomodulatory effects of mesenchymal stromal cells revisited in the context of inflammatory cardiomyopathy. *Stem cells international*. 2013;2013:353097.
147. De Filippo K, Henderson RB, Laschinger M and Hogg N. Neutrophil chemokines KC and macrophage-inflammatory protein-2 are newly synthesized by tissue macrophages using distinct TLR signaling pathways. *Journal of immunology*. 2008;180:4308-15.
148. Vogl T, Ludwig S, Goebeler M, Strey A, Thorey IS, Reichelt R, Foell D, Gerke V, Manitz MP, Nacken W, Werner S, Sorg C and Roth J. MRP8 and MRP14 control microtubule reorganization during transendothelial migration of phagocytes. *Blood*. 2004;104:4260-8.
149. Croce K, Gao H, Wang Y, Mooroka T, Sakuma M, Shi C, Sukhova GK, Packard RR, Hogg N, Libby P and Simon DI. Myeloid-related protein-8/14 is critical for the biological response to vascular injury. *Circulation*. 2009;120:427-36.
150. Cheng P, Corzo CA, Luetteke N, Yu B, Nagaraj S, Bui MM, Ortiz M, Nacken W, Sorg C, Vogl T, Roth J and Gabrilovich DI. Inhibition of dendritic cell differentiation and accumulation of myeloid-derived suppressor cells in cancer is regulated by S100A9 protein. *The Journal of experimental medicine*. 2008;205:2235-49.
151. Schnekenburger J, Schick V, Kruger B, Manitz MP, Sorg C, Nacken W, Kerkhoff C, Kahlert A, Mayerle J, Domschke W and Lerch MM. The calcium binding protein S100A9 is essential for pancreatic leukocyte infiltration and induces disruption of cell-cell contacts. *Journal of cellular physiology*. 2008;216:558-67.
152. Cabassi A, Binno SM, Tedeschi S, Graiani G, Galizia C, Bianconcini M, Coghi P, Fellini F, Ruffini L, Govoni P, Piepoli M, Perlini S, Regolisti G and Fiaccadori E. Myeloperoxidase-Related Chlorination Activity Is Positively Associated with Circulating Ceruloplasmin in Chronic Heart Failure Patients: Relationship with Neurohormonal, Inflammatory, and Nutritional Parameters. *BioMed research international*. 2015;2015:691693.
153. Averill MM, Barnhart S, Becker L, Li X, Heinecke JW, Leboeuf RC, Hamerman JA, Sorg C, Kerkhoff C and Bornfeldt KE. S100A9 differentially modifies phenotypic states of neutrophils, macrophages, and dendritic cells: implications for atherosclerosis and adipose tissue inflammation. *Circulation*. 2011;123:1216-26.
154. Zhang R, Brennan ML, Shen Z, MacPherson JC, Schmitt D, Molenda CE and Hazen SL. Myeloperoxidase functions as a major enzymatic catalyst for initiation of lipid peroxidation at sites of inflammation. *The Journal of biological chemistry*. 2002;277:46116-22.
155. Heymes C, Bendall JK, Ratajczak P, Cave AC, Samuel JL, Hasenfuss G and Shah AM. Increased myocardial NADPH oxidase activity in human heart failure. *Journal of the American College of Cardiology*. 2003;41:2164-71.
156. Dhalla NS, Temsah RM and Netticadan T. Role of oxidative stress in cardiovascular diseases. *Journal of hypertension*. 2000;18:655-73.
157. Ide T, Tsutsui H, Kinugawa S, Suematsu N, Hayashidani S, Ichikawa K, Utsumi H, Machida Y, Egashira K and Takeshita A. Direct evidence for increased hydroxyl radicals originating from superoxide in the failing myocardium. *Circulation research*. 2000;86:152-7.

158. Kerkhoff C, Nacken W, Benedyk M, Dagher MC, Sopalla C and Doussiere J. The arachidonic acid-binding protein S100A8/A9 promotes NADPH oxidase activation by interaction with p67phox and Rac-2. *FASEB journal : official publication of the Federation of American Societies for Experimental Biology*. 2005;19:467-9.
159. Kojima A, Matsumoto A, Nishida H, Reien Y, Iwata K, Shirayama T, Yabe-Nishimura C and Nakaya H. A protective role of Nox1/NADPH oxidase in a mouse model with hypoxia-induced bradycardia. *Journal of pharmacological sciences*. 2015;127:370-6.
160. Muller F, Froland SS, Aukrust P and Fagerhol MK. Elevated serum calprotectin levels in HIV-infected patients: the calprotectin response during ZDV treatment is associated with clinical events. *Journal of acquired immune deficiency syndromes*. 1994;7:931-9.
161. Hiraoka Y, Kishimoto C, Takada H, Kurokawa M, Ochiai H, Shiraki K and Sasayama S. Role of oxygen derived free radicals in the pathogenesis of coxsackievirus B3 myocarditis in mice. *Cardiovascular research*. 1993;27:957-61.
162. Muralidharan S and Mandrekar P. Cellular stress response and innate immune signaling: integrating pathways in host defense and inflammation. *Journal of leukocyte biology*. 2013;94:1167-84.
163. Nathan C and Shiloh MU. Reactive oxygen and nitrogen intermediates in the relationship between mammalian hosts and microbial pathogens. *Proceedings of the National Academy of Sciences of the United States of America*. 2000;97:8841-8.
164. Doitsh G, Galloway NL, Geng X, Yang Z, Monroe KM, Zepeda O, Hunt PW, Hatano H, Sowinski S, Munoz-Arias I and Greene WC. Cell death by pyroptosis drives CD4 T-cell depletion in HIV-1 infection. *Nature*. 2014;505:509-14.
165. Gastaldello S, Chen X, Callegari S and Masucci MG. Caspase-1 promotes Epstein-Barr virus replication by targeting the large tegument protein deneddylase to the nucleus of productively infected cells. *PLoS pathogens*. 2013;9:e1003664.
166. Guarda G, Braun M, Staehli F, Tardivel A, Mattmann C, Forster I, Farlik M, Decker T, Du Pasquier RA, Romero P and Tschopp J. Type I interferon inhibits interleukin-1 production and inflammasome activation. *Immunity*. 2011;34:213-23.
167. Foell D, Wittkowski H, Vogl T and Roth J. S100 proteins expressed in phagocytes: a novel group of damage-associated molecular pattern molecules. *Journal of leukocyte biology*. 2007;81:28-37.
168. Turovskaya O, Foell D, Sinha P, Vogl T, Newlin R, Nayak J, Nguyen M, Olsson A, Nawroth PP, Bierhaus A, Varki N, Kronenberg M, Freeze HH and Srikrishna G. RAGE, carboxylated glycans and S100A8/A9 play essential roles in colitis-associated carcinogenesis. *Carcinogenesis*. 2008;29:2035-43.
169. Kuipers MT, Vogl T, Aslami H, Jongsma G, van den Berg E, Vlaar AP, Roelofs JJ, Juffermans NP, Schultz MJ, van der Poll T, Roth J and Wieland CW. High levels of S100A8/A9 proteins aggravate ventilator-induced lung injury via TLR4 signaling. *PloS one*. 2013;8:e68694.
170. Grevers LC, de Vries TJ, Vogl T, Abdollahi-Roodsaz S, Sloetjes AW, Leenen PJ, Roth J, Everts V, van den Berg WB and van Lent PL. S100A8 enhances osteoclastic bone resorption in vitro through activation of Toll-like receptor 4: implications for bone destruction in murine antigen-induced arthritis. *Arthritis and rheumatism*. 2011;63:1365-75.
171. Boyd JH, Kan B, Roberts H, Wang Y and Walley KR. S100A8 and S100A9 mediate endotoxin-induced cardiomyocyte dysfunction via the receptor for advanced glycation end products. *Circulation research*. 2008;102:1239-46.
172. Wu Y, Li Y, Zhang C, A X, Wang Y, Cui W, Li H and Du J. S100a8/a9 released by CD11b+Gr1+ neutrophils activates cardiac fibroblasts to initiate angiotensin II-Induced cardiac inflammation and injury. *Hypertension*. 2014;63:1241-50.
173. Bangert A, Andrassy M, Muller AM, Bockstahler M, Fischer A, Volz CH, Leib C, Goser S, Korkmaz-Icoz S, Zittrich S, Jungmann A, Lasitschka F, Pfitzer G, Muller OJ, Katus HA and

Kaya Z. Critical role of RAGE and HMGB1 in inflammatory heart disease. *Proceedings of the National Academy of Sciences of the United States of America*. 2016;113:E155-64.
174. Yu Y, Yu Y, Liu M, Yu P, Liu G, Liu Y, Su Y, Jiang H and Chen R. Ethyl pyruvate attenuated coxsackievirus B3-induced acute viral myocarditis by suppression of HMGB1/RAGE/NF-KappaB pathway. *SpringerPlus*. 2016;5:215.
175. Hofer S, Uhle F, Fleming T, Hell C, Schmoch T, Bruckner T, Weigand MA and Brenner T. RAGE-mediated inflammation in patients with septic shock. *The Journal of surgical research*. 2016;202:315-27.
176. Li J, Schwimmbeck PL, Tschope C, Leschka S, Husmann L, Rutschow S, Reichenbach F, Noutsias M, Kobalz U, Poller W, Spillmann F, Zeichhardt H, Schultheiss HP and Pauschinger M. Collagen degradation in a murine myocarditis model: relevance of matrix metalloproteinase in association with inflammatory induction. *Cardiovascular research*. 2002;56:235-47.
177. Raphael R, Purushotham D, Gastonguay C, Chesnik MA, Kwok WM, Wu HE, Shah SJ, Mirza SP and Strande JL. Combining patient proteomics and in vitro cardiomyocyte phenotype testing to identify potential mediators of heart failure with preserved ejection fraction. *Journal of translational medicine*. 2016;14:18.
178. Mason JW. Myocarditis and dilated cardiomyopathy: an inflammatory link. *Cardiovascular research*. 2003;60:5-10.
179. Tada Y and Suzuki J. Oxidative stress and myocarditis. *Current pharmaceutical design*. 2016;22:450-71.
180. Schiopu A and Cotoi OS. S100A8 and S100A9: DAMPs at the crossroads between innate immunity, traditional risk factors, and cardiovascular disease. *Mediators of inflammation*. 2013;2013:828354.
181. Ma LP, Haugen E, Ikemoto M, Fujita M, Terasaki F and Fu M. S100A8/A9 complex as a new biomarker in prediction of mortality in elderly patients with severe heart failure. *International journal of cardiology*. 2012;155:26-32.
182. Bengtsson AA, Sturfelt G, Lood C, Ronnblom L, van Vollenhoven RF, Axelsson B, Sparre B, Tuvesson H, Ohman MW and Leanderson T. Pharmacokinetics, tolerability, and preliminary efficacy of paquinimod (ABR-215757), a new quinoline-3-carboxamide derivative: studies in lupus-prone mice and a multicenter, randomized, double-blind, placebo-controlled, repeat-dose, dose-ranging study in patients with systemic lupus erythematosus. *Arthritis and rheumatism*. 2012;64:1579-88.
183. Miteva K, Van Linthout S, Pappritz K, Muller I, Spillmann F, Haag M, Stachelscheid H, Ringe J, Sittinger M and Tschope C. Human Endomyocardial Biopsy Specimen-Derived Stromal Cells Modulate Angiotensin II-Induced Cardiac Remodeling. *Stem cells translational medicine*. 2016.

9. MANUSCRIPTS

1. Savvatis K, **Müller I**, Fröhlich M, Pappritz K, Zietsch C, Hamdani N, Grote K, Schieffer B, Klingel K, Van Linthout S: Interleukin-6 receptor inhibition modulates the immune reaction and restores titin phosphorylation in experimental myocarditis. *Basic research in cardiology* 2014, **109**(6):449[138].
2. Miteva K*, Van Linthout S*, Pappritz K, **Müller I**, Haag M, Stachelscheid H, Ringe J, Sittinger M, Tschöpe C: Human cardiac biopsy-derived stromal cells improve angiotensin II-induced cardiac remodeling. *Stem cells Translational Medicine[183]* 2016. * equal contribution.
3. Tschöpe C, **Müller I**, Xia Y, Savvatis K, Lassner D, Heimesaat MM, Bereswill S, Schultheiss H-P, Pieske B, Kühl U, Van Linthout S: Role of NOD2 in experimental and clinical Coxsackievirus B3-induced myocarditis (Manuscript submitted to *Circulation*).
4. **Müller I**, Vogl T, Pappritz K, Miteva K, Savvatis K, Rohde D, Most P, Lassner D, Pieske P, Kühl U, Van Linthout S*, Tschöpe C*: Pathogenic role of the damage-associated molecular patterns S100A8 and S100A9 in Coxsackievirus B3-induced myocarditis (Manuscript submitted to *Circulation research*). * equal contribution.
5. **Müller I***, Pappritz K*, Van Linthout S, Tschöpe C: Role of CX3CR1 in Coxsackievirus B3-induced myocarditis * equal contribution. (Manuscript in process).

10. ABSTRACTS AND ORAL PRESENTATIONS

1. **Müller I**, Xia Y, Savvatis K, Van Linthout S, Tschöpe C: NOD2 inhibition induces cardiobeneficial effects in murine Coxsackievirus B3-induced myocarditis. *Clin Res Cardiology* 104, Suppl 1, April 2015: V959 (accepted as oral presentation at the DGK Congress, Mannheim).
2. Tschöpe C, **Müller I**, Xia Y, Zietsch C, Savvatis K, Lassenr D, Kühl U, Schultheiss H-P, Pieske B, Van Linthout S: NOD2 knockdown improves left ventricular function and attenuates pathophysiological key mechanisms in experemental Coxsackievirus B3-induced myocarditis. *Circulation* 2015, 132: A19779 (accepted as poster presentation at the AHA Congress, Orlando).

3. Tschöpe C, **Müller I**, Vogl T, Pieske B, Van Linthout S: Role of S100A8 and S100A9 alarmins in Coxsackievirus B3-induced myocarditis. *JACC* April 5, 2016 Volume 67, Issue 13: 1398 (accepted as poster presentation at the ACC Meeting, San Diego).
4. Tschöpe C, **Müller I**, Vogl T, Savvatis K, Schultheiss H-P, Pieske B, Van Linthout S: Role of S100A8 and S100A9 alarmins in Coxsackievirus B3-induced myocarditis. *Clin Res Cardiology* 105, Suppl 1, March 2016 (accepted as poster presentation at the DGK Meeting, Mannheim).
5. Tschöpe C, **Müller I**, Xia Y, Savvatis K, Lassner D, Schultheiss H-P, Pieske B, Kühl U, Van Linthout S: NOD2 knockdown improves left ventricular function and attenuates NLRP3 inflammasome activity in experemental Coxsackievirus B3-induced myocarditis. *European Journal of Heart Failure Abstract,* 2016, Suppl 1, 18, 138: P542 (accepted as poster presentation at the Heart Failure Meeting, Florence).
6. **Müller I**, Van Linthout S, Vogl T, Pieske B, Tschöpe C: Role of S100A8 and S100A9 alarmins in Coxsackievirus B3-induced myocarditis. *European Journal of Heart Failure Abstract*, 2016, Suppl 1, 18, 137: P541 (accepted as poster presentation at the Heart Failure Meeting, Florence).

11. DANKSAGUNG

In erster Linie möchte ich Herrn Prof. Dr. Carsten Tschöpe danken, dass er mir die Möglichkeit gab auch nach einer 5-jährigen Laborpause in seiner Arbeitsgruppe die vorliegende Doktorarbeit durchführen zu können. Es war eine große Ehre in solch einer international anerkannten Arbeitsgruppe meinen wissenschaftlichen Werdegang fortzuführen. Ich hatte die großartige Gelegenheit auf dem Feld der Herzinsuffizienz und inflammatorischen Kardiomyopathie zu forschen, mit immer wieder neuen Herausforderungen, die meine Dissertation bereichert haben. Ich bin sehr dankbar dafür, dass Herr Prof. Dr. Carsten Tschöpe immer Zeit für anregende und zielführende Diskussionen fand.

Ein großes Dankeschön an PD Dr. Sophie Van Linthout, für ihre herzliche Aufnahme in die Arbeitsgruppe und die großartige Möglichkeit am Berlin-Brandenburger Centrum für Regenerative Therapien meine Dissertation verfassen zu dürfen. Ihre hervorragende wissenschaftliche Unterstützung und ihre Geduld, haben mich motiviert, und mich zu meinen persönlichen Höchstleistungen angetrieben. Sie hatte immer ein offenes Ohr und eine offene "Bürotür" für Diskussionen. Neben meiner wissenschaftlichen Expertise habe ich von Sophie gelernt, schwierigen Situationen mit Ruhe zu begegnen und niemals aufzugeben.

Meiner Arbeitsgruppe würde ich gerne für die großartige Zeit danken. Sie haben mich von Anfang an sowohl wissenschaftlich als auch moralisch unterstützt. Nach einer 5-jährigen Laborabstinenz, hatte ich das Glück durch Kerstin Puhl, Kathrin Hinz und Nadine Orrin wieder in das Laborleben eingearbeitet zu werden. Herrn Zingler möchte ich für die tolle Unterstützung bei der Immunhistologie danken. Mein Dank gilt auch Annika Koschel, Dr. Kapka Miteva, Marzena Sosnowski und Gwendolin Matz, die mich fortwährend im Labor unterstützt und eingearbeitet haben. Dr. Kathleen Pappritz und Dr. Christin Zietsch, meine Vorgängerinnen, euch danke ich für die fortwährende Unterstützung während meiner gesamten Promotion, die zahlreichen Diskussionen und natürlich die amüsanten Abende, die nicht nur der Wissenschaft galten. Ich bin sehr froh darüber euch alle als Kollegen gehabt zu haben.

Meinen Freunden möchte ich mich für die Begleitung und unendliche Unterstüzung danken, die Sie mir während meiner gesamten Doktorarbeit gegeben haben.

Zum Schluss möchte ich meiner gesamten Familie danken. Meinen Eltern möchte ich einen besonderen Dank aussprechen. Sie haben mich in jeder Lebenslage unterstüzt und haben mir die großartige Möglichkeit gegeben, mein Studium und die anschließende Promotion zu machen. Ohne die großartige Unterstützung meiner Eltern, hätte ich es nicht so weit geschafft. Vielen Dank!